New Ultra Scale-down Principles for Monoclonal Antibody Recovery and Purifications

Nicholas Hutchinson

UCL

Engineering Doctorate Thesis

I, Nicholas Hutchinson, confirm that the work presented in this thesis is my own. Where information has been derived from other sources, I confirm that this has been indicated in the thesis.

ProQuest LLC
789 East Eisenhower Parkway
P.O. Box 1346
Ann Arbor, MI 48106-1346

Abstract

The development of manufacturing processes for biopharmaceuticals is carried out by performing experiments in the laboratory and then the pilot plant. These laboratory – scale experiments are often misleading as they do not allow for the effect of the large-scale processing environment on the properties of biological process material. The research contained within this thesis seeks to develop laboratory techniques capable of eliciting the effects of the processing environment on the material and of predicting the performance of large-scale unit operations used in the purification of monoclonal antibody (MAb) biopharmaceuticals using milliliter volumes of process material. Two key interactive stages were examined; firstly, an early centrifugation clarification stage designed to prepare material for subsequent filtration which precedes the second stage studied, a high affinity antibody capture step. The first focuses on the whole cell broth, containing the contaminants and the antibody product, the latter on the antibody product itself. A scale-down centrifuge technique which employed a rotating-disc, centrifuge feed zone mimic along with a laboratory-scale centrifugation method were developed to predict the clarification performance of two pilot, disc stack centrifuges with differing feed zone configurations and a manufacturing-scale disc stack centrifuge. The material obtained from the scale-down centrifuge protocol was shown to be equivalent to that from one of the pilot centrifuges to which it had been compared and, hence, could be used for the development of subsequent unit operations, such as chromatography processes. A method was developed to predict the elution profile of an 18 L pilot affinity chromatography column using a scale-down column with a column volume of one milliliter. A regime analysis of the laboratory-scale

chromatography system was performed using conductivity transitions to determine the extent of additional zone broadening occurring at the small scale so that the prediction of the large-scale elution volume and eluting product concentration could be significantly improved.

Acknowledgments

The help of so many people at University College London and Lonza Biologics has been required during the course of my doctorate that unfortunately there isn't room to mention them all. However, if you are reading this and feel you should be acknowledged, I assure you that you are.

I would like to thank Professor Mike Hoare for teaching me such a lot about how to conduct and present research. I could never have completed this work without his patience and positive attitude which have been so invaluable over the past five years.

I'd like to acknowledge the never ending support of my wonderful family especially Mum and Dad, Vicky, Mike, Spike and Jared.

Many thanks to Claire for her support and patience, for her gentle encouragement to get this done and for all the good times we've had together.

The financial support from the EPSRC and Lonza Biologics is gratefully acknowledged.

Finally, thanks to London, an amazing city "full of sordid sinners and splendid sins", undivided and undefeated by terrorism, home for the past six years and an education in itself.

Table of contents

List of figures

Chapter 1

Chapter 2

List of tables

Chapter 1

Chapter 1 - Introduction

Lonza Biologics is a contract manufacturer of therapeutic proteins derived from animal cell culture. The majority of the processes operated are for the production of monoclonal antibody therapeutics. A typical production process can be divided up into three phases (Figure 1.1). During the cell culture phase, animal cells are grown in suspension culture and secrete the protein product into the surrounding growth medium. At the end of the cell culture, the material generated is clarified by processing through centrifuges (that remove most of the cells and cell debris) and filters (that remove any remaining solids) giving a clarified broth that can be purified in the final phase of the process. A typical purification process utilizes two or three chromatography columns with associated ultrafiltration steps that remove impurities such as proteins and nucleic acids produced by the cells along with the product.

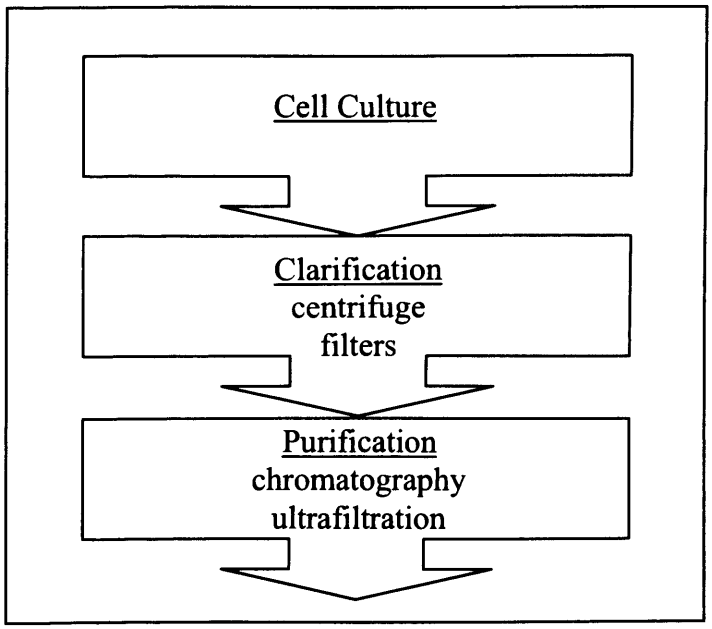

Figure 1.1. Overview of a therapeutic protein production process

Process development scientists seek to develop manufacturing processes that yield products that meet pre-defined criteria of safety and effectiveness. Development studies must be completed within short timelines (to allow early market entry of the product enabling the product's sponsor to recoup drug development costs), give a robust process to ensure product safety and minimise the risk of batch failure and provide an optimised process that minimises Cost of Goods.

Conventional development methods have been used successfully in the past to bring products to the market. They use scale-up methodologies based on established theory and hence both industry and regulators are comfortable with these approaches. However, they typically require large amounts of product/process material to yield relatively small amounts of process information and are often poorly predictive of the performance of large-scale processes. For example, centrifugation process development to identify an operating flow rate that gives the target level of process stream clarification while maximising plant throughput necessitates a 500 L cell culture to generate sufficient material for the development experiment, which is both costly and time consuming. Further, pilot-scale centrifugation studies can over-predict the clarification performance of large-scale equipment due to critical differences between the hydrodynamic environment of the equipment at the two scales and its impact on shear-sensitive process materials. Novel technology is required that permits more rapid manufacturing process development with reduced material requirements. This would allow more information and greater process understanding to be acquired which, in turn, will lead to more robust and optimised processes being developed in a shorter timeframe.

The aims of the work contained within this thesis were as follows,

- To develop and verify a centrifuge process development tool requiring small volumes of process material capable of predicting the performance of large-scale equipment.
- To develop and verify a chromatography process development tool capable of using the material generated by the centrifugation tool and capable of predicting the performance of large-scale columns.
- To develop appropriate models and visualisation tools to facilitate the use of the data generated by the process development tools for process design.

Literature Review

1.1. Antibodies

Antibodies or immunoglobulins are soluble proteins produced by the immune system of vertebrates to recognize and initiate the destruction of foreign molecules such as those derived from microorganisms. Any given antibody molecule has a specific affinity for the foreign macromolecule that stimulated its synthesis. Macromolecules capable of eliciting an antibody-producing response by the immune system are called antigens and include proteins, polysaccharides and nucleic acids. An antibody will recognize a highly specific site on an antigen molecule called an epitope.

1.1.1. Antibody structure

Antibodies typically share a common Y-shaped structure consisting of four polypeptide chains: two identical heavy chains that each carry covalently-attached oligosaccharide groups; and two identical, non-glycosylated light chains. The two heavy chains are joined together by disulphide bonds that are located in a flexible region of each polypeptide called the hinge. The hinge is typically 12 amino acid residues long and is exposed to both enzymatic and chemical cleavage. A single disulphide bond joins each of the light chains to one of the heavy chains.

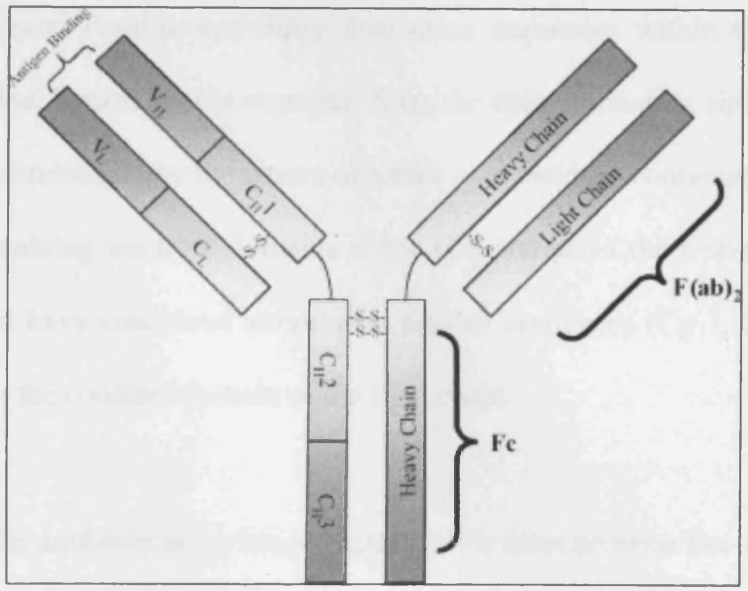

Figure 1.2. The structure of a human antibody (IgG) showing the 'Y'-shaped structure, the location of the heavy and light chains, the disulphide bridges (-s-s-), the antigen binding site, the antibody-binding fraction (F_{ab}) and the crystalizable fraction (F_c) and the various domains (C_H 1 -3, V_H & V_L, C_L). Reproduced from Sommerfeld & Strube, 2005.

Antibody light chains contain around 214 amino acids and have a molecular weight of around 25 kDa. The light chains consist of two domains, a variable domain (V_L) at the N-terminus (amino acid residues 1 to 108) which exhibit considerable amino acid residue sequence variability between different antibodies and a constant domain (C_L) at the C-terminus (residues 109-214) which has a highly conserved amino acid sequences. The heavy chains consist of 446 amino acid residues that fold into four domains and have a molecular weight of approximately 50 kDa. As with the light chain the residue sequence of the N-terminal domain varies between antibodies and is 109 amino acid residues in length (V_H). Three sequences within the variable domain of the light chain and three within the variable domain of the heavy chain

exhibit far greater residue variability than other sequences within these domains. These, so called, hypervariable segments form the epitope-binding site and antibody specificity is determined by the nature of amino acid residues contained within them. The three remaining constant domains at the C-terminus of the heavy chain are of equal size and have conserved amino acid residue sequences (C_H 1, 2 & 3) to one another and to the constant domain of the light chain.

Cleavage of the antibody at the hinge region yields three proteins two of which bind antigen and are known as F_{ab} fragments (*ab* is an abbreviation of 'antigen binding') and one that does not bind antigen and is known as the F_c fragment because a solution of these fragments will crystallize readily. F_{ab} fragments are composed of the entire light chain of the antibody bound to the N-terminal half of the heavy chain. The F_c fragment consists of the C-terminal half of the heavy chain consisting of the seconds and third constant domains. The role of the F_{ab} section of the antibody is to bind antigen and hence each antibody is bivalent while the F_c region is responsible for mediating protective responses known as effector functions such as compliment fixation which ultimately lead to pathogen lysis.

1.1.2. Antibody classes

There are five classes antibody IgG, IgM, IgA, IgD and IgE. The constant regions of the heavy chains vary from one class to another and give each class distinct biological characteristics.

IgM is composed of five of the monomeric units described above giving each IgM molecule ten antigen binding sites and allowing them to bind tightly to antigens containing multiple identical epitopes. They are the first antibody to be produced in an immune response but have lower affinity for antigens than antibody classes subsequently produced.

IgG is the principal antibody in the serum while IgA is the major class of antibody in external secretions such as saliva, tears, bronchial mucus and intestinal mucus where it forms dimers of monomeric units. IgA acts as the first line of defense against bacterial and viral antigens. IgG and IgA can further be divided into subclasses that result from minor differences in the amino acid sequence of the heavy chain. In humans there are four subclasses of IgG and two subclasses of IgA.

IgD is found in low levels in serum where its roles is uncertain, however, it is also found on the surface of B cells where it acts as an antigen receptor.

IgE is important in providing protection from parasites. Binding of IgE antibodies to an antigen leads to the degradation of mast cells and the release of a number of agents including histamine that induce smooth muscle contraction and the secretion of mucus (Stryer, 1995) .

1.1.3. Polyclonal antibodies

When infected by a pathologic agent a host organism's immune response will generate a large number of different antibodies that recognize different antigens and

different epitopes on an individual antigen. Each antibody is produced from an individual clone of white blood cell called plasma cells. Serum from immunized animals is a good source of polyclonal antibodies which can be used as reagents in immunochemical techniques. Polyclonal antibody containing sera from rodents immunized with infectious agents has been used for therapeutic purposes in humans; however, such crude preparations were ineffective and the rodent serum itself produced an adverse immune reaction in patients. More notably, polyclonal antibody therapeutics have been used as neutralizing venoms for the treatment of snake-bite victims (http://www.protherics.com/, 2005).

1.1.4. Monoclonal antibodies

In 1975, Georges Köhler and César Milstein invented hybridoma technology and were later awarded the Nobel Prize. A hybridoma is created by fusing an antibody-producing plasma cell from an immunized rodent with a cell derived from a rodent myeloma tumour (Köhler & Milstein, 1975). Such hybrid cells can be cloned and cultured indefinitely and, along with advanced cell culture techniques, allow the mass production of individual murine monoclonal antibodies.

1.1.5. Therapeutic monoclonal antibodies

Monoclonal antibodies can be raised against a vast number of epitopes including those contained within antigenic proteins involved in causing disease. By generating and then mass producing antibodies that could be administered to patients it appeared, in the 1980's, that modern medicine had discovered its 'Magic Bullets',

capable of binding to disease-implicated proteins with high specificity and bringing about their destruction. Such therapeutics, it was believed, would be ideal for identifying and destroying cancerous cells which frequently express tumour-specific antigens. An example of one such monoclonal antibody is trastuzumab (Herceptin^{TM}), marketed by Genentech, which targets and blocks a growth receptor on the surface of breast cancer cells. In a clinical trial consisting of 469 women with late stage breast cancer and testing positive for the receptor, a combination of Herceptin^{TM} and a standard chemotherapeutic agent reduced the size of tumours and led to an average increase in life expectancy of 5 months (Slamon *et al.,* 2001). The effectiveness of monoclonal antibody therapies can be increased by attaching toxins or radionucleotides. For example, IDEC Pharmaceuticals' radio-antibody, ibritumomab tiuxetan (Zevalin^{TM}) was approved by the US Food and Drug Administration in February 2002 for the treatment of non-Hodgkin's lymphoma. FDA approved monoclonal antibody therapies, their degree of humanization, indication, company and approval date are shown in Table 1.1

Product	Type	Indication	Company	Approved
Muromonab -CD3	Murine	Transplant rejection	Johnson & Johnson	1986
Abciximab	Chimeric	Cardiovascular disease	Centocor	1994
Rituximab	Chimeric	B-cell lymphoma	Genentech	1997
Daclizumab	Humanized	Transplant rejection	Hoffmann-La Roche	1997
Basiliximab	Chimeric	Transplant rejection	Novartis	1998
Palivizumab	Humanized	Respiratory syncytial virus	MedImmune	1998
Infliximab	Chimeric	Rheumatoid arthritis/ Crohn's Disease	Centocor	1998
Trastuzumab	Humanized	Breast cancer	Genentech	1998
Gemtuzumab-ozogamicin	Humanized	Acute myeloid leukaemia	Wyeth	2000
Alemtuzumab	Humanized	Chronic leukaemia	Genzyme	2001
Ibritumomab	Chimeric	Non-Hodgkin's leukemia	Biogen IDEC	2002
Adalimumab	Human	Rheumatoid arthritis	Abbott	2003
Omalizumab	Humanized	Allergic asthma	Genentech	2003
Tositumab-I131	Murine	Non-Hodgkin's leukemia	Corixa	2003
Efalizumab	Humanized	Moderate to severe psoriasis	Genentech	2003
Cetuximab	Chimeric	Various cancers	Imclone	2004
Bevacizumab	Humanized	Various cancers	Genentech	2004
Natalizumab	Humanized	Multiple sclerosis	Biogen Corp	2004
Etanercept	Fusion	Rheumatoid Arthritis	Immunex	1998
Alefacept	Fusion	Chronic plaque psoriasis	Biogen Corp	2003

Table 1.1 showing FDA approved monoclonal antibody therapies, their degree of humanization, indication, company and approval date.

1.1.5.1. Murine monoclonal antibodies and the HAMA response

Initial optimism over therapeutic monoclonal antibodies was met with limited clinical success as murine monoclonal antibodies were found to be antigenic in humans. Patients who received these therapeutics frequently developed immune responses to the drugs and produced human anti-mouse antibodies (HAMA) to these murine molecules which their immune systems recognized as foreign. The HAMA response led to the destruction of the therapeutic antibody, thereby reducing drug effectiveness (Winter & Milstein, 1991). Furthermore, murine monoclonal antibodies were found to be ineffective at triggering human effecter cells, such as the macrophages required to destroy the antibody-antigen complex, due to subtle differences between the heavy chains of murine and human antibodies. Of the murine antibodies only muromonab-CD3 (OKT-3^{TM}), sponsored by Ortho Biotech and marketed by Johnson & Johnson, has been approved by the US Food and Drug Administration for the reversal of acute rejection of kidney transplants. Muromonab-CD3's mechanism of action involves targeting a glycoprotein on the surface of T-cells in the immune system thereby preventing them from recognizing the transplanted organ as foreign. The success of this product lies not only in the fact that the product shuts down part of the immune system which could clear the drug but also that patients undergoing kidney transplants are treated with immunosuppressive drugs and are subsequently less likely to generate the HAMA response (Guru, 2002).

1.1.5.2. Chimeric monoclonal antibodies

Chimeric antibodies are genetically engineered by constructing genes in expression vectors that contain mouse and human DNA sequences. The resulting translated protein has human constant domains with murine variable domains (Morrison *et al.,* 1984; Boulianne *et al.,* 1984). The human constant regions are capable of communicating with patients' immune systems while the proportion of antigenic murine sequences is significantly reduced. The application of chimeric antibody technology led to a number of new products being approved such as abciximab (Reopro^{TM}), sponsored by Centocor, which reduces the risk of blood clots in patients suffering from cardiovascular disease by targeting receptors on the surface of platelets and rituximab (Rituxan^{TM}), sponsored by Genentech, for the treatment of non-hodgkins' lymphoma.

1.1.5.3. Humanized and human antibodies

To further improve the effectiveness of monoclonal antibody therapies, research continued into reducing the proportion of murine sequences in the protein. In 1986, Greg Winter, working at Cambridge University, reduced the mouse component of chimeric antibodies to between 5 and 10 % by replacing the entire murine gene with human DNA sequences except for those sequences that code for the hypervariable regions of the epitope binding site (Jones *et al.,* 1986). Such humanized antibodies evaded patients' immune systems and a number have since been approved by the FDA, the first of which, daclizumab (Zenapax^{TM}), was approved in 1997 and binds to and inhibits a receptor on activated white blood cells which would otherwise

stimulate tissue rejection of transplanted organs. In 2003 adalimumab (Humira™) became the first human antibody to be approved by the FDA for therapeutic use and was created using phage display technology. The process of phage display technology involves the harvesting of genes that code for antibody variable regions from populations of lymphocytes and cloning them for display of the associated heavy and light chain variable domains on the surface of viruses that infect bacteria or bacteriophage. Bacteriophage expressing proteins with the desired specificity and affinity can be selected by antigen affinity techniques and then further improved by mutation allowing a desired human antibody to be produced without any need for immunization (Winter *et al.*, 1994).

1.1.5.4. Fusion proteins

Etanercept (Enbrel™) and alefacept (Amevive™) are both FDA approved recombinant fusion proteins that contain antibody constant domains that are required for product functionality. The F_{ab} regions of the antibody molecule are replaced with a protein such as the Tissue Necrosis Factor (TNF) receptor component of Enbrel™ (http://www.enbrel.com/). Fusion proteins are manufactured in a similar way to monoclonal antibodies.

1.2. Manufacturing therapeutic monoclonal antibodies

Annual production of therapeutic monoclonal antibody products is small when compared to small molecule drugs due both to the specific and potent nature of antibody therapeutics. Demand varies considerably between products; however, even

for a more common indication such as rheumatoid arthritis production is unlikely to exceed 500 kg per annum equivalent to 100,000 patients being administered 5 grams of antibody per annum. Production costs are also typically much higher than small molecule therapeutics which can be synthesized for approximately US$ 5 per gram while antibody drugs incur production costs of US$ 100-1000 per gram. The relatively low volume of product required by the market allows demand to be met through campaigns of batch production while simultaneously minimizing the risks, such as contamination, of operating a continuous process. Commercial production processes for the large-scale manufacture of monoclonal antibodies are typically divided into three main phases. During the first phase, mammalian cells capable of expressing the desired antibody are grown in culture and secrete the product into the surrounding growth medium. Secondly, the product-containing growth medium is recovered by removal of the cells and finally the product is purified from impurities within the growth medium.

1.2.1. Cell culture

A characteristic of monoclonal antibody production along with the manufacture of other recombinant proteins is that the product is produced using living organisms grown under controlled conditions. The majority of full length therapeutic antibodies are produced in mammalian cell lines (Anderson & Reilly, 2004) because of their capacity for proper folding, assembly and post-translational modification of the product (Wurm, 2004). Table 1.2 below shows the cell culture methods used in the production of seven licensed therapeutic monoclonal antibodies.

Antibody	Cell Line	Format	Suspension or attached	Medium
Etanercept (Enbrel™)	CHO	Stirred tank bioreactor	Suspension	Not revealed
Trastuzumab (Herceptin™)	CHO	Stirred tank bioreactor	Suspension	Serum-free, Gentamicin containing
Infliximab (Remicade™)	Murine Myeloma	Stirred tank bioreactor, perfusion with spin filter	Suspension	Serum-free, protein hydrolysates, bovine transferrin, insulin, serum albumin
Palivizumab (Synagis™)	NS0	Stirred tank bioreactor, fed-batch	Suspension	Serum-free
Basiliximab (Simulect™)	Murine Myeloma	Stirred-tank bioreactor, perfusion	Suspension	Serum-free
Daclizumab (Zenapax™)	SP2/0	Not revealed	Not revealed	Not revealed
Rituximab (Rituxan™)	CHO	Stirred-tank bioreactor	Suspension	Contains Gentamicin

Table 1.2 showing cell culture methods used in the production of seven approved therapeutic monoclonal antibodies (adapted from Chu & Robinson, 2001).

1.2.1.1. Cell lines

Although monoclonal antibodies were originally produced in hybridoma cells (Kohler & Milstein, 1975) regulatory approval has been gained for recombinant protein production in immortalized chinese hamster ovary (CHO), mouse myeloma (NS0 & Sp2/0), monkey kidney (COS), baby hamster kidney (BHK), human embryo kidney (HEK-293) and human retinal cells (PER-C6) (Wurm, 2004). The choice of cell line for production is usually based on the ability of the line to produce product with human-like glycosylation patterns, to express the product in a stable fashion following gene insertion and to achieve high specific production rates (Sommerfeld & Strube, 2005). CHO and mouse myeloma cells fulfill these criteria well and hence are frequently used cell lines (see Table 1.2). These cell lines produce product with near human glycosylation patterns, stably express the protein and are capable of achieving final product concentrations of 4.7 $g.L^{-1}$ (Wurm, 2004). Both the culture and genetic manipulation of these cell lines have been extensively studied permitting considerable cell culture process control (Peakman *et al.,* 1994). Genetic manipulation of cell lines can be carried out in order to confer on the cell lines properties enabling improved bioreactor performance such as controlling cell growth (Bi *et al.,* 2004) (Chiang & Sisk, 2005), preventing cell death (Ibarra *et al.,* 2003) or influencing glycosylation (Shields *et al.,* 2002).

1.2.1.2. Cell culture media

High antibody titre cell culture processes are a result, in part, of the considerable research undertaken to optimize the growth media that provides cells with the

necessary compounds required for growth. Commercially available media can be obtained from suppliers; however, leading recombinant protein manufacturers develop and optimize their own formulations which are valuable commercial secrets. More than one media will be used in a single manufacturing process each tailored to a specific phase. For example, production media which is used for up to 21 days in the large-scale bioreactor is unlikely to be the same as that used for the sub-cultivation of rapidly growing cells lasting only 3-5 days that takes place in seed bioreactors. Media development is important for the productivity of the process and is carried out for each process and cell line. In the past fetal bovine serum was required for mammalian cell culture and added at a concentration of 1-20%. Serum contains peptides, growth factors, proteins, lipids, carbohydrates and small molecules that promote cell growth; however, modern media formulations support growth in the absence of serum. Using serum-free media reduces the cost of the media, the risk of transmission of adventitious agents such as prions and the cost of purifying the product (Wurm, 2004) hence manufacturers of antibodies prefer to use chemically defined media containing essential amino-acids, trace elements and proteins (Moran *et al.,* 2000). However, cell lines frequently require adapting to growth in the absence of serum which is a time consuming process and frequently leads to a reduction in the specific productivity of the cell line (Sommerfeld & Strube, 2005). Cell culture is possible in completely protein-free media (Hamilton & Ham, 1977) leading to further decreases in purification costs as the product is at least twice as pure as that produced in a protein-containing culture media (Sommerfeld & Strube, 2005).

1.2.1.3. Recombinant protein expression systems

Cell lines are genetically engineered to express the required therapeutic antibody by transfecting the cells with foreign DNA containing the gene encoding the protein product. To maximize cell culture productivity a stable expression system is required that ideally fulfils two criteria. Firstly it should be selective and hence will not permit non-product producing cells to grow and secondly it should be stringent in that it favours the growth of cells with high specific production rates. One common expression system is the glutamine synthetase (GS) system licensed to Lonza Biologics (Brown *et al.,* 1992). Glutamine synthetase is an enzyme that catalyses the synthesis of glutamine from glutamate and ammonium. Mammalian cells have no other mechanism for producing this essential and unstable amino acid. Mouse myeloma cells such as NS0 cell lines are unable to produce sufficient glutamine synthetase to grow in media that does not contain glutamine. If the genes encoding the product and glutamine synthetase enzyme are incorporated into the same segment of DNA only cells containing the gene encoding the product will be able to grow in glutamine free media. Although CHO cells produce sufficient endogenous glutamine synthetase to permit growth in glutamine free media the specific glutamine synthetase inhibitor methionine sulphoximine (MSX) can be used at concentrations of 10-100 μM to limit the enzymes activity so that only transfected cells with additional enzyme activity through vector amplification are capable of survival (Barnes *et al.,* 2000). A further advantage of the glutamine synthetase system is that transfected cells metabolize ammonia in the media, a toxic and unwanted by-product of cell growth (http://www.lonza.com/, 2005).

An alternative to the glutamine synthetase system is the dihydrofolate reductase (DHFR) system. DHFR is an enzyme, the activity of which is blocked by exposing cells to the drug methotrexate (MTX) (Gandor *et al.,* 1995). Most cells exposed to MTX will die; however, a small proportion that overproduce DHFR will survive. If the concentration of MTX is steadily increased over successive cell generations surviving cells can contain a few thousand copies of the length of DNA encoding product and DHFR enzyme (Wurm *et al.,* 1986). Most cells in which amplification has occurred produce more recombinant protein than those cells in which it has not and the improvement of specific productivities can be 10- to 20-fold (Zettlmeissl *et al,.* 1988).

1.2.1.4. Bioreactor formats

Historically mammalian cell culture was carried out using cell lines that grew while attached to a solid support such as the surface of a roller bottle or porous microcarrier beads. Today many cell types have been adapted to grow in suspension culture facilitated by the use of shear-protecting agents such as Pluronic F68 (van der Pol & Tramper, 1998). Suspension cell culture processes now dominate processes for the production of recombinant proteins as the scaling parameters are well understood and process control is facilitated in a homogeneous system (Chu & Robinson, 2001). Both stirred tank reactors and airlift reactors are frequently used for the growth of mammalian cells in suspension culture (Osman *et al.,* 2004). Stirred tank reactors are mechanically agitated using an impeller to ensure a homogeneous environment throughout the culture and support adequate bubble dispersion. Baffles are used to prevent the culture medium from vortexing while

oxygen/air is supplied to the cells via a gas sparger at the bottom of the reactor. Airlift reactors are not mechanically agitated and hence generate a less shear-intensive environment as shear forces can be detrimental to cell growth. Gas is sparged into part of the vessel called the riser reducing the liquid density and causing it to rise. Gas disengagement at the surface of the liquid leaves less dense, gas-free medium to re-circulate through the down-comer (Doran, 1994).

An important innovation in reactor design within the past decade has been the use of disposable cell culture bioreactors that rely on wave-induced agitation. These reactors can be operated at scales of up to 500 L and give similar growth rates and productivities to stirred-tank reactors (Singh, 1999). In addition, their disposable nature means that culture vessel preparation, usually involving cleaning and sterilization, is significantly simplified and can be achieved in one day rather than in three to four days (Tong *et al.*, 2004).

1.2.1.5. Feeding strategies

Basic batch suspension processes in a stirred tank reactor are becoming less frequently used, as nutrient feeding reduces waste accumulation and nutrient fluctuations allowing higher cell densities and productivities to be reached (Chu & Robinson, 2001). The use of fed-batch processing techniques permits the maintenance of high cell densities at high specific productivities for prolonged periods of time resulting in high final product titres. A typical batch process would, in the past, yield around 2 x 10^6 cells/mL, have a production phase of around 7 days and have a specific productivity of around 10 pg/cell/day. Today's extended batch

processes can yield 10 x 10^6 cells/mL, maintaining cell viability over 3 weeks with a specific productivity of ~90 pg/cell/day (Wurm, 2004). Palivizumab (Synagis®)is an example of a product manufactured using a fed-batch process, in which glucose is fed into the reactor to replace that utilized by cells (Schenerman *et al.,* 1999). In perfusion culture systems, several reactor volumes of fresh medium can be fed into the culture per day while the same volume of fluid, containing product for purification is withdrawn from the reactor. In order to retain the cells within the bioreactor perfusion systems rely on cell retention mechanisms such as centrifuges, spin filters (Idling *et al.,* 2000), hollow fibre modules (Yang *et al.,* 2000) and acoustic devices (Dalm *et al.,* 2005), thus allowing achievement of higher cell densities than could be obtained in fed-batch culture. The concepts of controlled feeding and perfusion have been combined at the 20 L scale (Yang *et al.,* 2000). A controlled glucose feed was introduced to the perfusion culture giving a cell density of 1.8 x 10^7 cells/mL and an antibody concentration of 275 U/L. The high productivity was attributed to the high cell density and minimized product dilution permitted by the glucose feed (Yang *et al.,* 2000).

1.2.1.6. Alternatives to cell culture

Expression systems capable of producing monoclonal antibodies have been investigated as potentially cheaper and more efficient methods of producing large volumes of antibody therapeutics. In 2000, Immunex's etanercept (Enbrel®) lost market share to Centocor's infliximab (Remicade®) because Immunex was unable to manufacture sufficient etanercept due to a lack of manufacturing capacity and was forced to ration available product among patients. This episode highlighted a

worldwide shortage of cell culture capacity. In 2001 industry analysts projected that demand for capacity would be four-fold greater than supply by 2005 (Molowa, 2001). Arguably, with the construction of new manufacturing facilities cell culture capacity supply has now matched demand (Thiel, 2004). However, future products requiring large dose sizes and the imposition by health care providers of limits on therapeutic prices continues to stimulate research into technologies to produce greater quantities of antibodies at a lower cost than cell culture. Full length antibodies have been produced in the bacterial species *Escherichia coli* (Simmons *et al.,* 2002). *E. coli* production can be easily scaled-up, is less prone to contamination than cell cultures, is rapid (as the organism population can double in 20 minutes, in comparison with mammalian cell populations that can take over 24 hours) and incurs lower fermentation capital costs than cell culture (Simmon *et al.,* 2002). The disadvantage of this microbial system and others like it is that these prokaryotic organisms are incapable of performing post-translational protein gylcosylation. This carbohydrate component of the antibody is often necessary for the correct functioning of the pharmaceutical (Shields *et al.,* 2002). However, in cases where it is not, such as when the antibody binds to soluble antigen, aglycosylated antibodies produced in bacteria could be suitable alternatives to glycosylated proteins derived from cell culture. Relative to *E.coli*, production of antibodies in fungal species such as *Aspergillus niger* or *Pichia pastoris* has the advantage that the protein is secreted by the organism into the culture medium. In contrast *E. coli* retains the expressed protein intracellularly, making recovery of the protein more complex and expensive. Filamentous fungal species have been shown to express homologous proteins at high concentrations. However, foreign proteins expressed following gene insertion are produced at a lower concentration and hence research has been carried out into

increasing heterologous expression (Sotiriadis *et al.*, 2001). Glycoproteins derived from fungal expression systems contain non-human carbohydrate residues which can be immunogenic in humans, precluding their use as therapeutic molecules. The glycosylation metabolic pathway of *P. pastoris* has been successfully genetically modified to yield humanized glycoforms of glycoproteins (Hamilton *et al.*, 2003). The use of plant species for the production of therapeutic glycoproteins such as monoclonal antibodies has been considered (Joh *et al.*, 2005). The advantages of production in plants include reduced capital costs, flexibility in production output depending on market demand and the lack of human adventitious agents in plant species. However, issues to be resolved before plant expressed proteins are likely to compete with those derived from cell culture include the long lead time to production, regulatory uncertainties, and concerns over plant glycosylation patterns in human therapeutic agents. The co-expression of human β1,4-galactosyltransferase and an antibody in tobacco plants has been achieved, yielding a galactosylation profile resembling that found in mammalian antibodies (Bakker *et al.*, 2001).

1.2.2. Product recovery

The purification of human therapeutic proteins derived from batch mammalian cell culture typically commences with the removal of cells and cellular debris. Separation of the cells from the cell culture medium removes intracellular contaminants such as host cell proteins, nucleic acids, carbohydrates and lipids. Furthermore, solid particulates such as cells and especially, colloidal cell debris, can foul downstream chromatographic steps and lead to unacceptable cross column pressure drops and a reduction in overall column performance.

1.2.2.1. Centrifugation

Centrifugation is a common technique used to harvest large-scale cell culture vessels as it combines low running costs with uncomplicated process development and operational robustness (Axelsson, 1999; Hanle, 1999; Abraham *et al.,* 2003). Centrifugal forces are generated and separation is achieved on the basis of the density difference between the heavy cell component and the lighter, liquid, component of the feed stream. Multi-chamber, tubular bowl and disc-stack designs are all available. However, the disc stack centrifuge is particularly convenient as it can provide intermittent solids discharge it does not require periodic disassembly and reassembly during the harvest to empty the bowl of solids.. The relatively low frequency of sediment discharge means that parallel discharge of entrained supernatant does not contribute strongly to product loss.

1.2.2.2. Normal flow filtration

Normal flow filtration, using depth filters, is routinely used to remove whole cells and cellular debris from pilot-scale cell culture broths (Charlton *et al.,* 2000). The technique is also often used downstream of centrifugation operations to remove small particles that failed to sediment in the centrifuge. During normal flow filtration the direction of flow of the harvested cell culture broth is perpendicular to that of the filter orientation, in contrast to tangential flow filtration. The deposition of a layer of filtered solids on the surface of the filter presents further resistance to cells in the process stream and prevents them passing through the membrane. As the filter cake builds up increasing pressure drops are experienced across the membrane and

eventually filtration must be stopped before the upper pressure limit of the equipment is reached. Positively charged filter units can be used, allowing the removal of particles whose size would otherwise permit their transmission through the filter pore. Such cationic filters also permit binding of contaminants such as nucleic acids, giving a more highly purified filtrate (Charlton *et al.*, 1999).

1.2.2.3. Tangential flow filtration

Tangential flow filtration which facilitates complete retention of solids provides an alternative to the combined use of centrifuges and normal flow filtration or normal flow filtration alone for the harvesting of cell culture vessels. During tangential flow filtration the direction of flow of the process stream is parallel to the orientation of the membrane, generating sufficient shear forces to prevent the deposition of a filter cake. Consequently greater volumes of cell culture broth can be filtered than in normal flow configurations without filter blockage. Harvesting of a 1250 L cell culture vessel at a flux rate of 27 L m^{-2} h^{-1}, over a three hour period, by tangential flow filtration has been described (van Reis *et al.*, 1991).

1.2.2.4. Expanded bed adsorption

Expanded bed adsorption provides an alternative harvesting strategy, allowing product capture, clarification and concentration in a single step. A bed of porous matrix particles, to which a product binding ligand is attached, is stably expanded in a column by pumping a buffer up through the bed. The flow rate is adjusted so that the expanded bed height is constant and the un-clarified cell culture broth is pumped

upwards through the bed under conditions allowing product-ligand binding. Cells and cell debris pass through the expanded bed in the spaces between the matrix particles, while product in the supernatant adsorbs to the ligand attached to the matrix. Once clarification and adsorption have occurred the expanded bed is settled and the product eluted by application of a buffer favouring product dissociation from the ligand. By eluting the product under settled bed conditions the elution volume is minimized and product concentration is achieved. A study comparing two different expanded bed adsorption processes for the combined clarification, capture, and concentration of a monoclonal antibody product has been reported (Blank *et al.*, 2001). An expanded bed adsorption process utilizing a negatively-charged ligand, capable of binding a positively-charged antibody, was found to be less effective at clearing impurities and product aggregates than traditional clarification and purification steps. This problem could be overcome the use of an affinity ligand and a different purification scheme; however, the more expensive affinity ligand was susceptible to damage from the harsh cleaning solutions required for expanded bed adsorption systems processing crude feed preparations. This led to a loss of adsorption performance over repeated cycles (Blank *et al.*, 2001).

1.2.3. Purification

According to FDA guidance (Zoon, 1997) purification schemes for monoclonal antibody products for human use should prevent the introduction of contaminants and eliminate impurities including animal proteins and materials, DNA, endotoxins, other pyrogens, culture medium components, compounds that may leach from chromatography columns and viruses Large-scale therapeutic antibody purification

processes usually incorporate three different chromatographic steps for contaminant removal and two different virus reduction steps. Virus reduction steps can usually be classified as virus inactivation or virus removal operations. Table 1.3 illustrates the purification sequences, post cell removal, employed for six marketed products.

	Herceptin	Rituxin	Campath™	Synagis	Remicade	Simulect
Affinity Chromatography	1	1	1		1	1
Virus Inactivation	2	2	2	3	2	2
Cation Exchange Chromatography	3	4	3	2	3	4
Anion Exchange Chromatography	4	3		1,5	5,6	3
Hydrophobic Interaction Chromatography	5					
Size Exclusion Chromatography			4	7		
Virus Clearance		5	5	4,6	4	5
Sterile Filtration	6	6	6	8	7	6

Table 1.3. Analysis of the order of unit operations employed during the purification of six different FDA-approved therapeutic monoclonal antibodies (Sommerfeld & Strube, 2005).

1.2.3.1. Chromatography

Table 1.3 demonstrates the current reliance of the bioprocessing industry on chromatographic separations for product purification. Chromatography separates solutes based upon their differing migratory speeds through a porous packed bed of matrix. Selective retardation of solutes, such as product or contaminants, can be achieved using matrices with characteristic surface chemistries. Chromatographic operations can typically be segregated into a number of distinct phases. Firstly, the column is equilibrated with buffer to ensure provision of homogeneous, non-eluting conditions within the column. Then, the column is loaded with the mixture of solutes to be separated. Finally, the column is washed with a buffer to remove those solutes that are least retarded by the column. Conditions within the column are then commonly changed by application of an elution buffer to reduce the affinity of the retarded solutes for the matrix, causing them to be eluted at the column outlet. The elution buffer can be applied in a step-wise fashion or by the gradual increase in its concentration to form a gradient. Although difficult to implement especially at the large-scale, gradient elution allows improved solute resolution. Finally, the column is regenerated using different buffers to strip residual solutes and re-equilibrated in preparation for the next batch.

1.2.3.1.1. Affinity chromatography

Affinity chromatography is frequently used when purifying monoclonal antibodies. The chromatographic matrix is derivatised with a molecule which binds a solute with high specificity under loading conditions. Two bacterial cell wall proteins have

evolved to promote pathogenesis when the bacteria invade the human host by binding the host's defending antibodies, primarily at the F_C region. These two bacterial proteins, Protein A and Protein G, can be isolated and attached to the inert support matrix to give a matrix with high antibody specificity. A single Protein A or Protein G chromatographic step can yield 90% pure antibody, explaining the popularity of the unit operation as demonstrated in Table 1.3. The remaining contaminants are present due to non-specific hydrophobic or ionic interactions with the matrix support. These interactions interfere with selectivity and can reduce column capacity by blocking antibody binding sites. Recombinant forms of both bacterial proteins are available in which non-essential sequences are removed leaving only the four antibody binding sites. Two particular problems associated with Protein A and G matrices are (i) their considerable cost, due to complex multi-step production methods (ii) and the leakage of bacterial protein ligand into the process stream requiring subsequent chromatographic removal. Such disadvantages have prompted some process operators to invest in cheaper, synthetic Protein A adsorbents with less potential for biological contamination (Newcombe *et al.*, 2005).

1.2.3.1.2. Ion-exchange chromatography

Ion-exchange chromatography separates contaminants from the product on the basis of the molecular charge of the solutes. The overall charge of macromolecules with multiple charged regions is determined by the pH of the solution. The pH of the solution at which the overall charge is neutral is called the p*I* of the molecule. At a pH lower than the p*I,* the molecule will have a net positive charge; the net charge is negative when the pH is higher than the p*I.* By manipulating buffer pH, successive

solute adsorption and desorption can be achieved, thus maximizing the separation. Elution of bound molecules is usually instigated by increasing the concentration of salts on the column until they have a higher affinity for the matrix than the solute of interest which is out-competed for binding sites, leading to net solute desorption.

Cation exchange matrices bind positively-charged molecules as they themselves are negatively-charged while anion exchange matrices which have a positive charge bind negatively-charged species. Anion exchange steps are often used as a second intermediate chromatographic step, following product capture by affinity chromatography. Positively-charged antibody molecules flow through the column unhindered, while negatively-charged contaminating molecules, such as nucleic acids from the cells in which the antibody was expressed and endotoxins from contaminating bacteria, are strongly retarded. These contaminant capture steps maximize column capacity, yield and productivity. Cationic exchange steps can be used as polishing steps for the removal of leached Protein A or as an alternative to methods such as size exclusion chromatography for the removal of product aggregates, which are often constrained by operating capacity and flow rate ranges.

1.2.3.1.3. Hydrophobic interaction chromatography

Hydrophobic interaction chromatography separates solutes on the basis of surface hydrophobicity and can be used to separate most proteins. Hydrophobic patches on the surface of the molecule bind to the hydrophobic matrix when in the presence of salt molecules. A reduction in the salt concentration leads to solute elution; and hence, product elution pools have low conductivities, thereby reducing buffer exchange requirements during product formulation.

1.2.3.1.4 Size exclusion chromatography

Size exclusion chromatography differs from the previously discussed chromatographic methods in that the matrix is not derivatized with a chemical ligand. Separation occurs on the basis of molecular size, with the matrix pore size controlling the separation. Large molecules are excluded to a greater extent than small molecules from the bulk of the column volume and thus, migrate rapidly through the column, eluting first. Smaller molecules access a greater proportion of the column volume and take longer to elute. As the degree of separation is a strong function of the column length, size exclusion columns are often much longer than other types of columns. Unlike affinity, ion-exchange and hydrophobic interaction chromatography, size exclusion processes do not require the various wash and elution phases. However, capacity is limited and the long thin columns, packed with porous, compressible matrices, must be operated at low flow rates, making the method most useful as a final polishing step to remove product fragments and aggregates.

1.2.3.2 Viral removal & inactivation

The International Conference for Harmonization (ICH) identifies two potential sources of viral contamination: those arising from the original cell line source, such as the master cell bank, and those introduced during production, such as the use of contaminated reagents, including animal serum components (ICH, 1998). The FDA recommends the incorporation of at least two robust orthogonal retrovirus removal steps into a purification protocol. Furthermore, demonstration of the ability of the

purification scheme to remove adventitious agents, including viruses, is required prior to Phase II/III clinical trials (Zoon, 1997). Viral inactivation steps are typically carried out using severe physico-chemical measures, such as acid, urea, detergent, heat or UV radiation treatment. Acid treatment is a convenient inactivation step after Protein A chromatography as elution is generally carried out at low pH. Methods such as these must be implemented with caution as they can impact negatively on product stability. Virus removal can be achieved using viral capture or flow-through chromatographic steps, the use of dead-end depth filters (20-40 nm pore size) or tangential-flow, ultrafiltration membranes with molecular cut-off points below 300 kilodaltons (Sommerfeld & Strube, 2005).

1.2.3.3 Ultrafiltration

Ultrafiltration is often required during the purification of therapeutic monoclonal antibodies in order to exchange the product into a different chromatography buffer by diafiltration, to concentrate the product or, as previously mentioned, for virus removal. Diafiltration can be used to purify the product by removing contaminants below the molecular weight cut-off of the membrane which can be in the range 30 – 500 KDa while the product is retained (Sommerfeld & Strube, 2005). The use of ultrafiltration as a high-resolution protein-protein fractionation method is attracting increasing interest as an alternative to chromatography (Filipe & Ghosh, 2005).

Formulation of the bulk purified antibody utilizes ultrafiltration to buffer exchange the product into the final antibody stabilizing excipient composition and concentrate the product prior to storage and vial filling for use. Size exclusion chromatography

can be used for formulation; however, as this method typically leads to a dilute eluted product it is impractical for the monoclonal antibodies formulation making ultrafiltration the method of choice for most manufacturers (van Reis & Zydney, 2001). Comparison of the two methods shows that ultrafiltration incurs lower material and labour costs, has a lower buffer consumption and requires less plant space and operating time (Kurnik *et al.*, 1995).

1.2.4 Characterization of therapeutic monoclonal antibodies

Ensuring product quality is of paramount importance when manufacturing any therapeutic agent. Complete physicochemical analysis of small molecule pharmaceuticals is a viable option due to their relatively simple structures, allowing product consistency to be monitored. In this manner, production batches of product can be easily compared with product used and proven to be safe in clinical trials.

Until recently, the complexity of biopharmaceuticals such as recombinant proteins, including monoclonal antibodies has meant that a complete physicochemical analysis of the product was not considered possible. Safety and efficacy were ensured by adopting the attitude that 'the manufacturing process defines the product'. In practice this meant that even minor changes to the manufacturing process could necessitate clinical studies to prove that no product change had occurred. Process scale-up required considerable process understanding and the manufacturer had to demonstrate rigorous process control within self-imposed limits.

Subsequent advances in analytical technology have changed the attitude of regulators to the extent that for a 'well-characterized biological' the process may no

longer define the product. Although this would seem to represent a significant change in regulatory policy, in order to ensure product safety manufacturers will need to (i) consider whether current analytical techniques adequately cover characteristics affecting function and potency and (ii) what degree of molecular structural change is permissible in a given product. This latter consideration would require a full understanding of the complex relationship between antibody structure and therapeutic function (Chirino & Mire-Sluis, 2004).

1.2.4.1. Sources of antibody heterogeneity

Antibody heterogeneity can occur due to variations in either carbohydrate side-chains or in the protein backbone. Carbohydrate side-chains are linked to a conserved asparagine residue in the CH2 region of the antibody. Figure 1.3 shows the typical structure of these oligosaccharide side-chains. This type of heterogeneity can arise due to changes in the manufacturing process eg. the fermentation conditions (Schmelzer & Miller, 2002). As the carbohydrate side-chains are an integral part of the F_c structure, variation in the side chains causes F_c structural heterogeneity which may, in turn, affect F_c-recepter interactions (Krapp *et al.*, 2003).

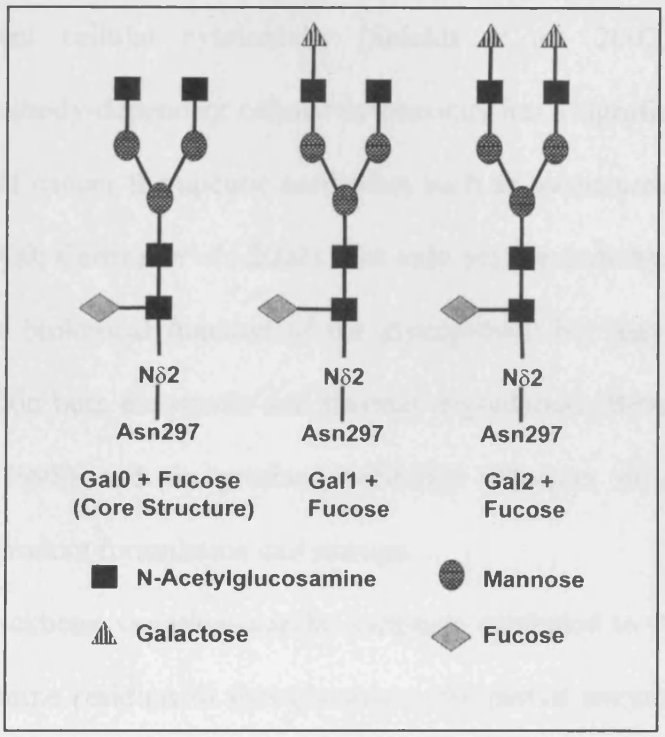

Figure 1.3. Schematic of IgG glycoforms. The core structure (*Gal0 + Fucose*) is normally composed of Asn^{297}-Nδ2-GlcNAc(fucose)-GlcNAc-mannose-(mannose-$GlcNAc)_2$, where GlcNAc is *N*-acetylglucosamine. Variation among individual glycoforms includes attachment of one (*Gal1 + Fucose*) or two (*Gal2 + Fucose*) terminal galactose units, attachment of sialic acid to the terminal galactose, and/or attachment of a third GlcNAc arm (bisecting GlcNAc). Reproduced from Shields *et al.*, 2002.

Terminal galactose levels correlate with complement-mediated cell killing *in vitro* (Tsuchiya *et al.*, 1989) while increased levels of core fucosylation decrease antibody-dependent cellular cytotoxicity (Shields *et al.*, 2002). Studies have suggested that antibody-dependent cellular cytotoxicity has a significant effect on the *in vivo* efficacy of cancer therapeutic antibodies such as trastuzumab and rituximab (Clynes *et al.*, 2000; Cartron *et al.*, 2002). Not only are the carbohydrate side chains important for the biological function of the glycoprotein but they have also been shown to impact on both enzymatic and thermal degradation (Bernard *et al.*, 1982; Runkel *et al.*, 1998) and on product solubility (Stowers *et al.*, 2002) with implications for product formulation and storage.

Protein backbone variations can be variously attributed to the cyclization of N-terminal glutamine residues to pyroglutamate, the partial enzymatic cleavage of C-terminal lysine residues by carboxypeptidases and unpaired cysteine residues. Degradative modifications, such as asparagine deamidation, aspartate isomerization and oxidation of methionine residues, can also be responsible for antibody heterogeneity (Harris *et al.*, 2004).

Shelf lives of 1.5-2 years are typically required in order to manage inventories of product. Product-degrading hydrolysis reactions that occur in liquid formulations of monoclonal antibody therapeutics can lead to undesirable protein heterogeneity and dose-to-dose variation. For example, isoaspartate formation of the aspartate 102 residue on trastuzumab (Herceptin) leads to a decrease in antigen-binding affinity (Chirino & Mire-Sluis, 2004). Pre-formulation studies are designed to help the developer of the therapeutic to determine solution conditions such as ionic strength and pH to minimize degradation which may affect drug efficacy and safety and to ensure product consistency. Several degradation routes may need to be

controlled to develop a marketable liquid formulation and the selected conditions may be sub-optimal for the control of any given degradation process (Kroon *et al.*, 1992).

Solid dosage forms, such as lyophilized protein, significantly reduce product degradation because the removal of water retards many degradative hydrolytic reactions such as aspartic acid residue isomerization (Harris *et al.*, 2004). During the lyophilization process the protein is frozen and dried by sublimation which subjects the protein to stresses that are typically controlled by the addition of excipients such as sugars. Such exipients control product aggregation which is the major degradative process for lyophilized proteins (Cleland *et al.*, 2001).

1.2.4.2. Analytical tests to assess heterogeneity

An extensive range of analytical techniques have become available for assessing the structure of protein therapeutics (Table 1.4). Mass spectroscopy in particular has become a valuable tool for detecting subtle changes in protein structure. Cell-based functional bioassays can be used to assess lot-to-lot comparability and have been used to detect differences between products not identified by physicochemical tests (Chirino & Mire-Sluis, 2004). Pharmacokinetic and pharmacodynamic studies in animal models are used to characterize bioavailability, clearance mechanisms and efficacy. Animal testing can provide structural/functional data allowing physicochemical product analysis to be of more use in comparability studies (Chirino & Mire-Sluis, 2004).

Form of Heterogeneity	Possible influencing factors	Analytical test
Amino acid sequence • Amino acid substitution • Deamidation • Oxidation	• Fermentation and purification process changes. • Cell line stability • Formulation • Sample handling	• Trypsin peptide mapping/mass spectrometry • Capillary electrophoresis • IEF • Ion-exchange-HPLC • Circular dichroism
Aggregation	• Formulation • High product concentrations • Sampling handling	• Analytical ultracentrifugation • Light scattering • Size-exclusion HPLC
Glycosylation	• Changes in fermentation process	• Capillary electrophoresis • Liquid chromatography/mass spectrometry • Electrospray ionization mass spectroscopy • Matrix-assisted laser desorption-time of flight mass spectroscopy
Truncation /fragmentation	• Fermentation changes • Manufacturing changes leading to protease/ peptidase contamination/ activation • Sample handling	• Mass spectroscopy • Size-exclusion chromatography • SDS-PAGE • IEF • Size exclusion HPLC
Disulphide rearrangement	• Fermentation changes • Sample handling	• Trypsin-peptide mapping / hydrophobic interaction

Table 1.4. Useful analytical tests to assess protein heterogeneity (adapted from Chirino & Mire-Sluis, 2004)

1.2.4.3. Controlling product quality

Regulatory authorities controlling the marketing of therapeutics demand manufacturing processes capable of repeatedly and reliably producing a finished product of a specified quality. Process validation is the act of demonstrating and documenting that a manufacturing process meets the requirements and covers all elements of a manufacturing process, from development through to final validation at the production scale.

The chosen manufacturing method must be defined, justified (based on consideration of the physical and chemical properties of the molecule) and then fully described. Data generated at different scales of operation throughout the development of the manufacturing process must verify the validity of the process employed. Laboratory-scale batches, at the research and early development stages, focus on the definition of critical product performance characteristics, thus facilitate the choice of the appropriate manufacturing process. Pilot-scale batches are used in the process development and optimization stages and should correspond to at least 10% of the future industrial-scale batch. The role of pilot batches is to ensure the smooth transition to the industrial scale product through development of a robust and reproducible manufacturing process. Pilot batches challenge the method proposed for routine production by identifying and evaluating the potential difficulties in and critical points of the manufacturing process; they also permit specification of apparatus and methods most appropriate to large-scale production. In this way pilot-scale batches provide a high level of assurance that the process will be feasible on an industrial scale without loss of product quality. Typically, full data for three

consecutive production-scale batches are required prior to the commencement of product marketing.

Proposed changes in the production process are controlled by clearly defined procedures. Data to demonstrate that the revised process will result in a product of the desired quality are required. Minor changes, which can be shown not to impact the quality of the product, are unlikely to require regulatory approval, however, significant changes to processes are typically subject to regulatory scrutiny and appropriate supporting data must be submitted by way of a variation to the marketing authorization.

1.3. Challenges of process specification

1.3.1 Centrifuge specification

Different approaches to the scale-down of industrial centrifuges have been adopted (Leung, 1998). Early attempts to address scale-down were based on reducing the capacity of the smallest scale disc stack centrifuges. For example, the separation capacity of a disc stack centrifuge has been reduced 10-fold by blanking off the majority of the separation discs and by carefully locating the remaining active discs within the stack in a position which best mimics overall centrifuge performance (Mannweiler & Hoare, 1992). In this fashion, a ten-fold reduction in the flow rate required to characterize centrifuge performance was achieved; this approach was successfully demonstrated for materials both sensitive and insensitive to shear effects in the feed zone. However, large feed volumes are still required to fill the centrifuge bowl. A series of interlocking inserts has been used to reduce the separation area by

76%, while also giving a 70% reduction in bowl volume, thereby reducing to 30% the volume and flow rate of process material required for characterization of the centrifuge recovery stage (Maybury *et al.*, 1998). Methods for using a bench-top centrifuge in order to mimic the recovery performance of industrial-scale centrifuges have also been described. For example, the recovery of polyvinyl acetate particles was well predicted by the bench-top centrifuge method; this was in contrast to the results for protein precipitates, where break-up of solids was found to reduce separator capacity 10-fold (Maybury *et al.*, 2000). A laboratory centrifuge was also used to mimic the recovery and dewatering performance of a multichamber-bowl centrifuge using a protein precipitate feed stream. Precipitate break-up in the continuous-flow centrifuge led to a reduction of approximately 50% in clarification performance (Boychyn *et al.*, 2001).

Computational fluid dynamics (CFD) has shown that significant energy dissipation occurs in the feed zone of tubular bowl (Jain *et al.*, 2005), multichamber-bowl, disc stack and CARR Powerfuge^{TM} centrifuges (Boychyn *et al.*, 2003). Maximum energy dissipation rates of 6 x 10^5 W kg^{-1} and 12 x 10^5 W kg^{-1} have been determined for a multichamber-bowl centrifuge, under flooded and non-flooded feed zone conditions, respectively. Both calculations were performed assuming a feed volumetric flow rate of 22 L hr^{-1} and a centrifuge bowl rotational speed of 167 rps. Similarly, a maximum value of 2 x 10^5 W kg^{-1} was determined for the disk stack centrifuge, operated at between 15 and 80 L hr^{-1} and at 165 rps; the maximum energy dissipation rate occurring in the feed zone of the CARR Powerfuge^{TM} was calculated to be 14 x 10^5 W kg^{-1}, at a flow rate of 20 L hr^{-1} and a bowl rotational speed of 255 rps (Boychyn *et al.*, 2004). A small, high-speed, rotating-disc device, designed to reproduce these energy dissipation rates in the centrifuge feed zone has been used to

shear milliliter quantities of process material prior to centrifugation in a laboratory test-tube centrifuge (Boychyn *et al.*, 2001. For shear sensitive materials, this shear treatment facilitated more accurate predictions of production-scale equipment than the use of the laboratory centrifuge alone (Boychyn *et al.*, 2001).

When developing a centrifugation process the objective is to achieve the target degree of clarification while maintaining high flow rates. To achieve this objective development scientists in pilot plants aim to predict the performance of the industrial-scale centrifuge, over an appropriate flow rate range, using the equivalent settling area or sigma theory for centrifuge scale-up. Sigma theory (Ambler 1959) is based on Stokes' law and can be used to describe the clarification process in a disc stack centrifuge. The settling velocity ($v_c(r)$) of a small, spherical particle in a laminar flow field is given by:

$$v_c(r) = \frac{d^2 \Delta\rho}{18\mu}\omega^2 r = \frac{v_g}{g}\omega^2 r \qquad \text{Equation 1.1}$$

where d is the particle diameter, $\Delta\rho$ is the density difference between the particle and the suspension, μ is the dynamic viscosity of the suspension, ω is the angular bowl velocity, r is the settling radius and v_g is the settling velocity of the particle under gravity. It is assumed that settling is unhindered and that laminar conditions apply, i.e. $Re(=v_c(r)\rho\, d/\mu) < 0.5$ where ρ is the liquid phase density.

The definition of the separation area, Σ, for the recovery of 100% of particles is (Ambler 1959):

$$\Sigma = \frac{V}{2 v_g t} = \frac{Q}{2 v_g} \qquad \text{Equation 1.2}$$

where V is the volume of material processed in time, t, for a batch centrifuge; Q is the flow rate for a continuous flow centrifuge.

Applying Stokes' law to a bottle centrifuge with swing-out rotor and integrating Equation 1.1 across the settling radius yields (Maybury *et al.*, 2000):

$$v_g t = \frac{\ln\left(\frac{2R_2}{R_1 + R_2}\right) g}{\omega^2} \qquad \text{Equation 1.3}$$

where t is the time during which the particle is being sedimented and R_1 and R_2 are the inner and outer radii, ie. the distances between the centre of rotation and the top of the liquid and the bottom of the tube, respectively. The group $v_g t$ indicates the equivalent distance settled in a gravity settling tank.

Rearranging and substituting Equation 1.2 into Equation 1.3 gives,

$$\Sigma_{lab} = \frac{V_{lab}\omega^2}{2g \ln\left(\frac{2R_2}{R_2 + R_1}\right)} \qquad \text{Equation 1.4}$$

The acceleration and deceleration phases of a centrifugation run can contribute significantly to settling when the spin time is short. If it is assumed that the rate of change in rotational speed is constant in each phase the following modified formula can be used (Maybury *et. al.* 2000):

$$\Sigma_{lab} = \frac{V_{lab}\omega^2(3 - 2x - 2y)}{6g \ln\left(\frac{2R_2}{R_2 + R_1}\right)} \qquad \text{Equation 1.5}$$

where, x and y are the fractional times required for acceleration and deceleration respectively.

In a disc stack centrifuge sedimentation of particles occurs in the channels between discs. Process suspension enters the separation channels at the outer radius and flows through the channels towards the centre of the disc stack. If a single channel is considered, a particle is considered to be separated when it reaches the upper boundary of the disc space. For a particle of gravity settling velocity, v_g,

following the most unfavorable particle trajectory, the hydrodynamic throughput capacity, Q, at which the particle will just be separated is given by considering the resultant particle motion, due to both hydrodynamic flow through the discs and to settling under the action of centrifugal force. Assuming the particle moves with the fluid, the velocity of the particle, *u(h)*, through the gap between the discs is given by,

$$u(h) = \frac{dQ^*/z}{dh.2\pi r} \qquad \text{Equation 1.6}$$

where Q^* is the limiting hydraulic throughput capacity for which the particles are just recovered, z is the number of discs and dQ^*/z is the flow rate through an area $dh.2\pi r$; r is the radius at any point during flow through the discs and h is the gap width between the discs. The particle velocity opposing this fluid flow is given by $v_c(r)sin\theta$ where $v_c(r)$ is defined in Equation 1.1; the particle velocity carrying the particles to the upper boundary of the disc space is $v_c(r)cos\theta$ where θ is the half-disc angle. The resultant particle trajectory with radius, r, is given by,

$$\frac{dr}{dh} = \frac{u(h)\tan\theta}{v_c(r)} \qquad \text{Equation 1.7}$$

Integration over the length of the disc gives the expression for the limiting hydraulic throughput capacity of the disc stack centrifuge (Mannweiler & Hoare, 1992):

$$Q^* = \frac{2}{3g}\pi z\omega^2 \cot\theta(r_2^3 - r_1^3)v_g = \Sigma_{ds} v_g \qquad \text{Equation 1.8}$$

where r_2 and r_1 are the outer and inner disc radii, respectively and Σ_{ds} is the so-called equivalent settling area of the disc stack centrifuge. The full derivation of the relationship, which is outside the scope of this thesis, is given by Mannweiler & Hoare (1992) and elsewhere.

By maintaining the ratio of flow rate to separation area, equivalent clarification efficiencies should be achieved between the development and industrial

scale centrifuges (Ambler, 1959). Sigma theory can be used to allow industrial scale equipment performance to be predicted using centrifuges of different sizes, geometries and modes of operation. Furthermore, a batch laboratory-scale centrifuge can be used to predict the clarification performance of a continuous, industrial disc-stack centrifuge, at different flow rates:

$$\frac{Q_{ds}}{C_{ds}\Sigma_{ds}} = \frac{V_{lab}}{t_{lab}C_{lab}\Sigma_{lab}} \qquad \text{Equation 1.9}$$

where Q_{ds} is flow rate through the disc-stack machine, Σ_{ds} and Σ_{lab} are equivalent separating areas for the disk stack centrifuge and laboratory centrifuge, respectively, t_{lab} is the residence time in the laboratory centrifuge, V_{lab} is the volume of material in the centrifuge tube and C_{ds} and C_{lab} are calibration factors to account for non-ideal flow conditions and are assumed to be independent of factors determining sedimentation performance. C_{lab} is considered as the reference case and, hence, is equal to 1. The correction factor for disc stack centrifuge, C_{ds}, is in the range 0.4 – 0.5 (Pinheiro & Cabral, 1993). C_{ds} is a compound group covering many aspects of centrifuge design. Values are based on actual system performance, primary under industrial conditions. For design purposes, a fixed value for C_{ds} is typically assumed; it must be understood that deviations from predicted performance of the order of ± 20% can be attributed to variations in C_{ds} (UCL pilot study experience).

1.3.2 Normal flow filter specification

Normal flow filters can be operated in two different modes. During constant-pressure filtration the pressure drop across the filter is maintained, leading to a reduction in

the filtration rate over time, as the build-up of a cake of filtered material increases resistance to flow. Alternatively, during constant-rate filtration, the flow rate is maintained by gradually increasing the cross-filter pressure drop. Of the two modes of operation, constant-rate filtration is more common. Scaling-up of filtration area from the pilot plant to manufacturing-scale is traditionally based upon maintaining an equivalent applied pressure profile, filter medium and ratio of filtrate volume to surface area. Filtration process development in the pilot plant involves identifying flow rates that allow the required level of productivity without causing excessive cross-filter pressure drops which could damage the filter and lead to equipment failure. Operating at high cross filter pressure drops maximizes productivity; however, it can lead to filter clogging as filtered solids can be driven into the filter pores and biological filter cakes are highly compressible.

Laboratory-scale filtration equipment is often used to select filter media, filter aids and pre-coats. Laboratory filters are often operated in batch mode, have simple geometries and utilize compressed air as the driving force for filtration. Constant pressure tests using such equipment can provide information about filtrate flux rates and filter cake dewatering at different pressures. Further, cake resistance and compressibility values can be determined from these experiments, allowing identification of a pressure profile which supports maintenance of a constant, specified filtration flux rate. However, such laboratory-scale equipment often poorly predicts large-scale filter performance, because they are operated in batch, rather than continuous mode, and because they are geometrically different. Superior predictions of the flux profile for a pilot filter have been achieved by modifying a traditional laboratory-scale Nutsche filter so that it could be operated semi-continuously and in a horizontal, rotating configuration, ensuring that the critical

parameter of filter cake structure resembled, as closely as possible, that of the large-scale system (Reynolds *et al.,* 2003). Automated, high-throughput evaluation of feed streams has been achieved using a custom-designed 8-24-well filter plate with a membrane area of 0.8 cm^2 per well (Jackson *et al.,* 2005). Different membrane types could be evaluated simultaneously and specific cake resistances determined for different feed suspensions.

1.3.3 Tangential flow filter specification

Tangential flow filtration has traditionally been scaled-up and -down by maintaining the filtrate volume-to-membrane surface area ratio. Membrane material, pore size and channel heights are also held constant while the number of channels is increased in order to provide additional membrane area. Development of tangential flow filtration processes involves the identification of the minimum trans-membrane pressure capable of achieving high permeate flux rates. Excessive trans-membrane pressures can lead to severe membrane fouling and reduced filter life-times. Increasing the linear velocity of the process fluid through the membrane channel increases the level of shear, thus reducing the protein gel-layer at the membrane wall and increasing flux rates. However, excessive shear rates can be damaging to protein products during ultrafiltration or to cells being removed by microfiltration and should be applied with caution.

Commercially available, small-scale tangential flow filters typically have shorter channel lengths than large-scale filters (Brose *et al.,* 1996); however, failure to maintain channel lengths can significantly impact on process parameters. The pressure drop between the filter inlet and outlet is a function of the channel length

and, in turn, determines the trans-membrane pressure drop which drives transport across the filter. Linear scaling of microporous membrane filtration systems, by maintaining constant channel length, has been described (van Reis *et al.,* 1991). Scaling of ultrafiltration membrane processes, by maintaining fluid dynamic parameters such as protein concentration at the membrane wall has also been achieved (van Reis *et al.,* 1997).

1.3.4 Chromatography process specifications

Scaling of chromatography columns is traditionally carried out by maintaining the process fluid linear velocity and the matrix bed height. If these two parameters are held constant, the residence time of fluid through the column will also be maintained. Scaling-up and-down is achieved by varying the column diameter. Process development involves identifying matrices and buffer conditions to maximize column capacity and yield. 'Scouting' experiments, using columns with reduced bed heights, have been used to select the most promising matrices and conditions and have the advantage of requiring significantly smaller volumes of feed material (Fahrner *et al.,* 1999). Predictions of large-scale column binding capacities and elution profiles, however, are typically determined at the large-scale bed height and operating linear flow rate. Shorter bed height columns typically have higher capacities per unit volume of matrix, as the concentration gradient between the bulk flow and the matrix is high at the entrance to the column. Further down in long bed height columns this gradient is reduced as bulk phase protein has bound higher up the column. The use of general rate models could aid the extrapolation of data from

columns with reduced bed heights to the large-scale, but are yet to be widely used in industry (Gu *et al.,* 1993).

Such models typically aim to predict phenomena occurring on the column itself; however, when using small columns with reduced bed heights, dispersion occuring in connecting tubing, dead volumes and detectors tends to predominate over column effects. In a study using a 1 mL chromatography column, the extra-column volume made up over 22 % of the total volume and extra-column broadening constituted over 60 % of the total broadening in the system (Kaltenbrunner *et al.,* 1997).

A further difficulty in the linear scale-up and -down of chromatography columns is that many commercially-available resins are highly porous to aid solute mass transfer kinetics; however, this also renders the material prone to compression and deformation. Obtaining heterogeneous matrix packing densities throughout columns is challenging (Shallikar *et al.,* 2003) and difficult to reproduce at varying scales. Narrow, laboratory-scale columns typically have less well-compressed beds, as the column wall supports the matrix. In wide diameter columns, increased levels of bed compression lead to increased cross-column pressure drops, which can prevent large-scale columns from being operated at the same linear flow rates as laboratory scale-columns. Models have been developed to predict the increased pressure drops and maximum operating flow rates of large-scale columns; however, the impact on performance characteristics such as column capacity and yield is less well understood (Stickel & Fotopoulos, 2001).

Chapter 2 – The use of ultra scale-down centrifugation for the prediction of normal and soft feed, industrial-scale, disc stack centrifuges, used for the clarification of mammalian cell culture broth at pilot scale.

2.1. Introduction

The development of primary recovery process for monoclonal antibody manufacturing processes occurs in the pilot plant. Typically, a flow rate excursion experiment is carried out in which a cell culture vessel is harvested at different flow rates through a pilot centrifuge and the degree of clarification achieved determined for each flow rate. Upper and lower flow rate limits for achievement of the target degree of clarification within a sensible time frame are determined. These limits are converted into upper and lower manufacturing flow rates by maintaining the flow rate-to-equivalent settling area ratio, according to sigma theory (Section 1.3.1). Such an experiment can require the generation of 500 L of cell culture broth and hence are frequently run only once, to minimize development costs. The consequence of having such a small body of data is that processes are frequently not fully optimized; the effects of harvesting at different time points during the fermentation are not fully understood. Thus centrifuge development is based on the 'worst-case scenario' in which harvesting occurs at the very latest time point, when cell viability is low, making cell separation the most difficult. The clarifying filter area, downstream of the centrifuge, is often oversized in order to avoid excessive cross filter pressures and associated equipment failure. Such contingency allowances add to product costs and dimishes the ability of the sponsor to recoup the cost of bringing the product to market.

Alternative techniques to centrifuge process development, making use of laboratory systems requiring significantly smaller volumes of process material, have been proposed (Section 1.3.1). Such methods offer not only the potential for improved process optimization but also allow process development studies to be undertaken earlier in the product lifecycle, thus reducing the 'time to market'.

This chapter describes the development of an ultra scale-down centrifugation technique for use with mammalian cell suspensions and its verification using two centrifuges operated, in the Lonza pilot plant, but equivalent in scale to systems used in the clarification of broth from 2000 L bioreactors in the manufacturing facility. One of the large-scale centrifuges had a standard design feed configuration; the other had a hermetic feed configuration. The use of hermetic feeds ensures feed-zone flooding and allows the energy dissipated as a result of process fluid acceleration towards the centrifuge rotational speed to occur in a greater fluid volume, thus reducing potential damage to fragile solids.

The use of the data generated by the ultra scale-down centrifuge technique for the development of a 'windows of operation' visualization tool is described. The window of operation method of presenting data allows process development engineers to rapidly identify operating conditions that will allow specified processing performance criteria to be met.

Finally, a product analysis study is included, to demonstrate product comparability between the large-scale and the ultra scale-down centrifuges. The study seeks to confirm that the equipment and processes used during the ultra scale-down technique do not negatively on impact product quality; thus, supernatant from the scale-down centrifuge can be used for development of subsequent downstream operations.

2.2. Materials and Methods

2.2.1. Experimental Overview

A sample of large-scale cell culture broth, collected at harvest point, was subjected to hydrodynamic forces in a rotating disc device in order to study shear susceptibility. The sheared cell suspension was subsequently transferred to a bench-top centrifuge in order to mimic the sedimentation occurring in the industrial scale equipment, at different flow rates, according to Equation 1.9. Broth clarification was studied at industrial scale, using disc stack centrifuges with standard and hermetic feed configurations.

2.2.2. Cell culture broth

Experiments were undertaken using cell culture broth, containing the GS-NS0 myeloma 6A1(100)3 expressing a chimeric B72.3 IgG4 antibody, raised against tissue from a metastatic breast carcinoma and recognizing a large tumour-associated glycoprotein termed TAG-72 (Johnson *et al.,* 1986). The broth was produced using a 500 L fed-batch, stirred-tank fermenter and protein-free media (Osman *et al.,* 2004). All studies were undertaken using broth from the late decline phase of growth when cell viability was below 10% and the concentration of solids was 1.5% v/v. An example of a growth profile and the harvest point is given in Figure 2.1

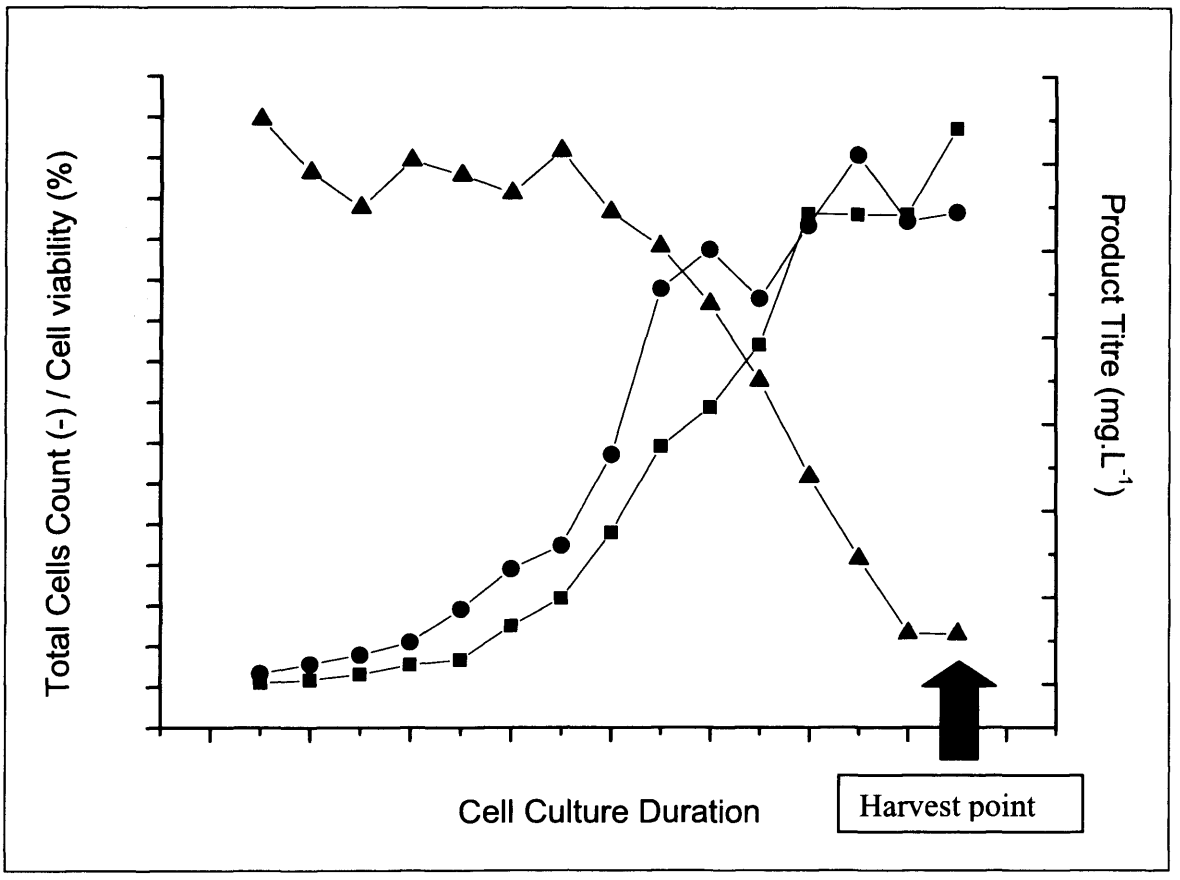

Figure 2.1. – Growth profile of cell culture material used in centrifugation experiments showing harvest point. The broth was produced using a 500 L fed-batch, stirred-tank fermenter and protein-free media. The cell line was the GS-NS0 myeloma 6A1(100)3 expressing a chimeric B72.3 antibody. Figure shows antibody titre (■) total cell count (●) and cell viability (▲).

2.2.3. Centrifuge equipment

Laboratory scale: Either a Beckman J2-MI laboratory centrifuge, fitted with the JS-13.1 swing-out rotor (Beckman Instruments (UK) Ltd, High Wycombe, UK) or an IEC Centra CL3 laboratory centrifuge, fitted with the '243' swing-out rotor (IEC International Equipment Company, Massachusetts, USA) was used to clarify cell suspension samples.

Industrial scale: Continuous-flow Alfa Laval BTPX 205 or Alfa Laval BTPX 305H disc stack centrifuges (Alfa Laval, Lund, Sweden) were used to process cell culture broths. The BTPX 205 is designed specifically for cell harvesting, broth clarification and cell debris separation at the pilot scale, is steam sterilizable and has cleaning-in-place capability (CIP). The BTPX 305H has many of the same features but is hermetically sealed and bottom-fed via a rotating feed line, in order to more gently accelerate the process stream to the speed of the bowl and to ensure the exclusion of air from the feed zone .

2.2.4. Centrifuge protocol

Laboratory scale: Oak Ridge Polycarbonate centrifuge tubes, 50 mL, filled with 40 mL of cell culture broth were used with the Beckman J2-M1 laboratory centrifuge. Polypropylene centrifuge tubes, 15 mL, filled with 10 mL of broth were used with the IEC Centra CL3 laboratory centrifuge. Following each centrifuge run the uppermost 15 mL or 5 mL of supernatant, respectively, was removed by pipette, taking care not to disrupt the sediment at the bottom of the tube. Samples were spun

for between 20 and 46 minutes at 4000 rpm in order to give $V/t\Sigma$ ratios of between 1.04 and 2.42 x 10^{-8} m s^{-1}.

Industrial scale: The mammalian cell culture broth was harvested using either an Alfa Laval BTPX205 or an Alfa Laval BTPX305H continuous disc stack centrifuge by over-pressurizing the vessel with compressed air. Flow rates were varied between 170 and 600 L hr^{-1}.

2.2.5. Rotating disc device

The rotating disc device consisted of a stainless steel chamber of diameter 50 mm and height 10 mm. The rotating elements were fabricated from a smooth aluminum alloy, coated with a thin layer of PTFE, mounted on a stainless steel shaft. The rotating disc had a diameter of 40 mm and a depth of 1 mm. The shaft of the element was extended through a PTFE bearing and was connected to a high speed DC motor powered from the mains, via a transformer. The transformer provided a range of speeds from 0 to 20,000 rpm measured using an optical probe.

The top and bottom of the stainless steel chamber are equipped with entrance and exit ports with fittings to allow the attachment of syringe fillers. The device was filled from the bottom allowing trapped air to escape though the top. Once the chamber was full, inlets and outlets were sealed prior to operation of the device. The assembly was mounted on a heavy metal base to reduce vibration during experiments.

Previous computational fluid dynamic analysis has allowed maximum dissipation rates to be determined for a variety of centrifuges with different feed-

zone configurations (Figure 2.2). Details of how the flow fields have been mapped have been provided elsewhere (Boychyn *et al.,* 2001). From this information and a similar analysis of maximum energy dissipation rates within the rotating-disc device at different rotating-disc speeds, the rotating-disc device can be operated at speeds that will subject shear-sensitive process material within the device to similar levels of energy dissipation as it would experience in the feed-zone of the centrifuge.

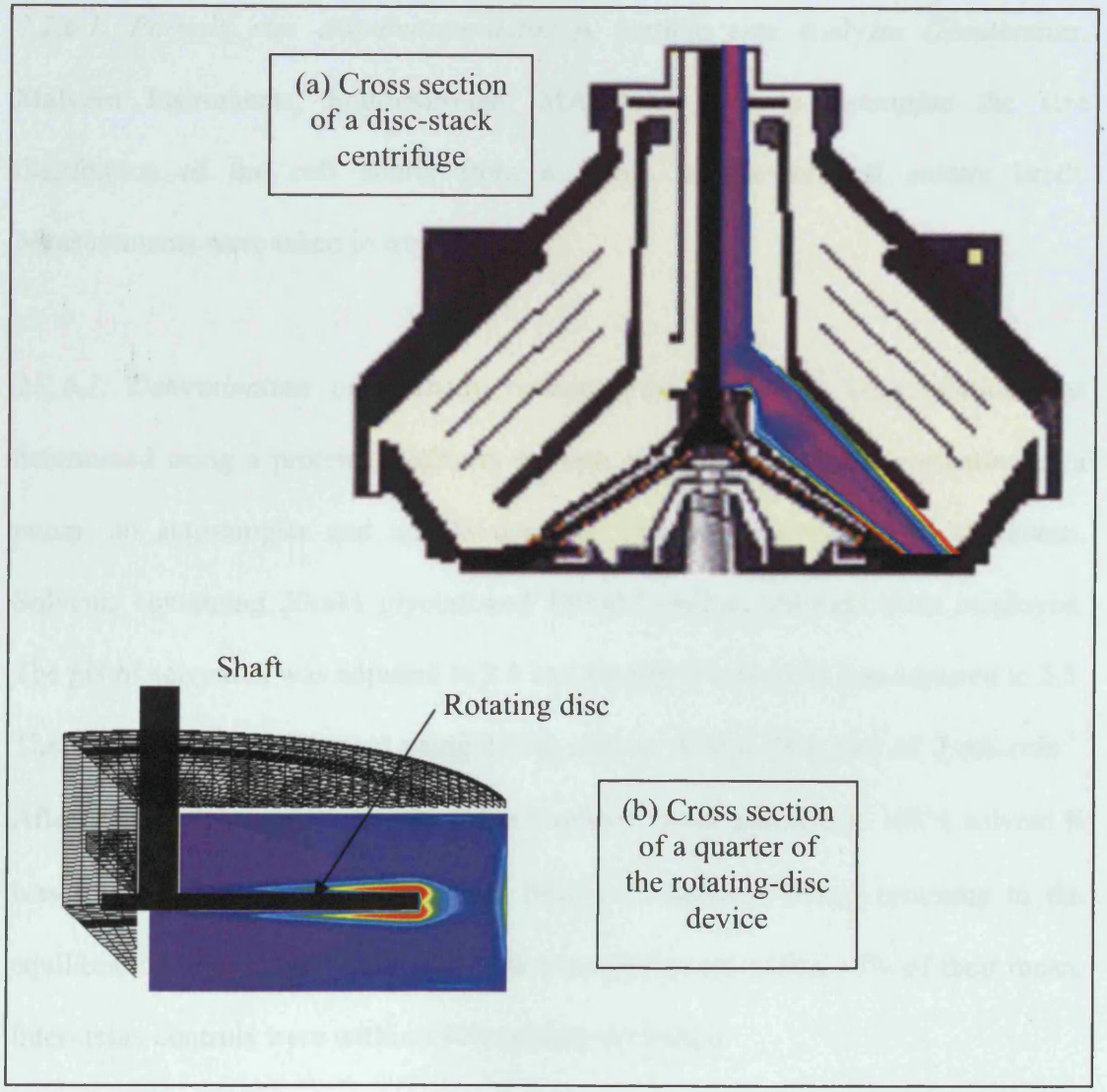

Figure 2.2. Computation Fluid Dynamic (CFD) analysis of the (a) feed zone of a disc-stack centrifuge and (b) the rotating disc device. The different colours represent different energy dissipations and together the analyses show that energy dissipation rates in the rotating-disc device can be generated which are comparable to those in the feed zone of the centrifuge (Boychyn *et al.*, 2001).

2.6.6. Analysis

2.2.6.1. Particle size distribution data: A particle size analyzer (Mastersizer, Malvern Instruments, Southborough, MA) was used to determine the size distribution of the cell debris from a 5 mL sample of cell culture broth. Measurements were taken in triplicate.

2.2.6.2. Determination of antibody concentration: Antibody concentration was determined using a protein A affinity column and a HPLC system consisting of a pump, an autosampler and an UV-detector. Effluent was monitored at 280nm. Solvents containing 50mM glycine and 150mM sodium chloride were employed. The pH of solvent A was adjusted to 8.0 and the pH of solvent B was adjusted to 2.5. The column was equilibrated using 100% solvent A at a flow rate of 2 $mL.min^{-1}$. After 200 μL of sample was injected, a 1-minute linear gradient to 100% solvent B was run and held at that point for a further 35 minutes before returning to the equilibration conditions. Replicates of test samples were within ±5% of their mean. Inter-assay controls were within ±10% of their set values.

2.2.6.3. Protein assay: The soluble protein concentration of feed and supernatant streams was measured by the method of Coomassie (Bradford,1976). The assay uses Coomassie brilliant blue (G250), which when in protonated form, is pale orange/red in colour. Proteins bind strongly to the dye forming both ionic and hydrophobic interactions that suppress protonation and result in a colour change to blue. A calibration curve was generated from standards of bovine serum albumin (BSA), 0-1500 μg/ml. The response was linear at protein concentrations between 0 – 1500 μg/mL (Figure 2.3). Samples were diluted into this range, using PBS. Diluted sample

was added to neat reagent in the volumetric ratio of 1:30 and the shift in optical density was monitored by a spectrophotometer, at 595 nm, after 5 minutes.

2.2.6.4. DNA assays: DNA quantification was carried out using a 2100 Bioanalyser (Agilent Technologies, Palo Alto, CA) system and a DNA 12000bp assay kit (Agilent Technologies, Palo Alto, CA). The bioanalyser sizes and quantifies the DNA in 12 samples simultaneously within the confines of a disposable microchip by comparison with a kit-supplied molecular weight ladder run on the same microchip. The microchip consists of a series of interconnecting micro-channels fabricated, in the glass, which are filled with a gel-dye matrix. DNA fragments are separated according to their size by means of molecular sieving in the gel matrix and are detected by laser-induced fluorescence. Associated software can quantify the DNA in a sample on the basis of the area below the peaks on the sample electropherogram.

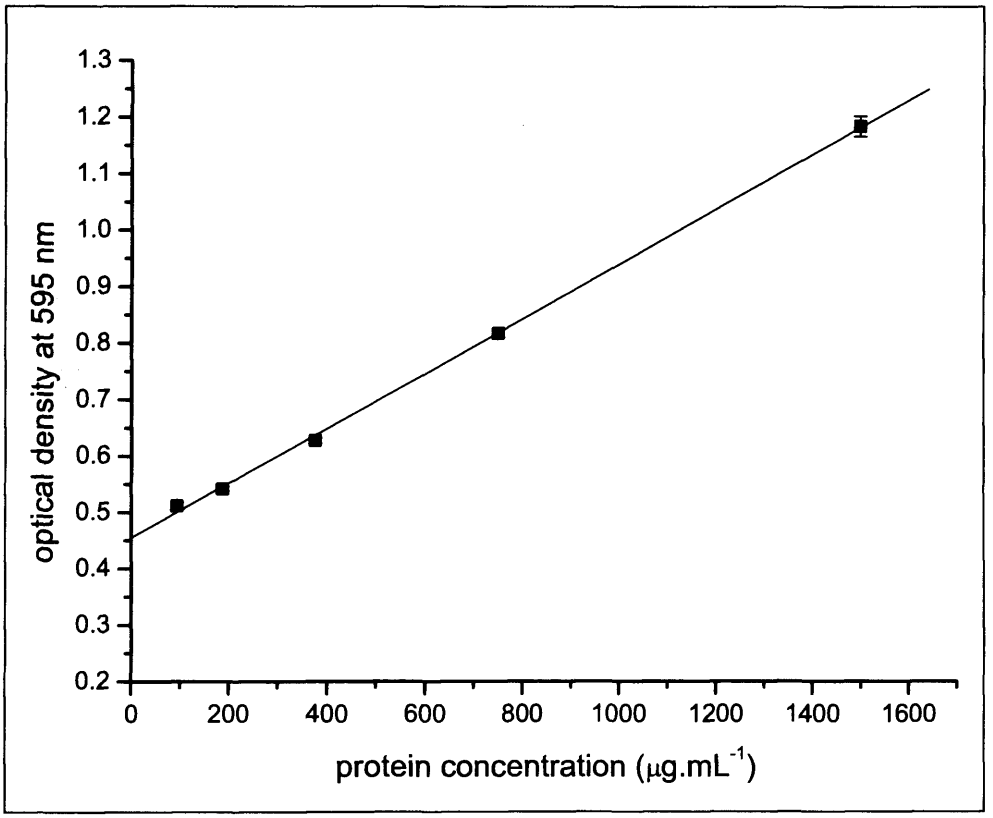

Figure 2.3. Standard curve used for determining protein concentrations by the Coomassie method. Data points are the means for three replicate measurement and error bars are standard deviation.

The microchips were prepared as recommended by the manufacturer, with minor modifications, using crude supernatant samples. 400 µl of DNA gel matrix was mixed with 20 µl of DNA dye concentrate and spin filtered at 3000 rpm for 10 minutes. The gel-dye mix was then loaded onto a new DNA chip. During this time the gel-dye mix was protected from the light. 5µl of DNA marker was added to the ladder well and all sample wells. 1µl of sample was added to each of the sample wells and 1µl of DNA ladder was added to the ladder well. The DNA sample chip was vortexed for 60 s before being inserted into the receptacle; the run commenced within 300 s of vortexing. The electropherograms of the ladder well and samples were checked to ensure all peaks were present and well-resolved, that the ladder baseline was flat and that marker readings were over 20 fluorescence units higher than baseline readings.

2.2.6.5 Percentage solids remaining in supernatant: Centrifuge performance was evaluated in terms of the percentage solids remaining in the supernatant, S, as follows:

$$S(\%) = \left(\frac{OD_s - OD_o}{OD_f - OD_o} \right) \times 100 \qquad \text{Equation 2.1}$$

where all OD values are measured at 550 nm wavelength; OD_o refers to the supernatant obtained after extended centrifugation (V = 5 mL, t = 5520 s, N = 66.7 rps, IEC centrifuge, giving $V/t.\Sigma = 5.2 \times 10^{-9}$ ms^{-1}); OD_s refers to the supernatant obtained in the centrifugation test procedure; OD_f to the feed stream prior to centrifugation.

2.2.6.6 Antibody comparability study: 40 mL samples of clarified cell culture broth and supernatant from the ultra scale-down centrifuge and industrial centrifuge were purified using 20mL disposable columns packed with rmp Protein A Sepharose FF matrix (Amersham Bioscience, Uppsala Sweden). The columns were packed and operated under gravity. Antibody-containing fractions were pooled and dialysed against phosphate-buffered saline before being concentrated using a spin ultrafiltration unit (Millipore, Billerica, MA).

Sample product integrity was analyzed using the 2100 Bioanalyzer (Lab on a chip) and a Protein 200 Plus Assay Kit (Agilent Technologies, Palo Alto, CA). The protein chip uses the same microfluidics technology as the DNA chip previously described (Section 2.2.6.4.). 4 μL of sample was added to 2 μL of sample buffer in the presence and absence of the reducing agent β-Mecaptoethanol and heated in boiling water for 60 s. Once the sample had cooled it was spun at 13,000 rpm for 15 s and the sample diluted with 84 μL of distilled water. 6 μL of diluted sample was applied to the protein chip wells, where proteins are separated by size via acrylamide sieving. The protein chip was loaded into the 2100 Bioanalyzer where, following the separation process, each protein was induced by fluorescent excitation at 633 nm.

10 μg samples of purified antibody were used to evaluate the protein pI; these were loaded onto an Isogel Precast Agarose IEF plate with pH range 3 – 10 (Cambrex, East Rutherford, NJ) and run according to the manufacturer's instructions with minor modifications. Isoelectric focusing standards with pIs between 3.5 and 9.5 (Pharmacia LKB, Piscataway, NJ) were run in order to determine the pI of product bands. The gel was developed using Coomassie Brilliant Blue R250 stain and the appropriate destaining solution and accepted on the criteria that all pI markers were clearly focused and in the expected pattern and pI range.

The presence of aggregates and antibody fragments was determined using a Zorbax Bioseries GF 250 column (9.4mm ID x 25cm) and an Agilent 1100 HPLC system (Agilent Technologies, Palo Alto, CA). The mobile phase was 0.2M Phosphate buffer, pH7.0 and 50 μL samples were injected at a protein concentration of 2mg/mL. The column was operated at 1mL/min at room temperature. Fragment peaks eluting at the tailing edge of monomeric antibody peak were integrated using the tangent skim method, while aggregates were integrated using the perpendicular drop method.

2.3. Results

2.3.1 Ultra scale-down centrifuge technique development and verification of clarification performance predictions

The mammalian cells and associated debris used in shearing trials were taken from are the late decline phase of growth when only a small proportion (less than 10%) of cells are viable; the particle size distribution is unimodal (Figure 2.4) Exposure of a sample of this feed suspension to a maximum energy dissipation rate of 2.04×10^6 W kg^{-1} for 20 s, in the high-speed rotating disc device, leads to solids break-up and results in decreased particle size (for example a reduction in modal size from 11 to 8 μm) and a bimodally distributed population. The consequence of this change on the efficiency with which solids can be removed by sedimentation, post-shear treatment, is described in the legend to Figure 2.4; a near doubling in the proportion of solids remaining in the supernatant following laboratory-scale centrifugation was observed (from 4.4 % to 7.5 % solids).

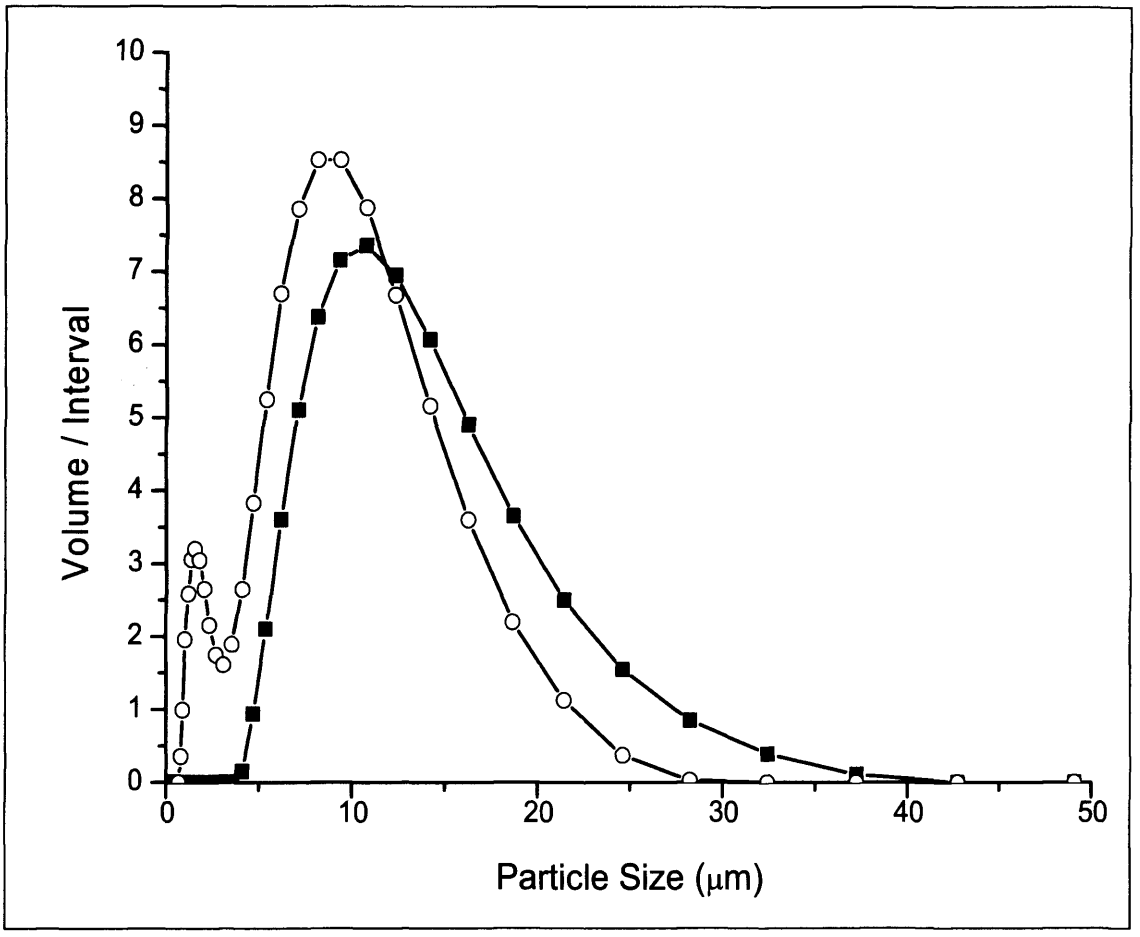

Figure 2.4. Particle size distributions for mammalian cell broth exposed to shear in the rotating-disc device: ■ non-sheared; O sheared at an equivalent energy dissipation rate of 2.04 x 10^6 W kg^{-1} for 30 s. The area under the graph between any two sizes is equivalent to the volume of particles in that size range.

Solids remaining in the supernatant after centrifugation (OD basis, see equation 2.1): non-sheared, 4.4% ± 0.1 sd based on four replicates; sheared, 7.5% ± 0.4 sd. (Samples were spun in the laboratory centrifuge under the following conditions, N = 71.7 rps, t = 1410 s, V = 40 mL, giving a V/t.Σ value of 2.5 x 10^{-8} m s^{-1}).

In practical terms the increased level of fine solids in the supernatant will reduce the filterability of the process stream due to blinding and could cause increased pressure drops across chromatography columns, due to fouling, if not eliminated prior to purification operations.

Figure 2.5 shows a visual (light microscopic) comparison between pre-shear NS0 mammalian cells (Figure 2.5 (a)) and a sample after exposure to a maximum energy dissipation rate of 3.67×10^5 W kg^{-1}, generated in the high-speed rotating disc device (Figure 2.5 (b)). Arrows 1 & 2 show damaged cells whose presence may be attributable to shear forces in the rotating disc device; while Arrow 3 shows an example of a debris particle with a diameter of less than 5 μm, corresponding to the smaller peak in the sheared sample particle size distribution (Figure 2.4).

A reduction in clarification performance is observed for samples exposed to shear for 5 s (Figure 2.6) No further significant reduction in clarification efficiency was observed when samples were exposed to shear for between 5 and 30 s. Some further evidence of additional attrition was observed at longer exposure times (up to 50 s). All subsequent rotating disc shear experiments were limited to exposure times of 20 s to allow reproducible operation to be more easily achieved and to avoid excessive break-up at longer times. This ensures sufficient time for exposure of the entire sample to the highest shear region at the tip of the disc for all the rotational speeds used (Boychyn *et al.,* 2001) based on the mixing time.

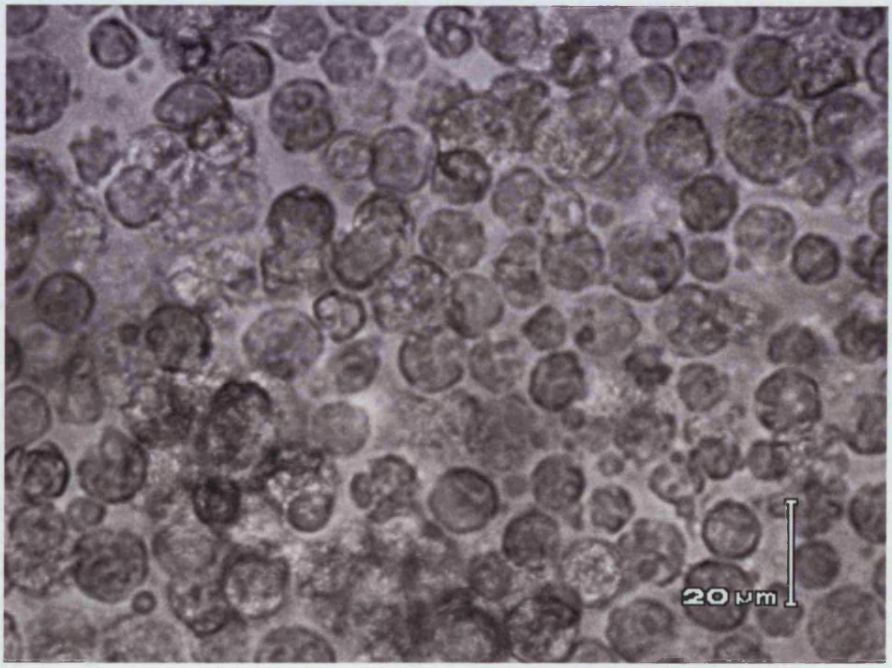

(a)

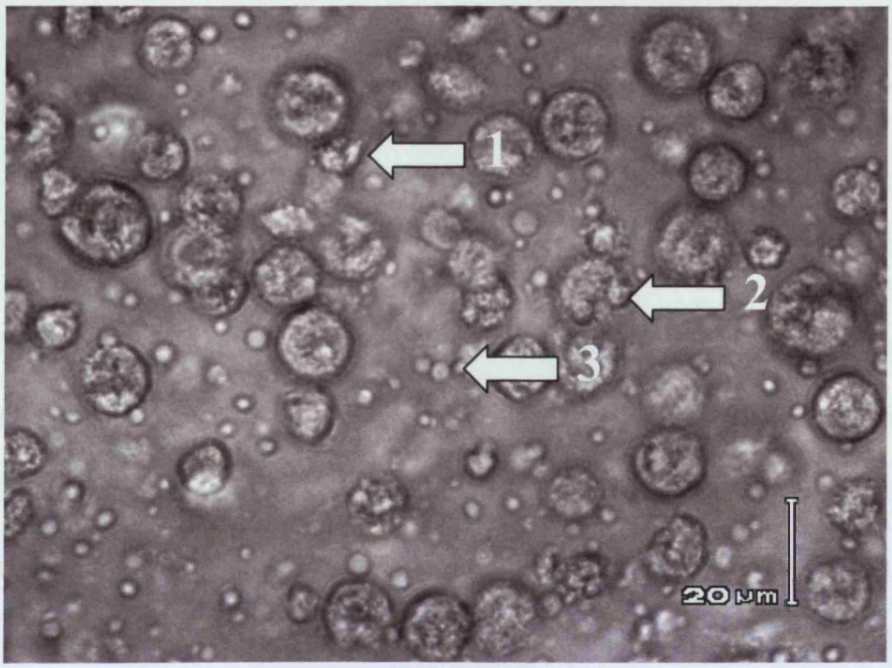

(b)

Figure 2.5 – Light micrographs of NS0 cells, (a) pre-shear and (b) after shearing in the rotating disc device at 3.67 x 10^5 W kg^{-1}.

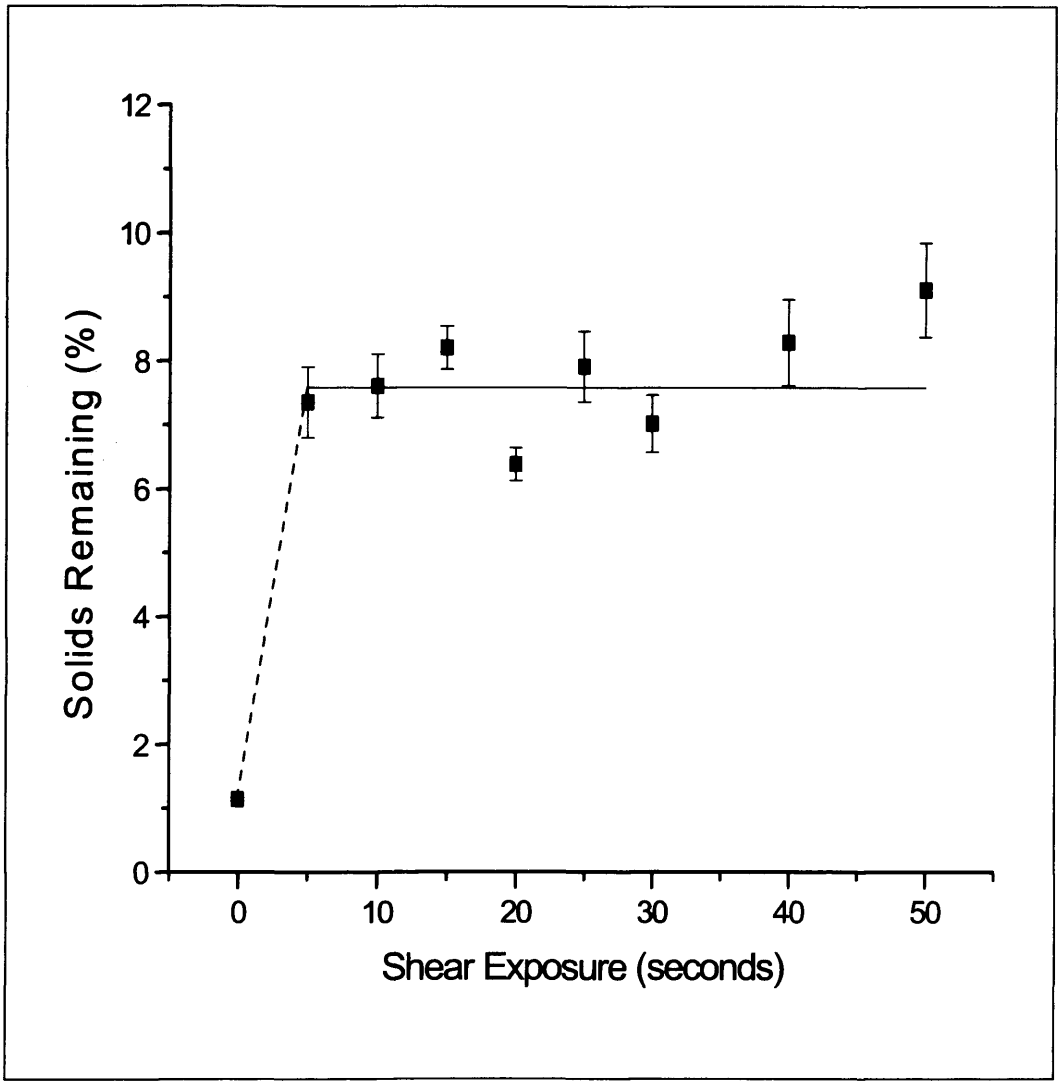

Figure 2.6. Dependence of the percentage of solids remaining in the supernatant following centrifugation on the duration of shear exposure prior to centrifugation. All particle damage appears to occur within the first 5 s of shear (χ^2 >99.5%, $t \geq 5$ s). Mammalian cell broth samples were exposed to an equivalent maximum energy dissipation rate of 3.67 x 10^5 W kg^{-1}. Sheared samples were spun in the laboratory centrifuge under the following conditions, N = 66.7 rps, t = 1200s, V = 10 mL giving a value of $V/t.\Sigma = 2.42 \times 10^{-8}$ m s^{-1}. Data points and error bars indicate mean values and propagated standard errors for triplicate measurements respectively.

The percentage of solids failing to sediment during centrifugation increases with the maximum energy dissipation rate during shearing (Figure 2.7). The result is attributed to higher rates of energy dissipation leading to the attrition of a greater proportion of the cell debris and a corresponding increase in the concentration of fines in the supernatant; such fines that cannot be sedimented under the centrifuge conditions tested. The extent of the reduction in clarification performance with increased shear stress diminishes as the number of susceptible cells decreases.

CFD analysis has allowed quantification of complex flow fields in an industrial disc stack centrifuge comparison with those found in the high-speed rotating disc device (Boychyn *et al.*, 2004). As a consequence, the operating rotating-disc device could be used to mimic the effect on shear-sensitive solids of conditions in the centrifuge feed zone.

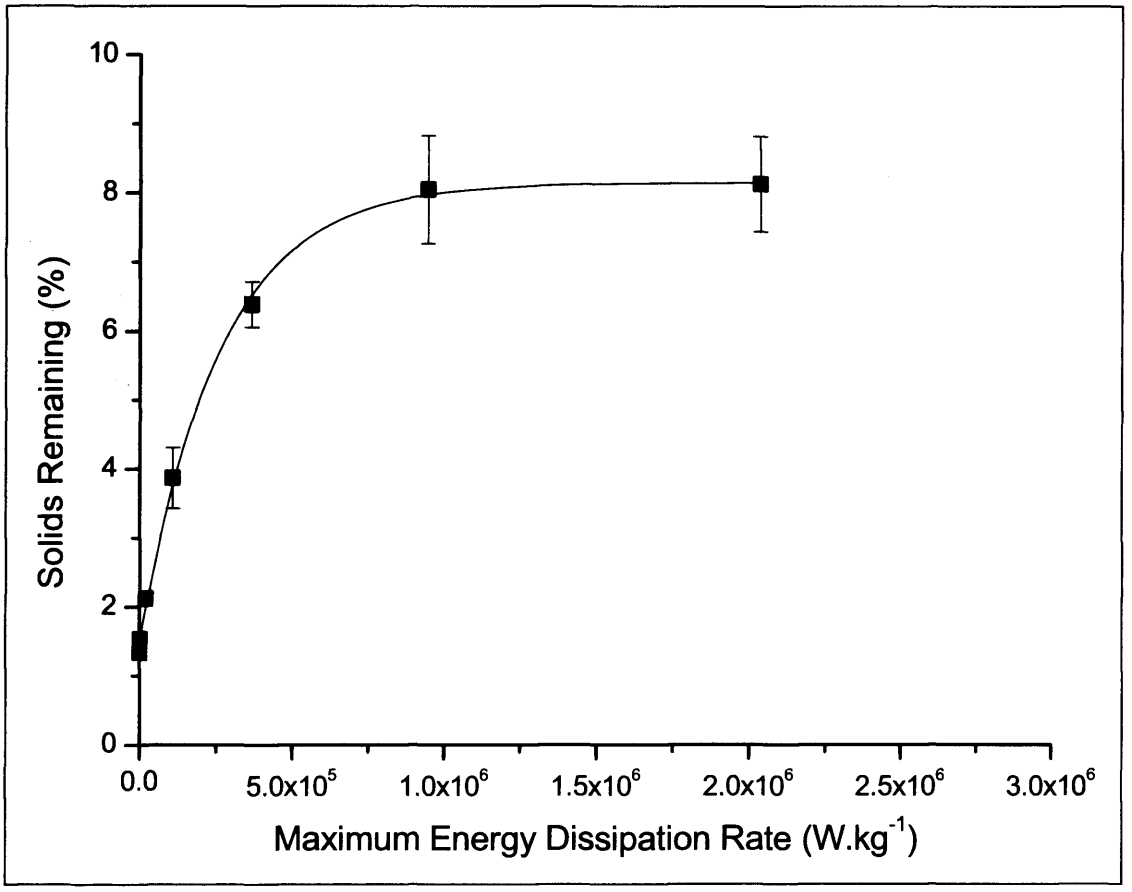

Figure 2.7. Dependence of the percentage of solids remaining in the supernatant following centrifugation on the maximum energy dissipation rate to which the mammalian cell broth sample is exposed prior to centrifugation. Mammalian cell broth samples were sheared for 20 s in the rotating disc device and centrifuged under the following conditions, N = 66.67 rps, t = 1200s, V = 10 mL, giving a value of $V/t.\Sigma = 2.42 \times 10^{-8}$ m/s. Data points indicate mean values; and error bars represent propagated standard errors for triplicate measurements. Least squares best fit given using exponential relationship.

Figure 2.8 shows that the percentage of solids remaining in the supernatant, following centrifugation, increases between 1.5 and 2.8 fold with the $V/t.\Sigma$ ratio, for unsheared samples and for samples exposed to maximum energy dissipation rates of 1.95×10^4 W kg^{-1} and 3.67×10^5 W kg^{-1}. Figure 2.8 shows that subjecting feed samples to increasing magnitudes of shear reduces the proportion of cell debris recovered over a range of centrifuge conditions as predicted in Figure 2.7. In each of these experiments the ratio $V/t\Sigma$ was adjusted by varying the time of centrifugation, t. The relationships are linear in all cases except for the samples exposed to the higher energy dissipation level at the low values of $V/t\Sigma$. A linear relationship in these probability-log plots indicates that the volume-based particle size distribution is Gaussian. Evidently the significance of the fine particles formed under high stress conditions and the resultant bimodal relationship becomes noticeable at the greater levels of centrifugation.

Clarification data from two industrial-scale disc-stack centrifuges of equivalent size but with different feed zone configurations, are shown in Figure 2.9 which compares the industrial data to predictions of industrial-scale performance based on ultra scale-down experiments made by the extrapolation of the least squares fits given in Figure 2.8. Industrial-scale data from the Alfa Laval BTPX 205 disc-stack centrifuge with a standard feed zone configuration correlates with laboratory-scale data predictions at all but the lowest feed flow rate for material pretreated at the highest shear rate. The leveling-off in solids removal at equivalent centrifuge conditions, at low $V/t\Sigma$ or Q/Σ values, is not observed. The leveling-off in solids removal observed for the laboratory centrifuge at the lowest $V/t\Sigma$ value studied after material exposure to high shear rates is not reproduced for the industrial-scale centrifuge. Effects such as

aggregation of the very fine debris in the static test tube centrifuge will lead to deviations, i.e. where the continuous flow nature of the disc stack prevents such effects occurring. Means of preventing such re-aggregation are currently under investigation. Otherwise good agreement is observed for the full range of extrapolated conditions for the low shear predictions and the recovery achieved in the Alfa Laval BTPX 305H with hermetic feed configuration. It is appropriate to note here the results of Lander *et al.* (2005), obtained using a CARR Powerfuge™ type centrifuge in which high feed zone stresses may be expected to lead to loss of clarification. In the paper, the inference is that no cell damage occurs. However, the low clarification efficiencies obtained are indicative of a high background of difficult-to-settle solids. In addition, the use of higher separation capabilities ($Q/\Sigma \approx 10^{-9}$ ms^{-1}) is likely to have been sufficient to mask effects of cell break up.

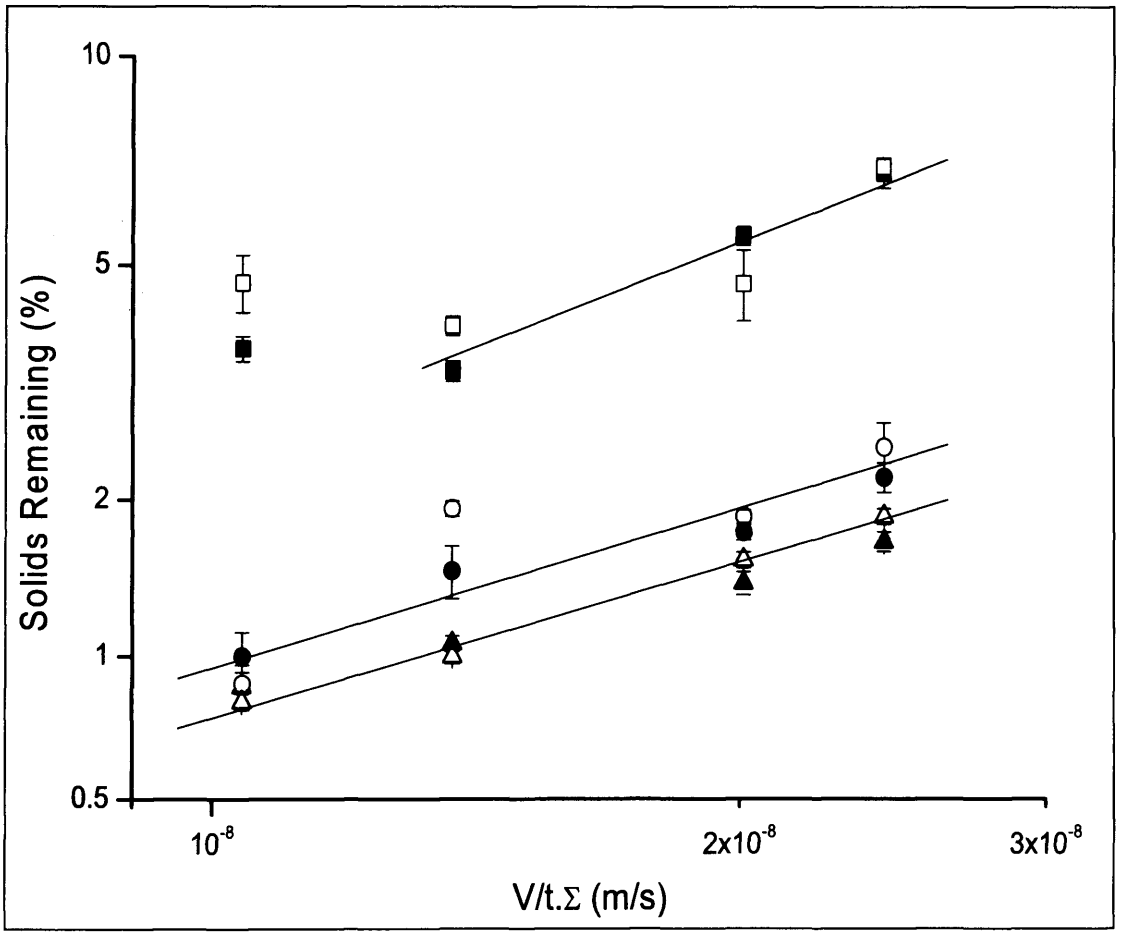

Figure 2.8. Relationship between the % solids remaining and the ratio of equivalent flow rate to centrifuge separation area, plotted on probability-logarithmic axes for ultra scale-down method. Mammalian cell broth exposed to the following shear conditions in the rotating disc-device: ▲, △, non-sheared; ●, ○ 1.95 x 10^4 W kg^{-1}; ■, □ 3.67 x 10^5 W kg^{-1}. Symbols represent means of two sets of replicate measurements, error bars represent propagated standard errors for triplicate measurements. Open and closed symbols represent two separately produced fermentation broths. Solid lines represent the line of best fit for each data set.

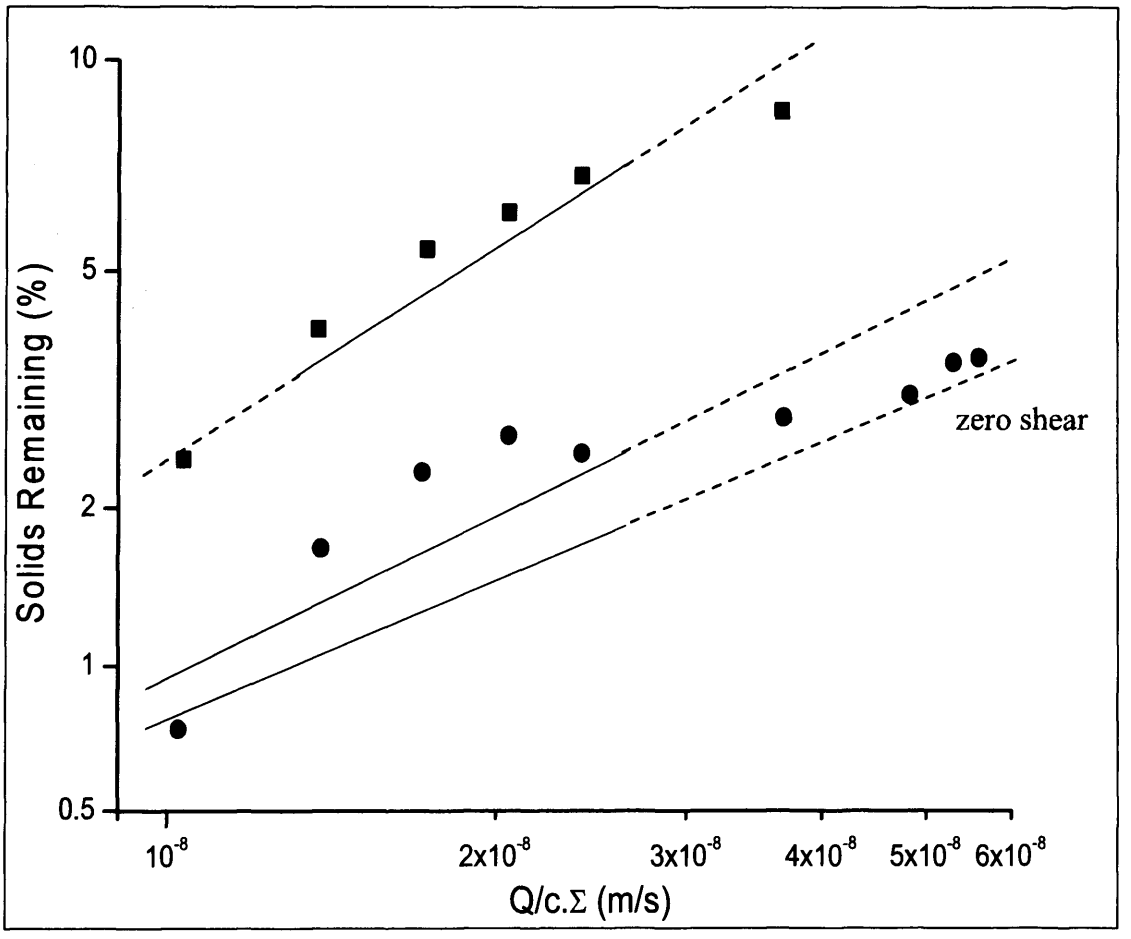

Figure 2.9. Relationship between the % solids remaining and the ratio of equivalent flow rate to centrifuge separation area, plotted on probability-logarithmic axes for industrial scale centrifugation:■, Alfa Laval BTPX 205; ●, Alfa Laval BTPX 305H. Solid lines represent ultra scale-down predictions (Figure 2.8), dashed lines represent extrapolations of these predictions. Zero shear ultra scale-down line also given for reference.

2.3.2 Centrifugation Windows of Operation

Data acquired from ultra scale-down experiments can be presented as in Figure 2.8; however, converting such information into a format permitting process design decisions can be difficult. It would be advantageous to use these data to define an "operating space" within which a design engineer could be confident that specified design parameters could be achieved. Figures 2.10(a) and 2.10(b) show how such operating windows can be generated for centrifuge process design. The x-axis of the operating window shows increasing equivalent settling area (Σ) while the y-axis shows increasing volumetric flow rate (Q). In Figure 2.10(a) the shaded region shows a possible operating space, confined between two lines corresponding to lower and upper flow rate constraints. Below the lower flow rate constraint the process fluid temperature will increase as heat generated by the friction within the centrifuge is dissipated into the slow moving process stream. This would be unacceptable from a processing perspective as it would be likely to lead to denaturation of the protein product. The upper flow rate constraint represents the maximum achievable flowrate. The limiting upper and lower flow rate values increase as the size of the centrifuge increases.

In contrast to Figure 2.10(a), the shaded region of Figure 2.10(b) shows a performance space. Within the shaded region, a solids carryover of 1.5% can be achieved. The clarification constraint that encloses the performance space has been determined using the ultra scale-down centrifuge data presented in Figure 2.8. The line of best fit from the data generated by operating the rotating disc device at an energy dissipation rate of 3.67×10^5 W kg^{-1} was extrapolated to a solids carryover value of 1.5% and the corresponding equivalent flow rate to equivalent settling area

($V/t.\Sigma$) ratio determined to be 6.8×10^{-9} $m.s^{-1}$ (Figure 2.11). Extrapolation of this line of best fit is questionable because of the failure of the data points at the equivalent flow rate to equivalent settling area ($V/t.\Sigma$) ratio of 1.04×10^{-8} to lie on the line. The reasons for this are discussed in Section 2.3.1 along with Figure 2.8. Data from the large-scale (Figure 2.9) suggest the relationship should continue to be linear and hence the linear extrapolation is used to here for the purposes of demonstrating the windows of operation approach. The clarification constraint illustrates this ratio over a range of equivalent settling areas and flow rates. It assumes that clarification performance obeys the sigma theory of centrifuge scaling which may not be true for a process stream containing shear sensitive solids, as larger centrifuges are likely to generate higher shear forces, cause greater solids break-up and hence clarify the process stream less well than sigma theory would project.

An operating window generated when the clarification performance constraint is superimposed on the operating constraints is given in Figure 2.10(c). The performance space fails to overlap with the operating space, showing clearly that the required level of performance cannot be achieved using a centrifuge with a feed zone in which this level of energy dissipation occurs. The design engineer can overcome this problem by sacrificing clarification performance in order to achieve a performance space that intersects with the operating space.

Figure 2.10(d) shows the outcome of increasing the performance constraint to a value of 3.5% solids carryover. The region of overlap shows the flow rates at which target clarification will be achieved for any given equivalent size. Relaxation of the performance constraints does not, however, come without cost. In this case, increasing the clarification limit means that more than twice the volume of solids are carried over from the centrifugation; these solids must be subsequently by (eg. depth

filtration) in order avoid solids fouling during the affinity capture chromatography step. Associated increases in the depth filtration area required to remove this particulate matter would substantially add to processing costs.

Impact of switching to a soft feed centrifuge with a feed zone that generates a maximum energy dissipation rate of 1.95×10^4 W kg^{-1}, as determined by the ultra scale-down centrifuge technique while maintaining the original performance constraint of 1.5 % solids carryover is shown in Figure 2.10(e). The resulting operating window shows that not only can the desired clarification performance be achieved by this technological shift but also that it can be achieved over a broader range of flow rates. This larger operating window indicates a more robust centrifugal clarification process.

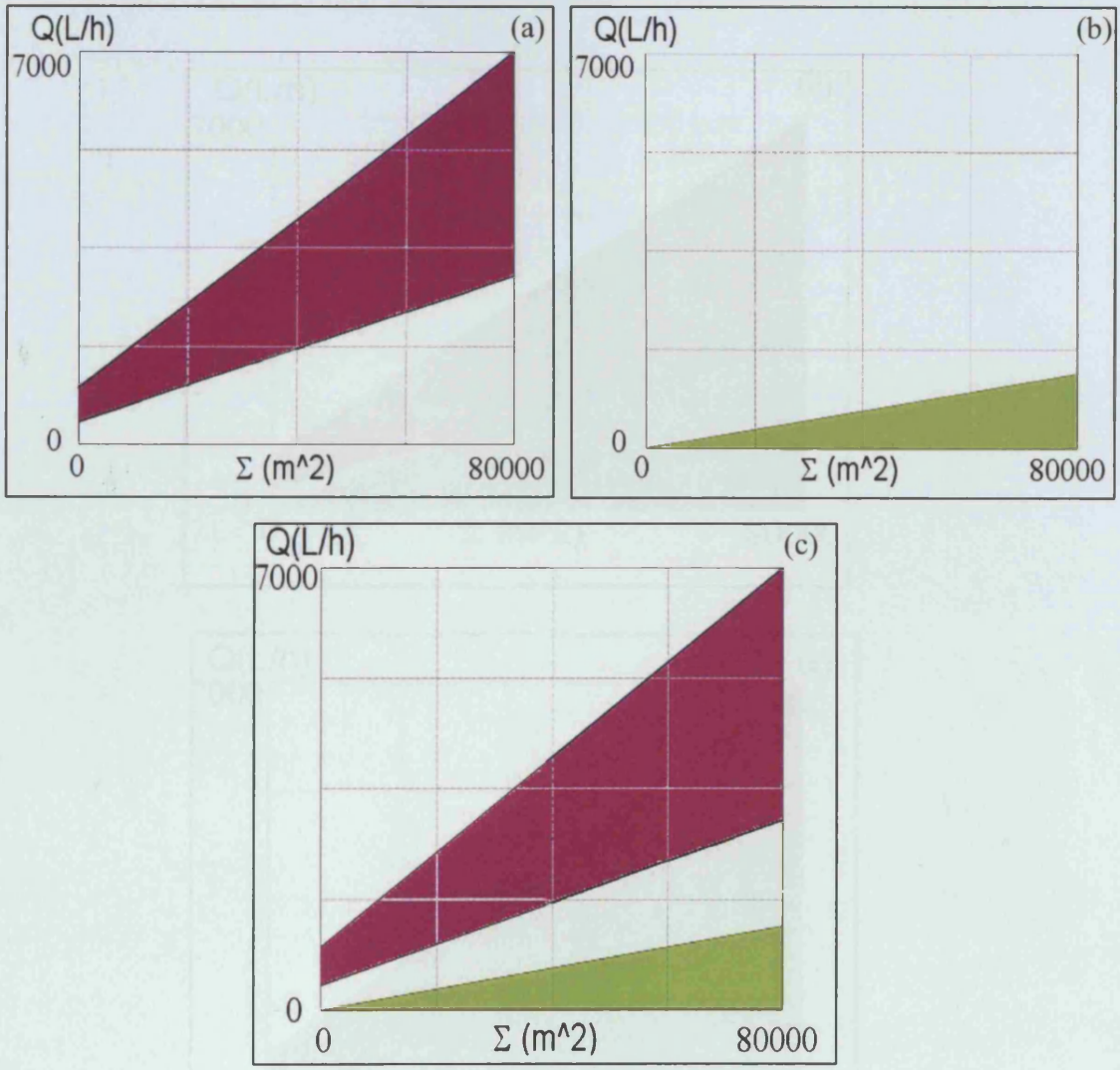

Figure 2.10 (a) showing how an operating window can be constructed. An (■) operating space is defined between two lines corresponding to lower and upper flow rate constraints. (b). an operating window. The coloured region (■) represents flow rate to equivalent settling area ratios allowing a maximum solids carryover of 1.5 % for a centrifuge with a feed zone maximum energy dissipation rate of 3.67 x 10^5 W kg^{-1}.(c) The figure shows the constructed operating window with the performance space superimposed over the top of the operating space. In this case the two spaces have failed to overlap, indicating that this centrifuge cannot deliver the desired level of clarification.

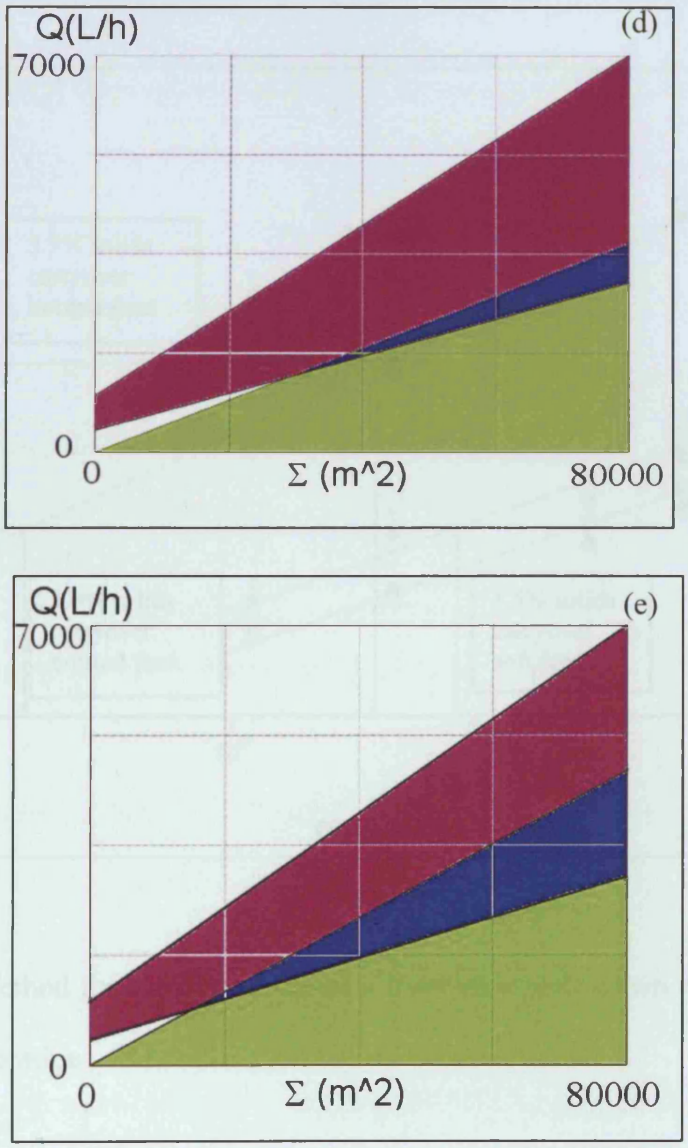

Figure 2.10 (cont.) (d) By adjusting the performance constraint to allow 3.5% solids carryover, overlapping performance and operating constraints produce an operating window (■). (e). Replacing the normal feed centrifuge with a soft feed centrifuge allows the original performance constraint of 1.5% solids carryover to be achieved and gives a larger operating window, demonstrating a more robust process.

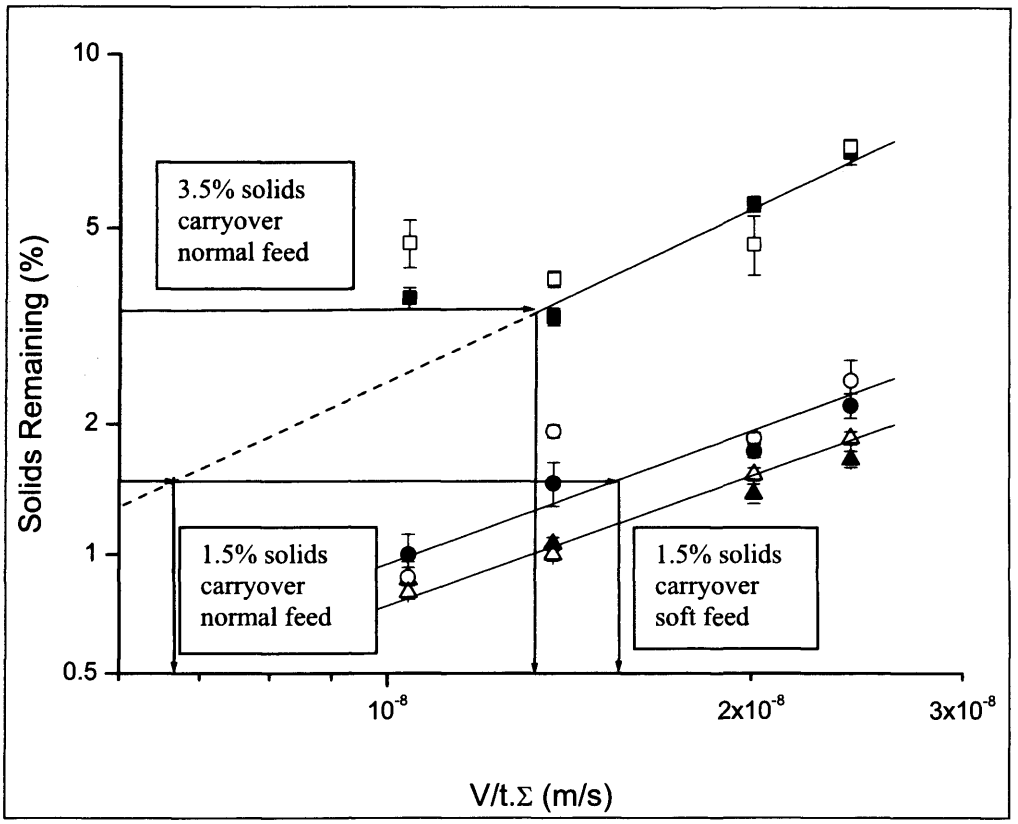

Figure 2.11. Method for converting the data from ultra scale-down experiments into windows of operation.

2.3.3 Product and process stream comparability study

The clarification results indicate that the performance of the industrial centrifuge can be predicted using the ultra scale-down centrifuge with appropriate pre-centrifugation shearing of the process suspension. It is, however, important to show that antibody levels and structure are comparable at both scales not least because it is desirable to use the supernatant from the ultra scale-down device to develop processes for subsequent unit operations such as ion-exchange and gel permeation chromatography steps.

Table 2.1 compares ultra scale-down predictions of normalized supernatant composition with industrial scale data. The levels of solids (debris) in the supernatant is seen to increase with increasing shear stress. An increase of 20% in the level of protein in the centrate is observed from the ultra scale-down centrifuge pre-sheared with a maximum energy dissipation rate of 3.67×10^5 W kg^{-1} which may indicate that at high levels of shear cell disruption and the release of subcellular proteins occurs. However, in general the level of DNA and product impurities do not appear to increase. The cell viability in the feed suspension at the point of harvest was low and it is likely that the majority of the cell contents had already been released so that the additional contaminant release caused by cell disruption in the centrifuge feed zones or in the feed zone mimics was relatively insignificant.

	USD 0 W kg^{-1}	USD 1.95×10^4 W kg^{-1}	Alfa Laval BTPX 305H	USD 3.67×10^5 W kg^{-1}	Alfa Laval BTPX 205
MAb	1	0.89	1.00	0.99	1.02
Protein	1	0.92	1.04	1.20	0.95
DNA	1	1.00	0.97	1.01	0.78
Debris	1	1.32	1.42	3.95	3.94

Table 2.1. Composition of supernatant obtained from industrial-scale and ultra scale-down (USD) centrifugation mimics. %Solids remaining measured at $V/t.\Sigma$ or $Q/c.\Sigma = 2.42 \times 10^{-8}$ m/s. Laboratory centrifuge conditions were as follows: N = 66.67 rps, t = 1200 s, V = 10 mL. Maximum energy dissipation rates generated during pre-shearing in the rotating disc device are given (W kg^{-1}).

A further concern is change in protein structure associated with exposure to air-liquid interfaces in well-mixed regions (Axelsson, 1999) While it is recognized that antibodies will have been exposed to such conditions within the cell culture vessel, the intensity of fluid mixing in the centrifuge feed zone is significantly different. Basic analysis of antibody structure is performed at Lonza Biologics by SDS-PAGE, iso-electric focusing and gel-permeation HPLC. The activity of products can be assessed by ELISA techniques or cell-based assays, however, these methods have not been developed for the cB72.3 antibody used in these experiments. Sophisticated product analysis techniques such as mass spectroscopy are available but are beyond the scope of this thesis.

Figure 2.12(a) shows the results of capillary-aided gel electrophoresis for the cB72.3 antibody, prior to centrifugation (lanes 1 & 6), following ultra scale-down centrifugation under three different shearing conditions (lanes 2, 3 and 4 & 7, 8 and 9) and following centrifugation in the Alfa Laval BTPX 205 (lanes 5 and 10). Under reducing conditions (lanes 1-5) the heavy and light chains have the expected molecular sizes of 62 and 25 kDa, respectively. Under non-reducing conditions, the assembled antibody has a molecular size again as expected of 159 kDa.

Very similar band patterns are obtained under reducing and non-reducing conditions for samples from fermentation broth, ultra scale-down centrifugation supernatant and industrial centrifuge supernatant, indicating that the hydrodynamic conditions experienced by the antibody during any of the conditions investigated did not affect the protein size by cleavage of peptide bonds.

IEF profiles of purified antibody from the supernatant of the ultra-scale centrifuge, under the three shearing conditions investigated are shown in Figure

2.12(b). The technique is used to demonstrate that no structural changes such as loss of N-terminal lysine residues which would result in an altered charge profile have occurred; capillary aided gel electrophoresis would be insufficiently sensitive to detect such changes. Samples of cell culture broth and supernatant from the Alfa Laval BTPX 205 centrifuge have been provided for reference. The *pI* profiles of each antibody sample are comparable, displaying four major bands in the range 6.55 to 7.35 indicating that no structural changes leading to altered charge profile have occurred during the ultra-scale or industrial scale clarification processes. This result is significant in that it bolsters the decision to use ultra scale-down centrifuge supernatant for the development of downstream chromatographic steps such as ion-exchange separations.

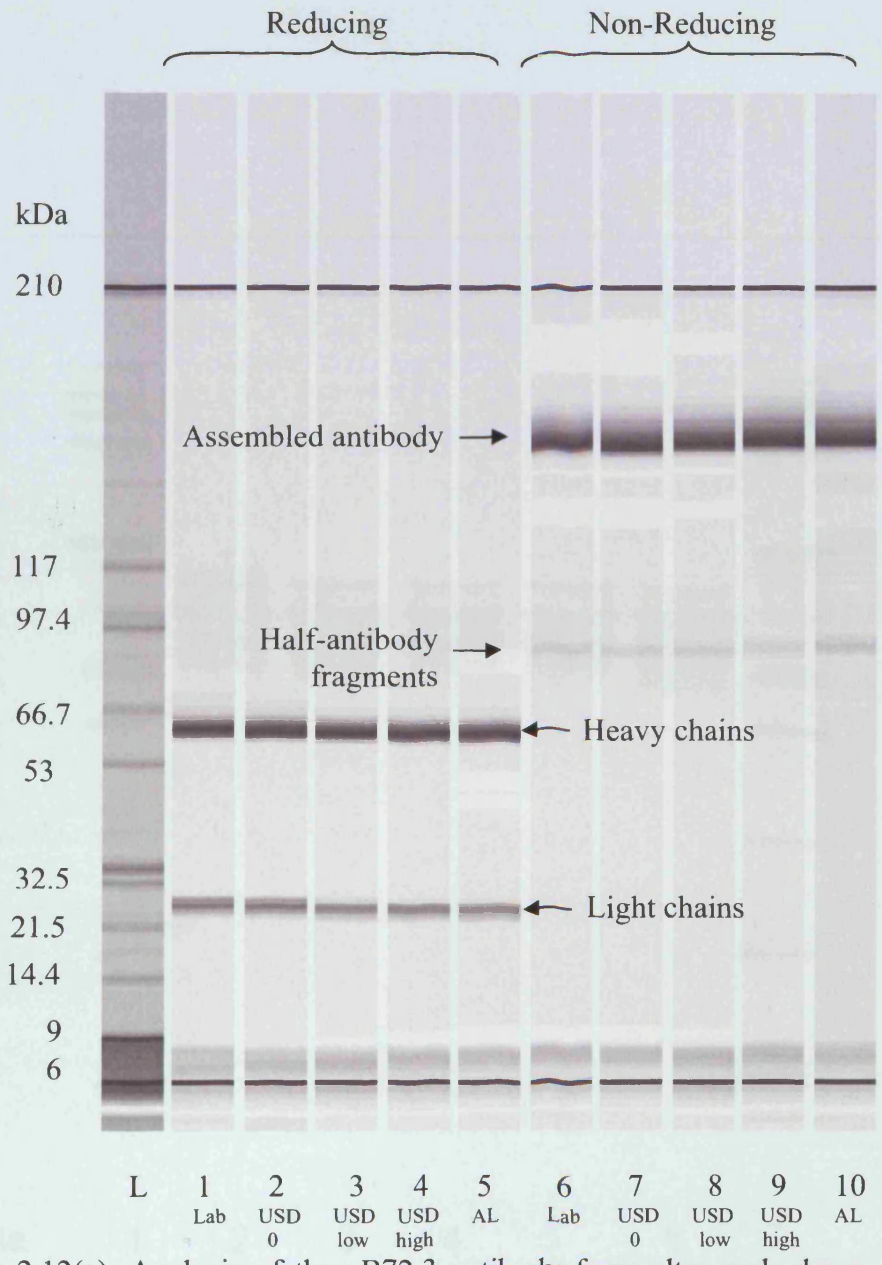

Figure 2.12(a). Analysis of the cB72.3 antibody from ultra scale-down and large-scale centrifuge supernatants. Samples analyzed by reducing (Lanes 1-5) and non-reducing (Lanes 6-10) capillary gel electrophoresis, after filtration and affinity (Protein A) separation. Reference samples prepared by laboratory centrifugation at 3200 g, 600 s (Lanes 1 & 6). Ultra scale-down centrifugation with feeds exposed to equivalent shear rates of zero shear (Lanes 2 & 7), 1.95×10^4 W kg^{-1} (Lanes 3 & 8), and 3.67×10^5 W kg^{-1} (Lanes 4 & 9). Alfa Laval BTPX205 supernatant (Lanes 5 & 10).Lane L represents molecular weight markers.

Figure 2.12(b). Samples analysed by isoelectric focusing after filtration and affinity (Protein A) separation. Reference sample prepared by laboratory centrifugation at 3200 g, 600 s (Lane 2). Ultra scale-down centrifugation with feed exposed to equivalent shear rates of zero shear (Lane 3), 1.95 x 10^4 W kg^{-1} (Lane 4), 3.67 x 10^5 W kg^{-1} (Lane 5). Alfa Laval BTPX205 supernatant (Lane 6). *pI* markers (Lanes 1 & 7)

The relative proportions of antibody aggregates, monomer and fragments in cell culture broth, ultra scale-down supernatant and industrial supernatant samples, as determined by gel-permeation HPLC, are shown in Figure 2.12(c). Both ultra scale-down and industrial samples show the same relative proportions (to within ±1%) of each species indicating that the product generated at all scales investigated is comparable, with respect to the levels of aggregated and cleaved product.

The gel-permeation HPLC results show that samples from the ultra scale-down centrifuge exposed to increasing levels of shear contain a greater proportion of fragments. These fragments, which can be observed in lanes 6-10 (non-reduced antibody) in Figure 2.12(a) correspond in size to half antibodies (87 kDa), consisting of one light and one heavy chain. These results suggest that hydrodynamic forces experienced by the antibody in the rotating-disc device may split the monomer. It is hypothesized that the fraction of the B72.3 antibody which lacks covalent interactions between the heavy chains and which is maintained as a four-chain structure via non-covalent bonds (Aalberse & Schuurman, 2002) may be susceptible to shear effects. Losses of recombinant proteins, specifically, molecular level changes in product properties, due to hydrodynamic conditions in processing equipment at the molecular level are the subject of further investigation (Qvist *et al.*, 2006). While the rotating disc device employed here provides very important insights into the centrifugation process, it is possible that further insight into subsequent, high resolution bioprocessing operations may be gained by detailed molecular analysis.

	Aggregates		Monomers		Fragments	
	Mean (%)	SD	**Mean (%)**	SD	**Mean (%)**	SD
Cell Culture Broth	**0.20**	0.002	**99.80**	0.003	**0.00**	0.000
USD Centrate exposed to 0 W kg^{-1}	**0.22**	0.003	**99.78**	0.003	**0.00**	0.000
USD Centrate exposed to 1.95 x 10^4 W kg^{-1}	**0.18**	0.001	**99.45**	0.003	**0.37**	0.003
USD Centrate exposed to 3.67 x 10^5 W kg^{-1}	**0.16**	0.002	**98.86**	0.007	**0.98**	0.005
Alfa Laval BTPX 205	**0.48**	0.002	**99.51**	0.003	**0.01**	0.001

Figure 2.12(c). Samples analyzed by gel permeation HPLC after filtration and affinity (Protein A) separation.

2.4 Conclusions

The use of data generated using the ultra scale-down centrifugation technique facilitates predictions of industrial-scale disc stack centrifuge clarification performance over a range of operating flow rates. The accuracy of these predictions is increased when the hydrodynamic forces in the feed zone of the industrial-scale centrifuge are mimicked using a high-speed rotating disc device. Windows of operation can be used, in conjunction with ultra scale-down methodologies, to allow rapid decisions to be made regarding process design. The ultra scale-down centrifuge has been shown to generate supernatant representative of that produced at the large scale. This material can be used for the study of downstream operations such as filtration and chromatography processes, in an effort to elucidate the impact of centrifuge operating variables on the complex interactions between centrifuges and purification equipment.

Chapter 3 – Verification of the ultra scale-down centrifugation technology by comparison of predictions with the performance of a manufacturing-scale, disc-stack centrifuge, used to harvest a 20,000 litre cell culture bioreactor.

3.1 Introduction

In the previous chapter the ultra scale-down technique was used to mimic the performance of normal and soft feed centrifuges with equivalent separating areas of 11,350 m^2. Centrifuges in the pilot plant were used to remove the Lonza Biologics NS0 cell line 6A1 (100)3 from cell culture broth produced in a 500 L fermentation in the Lonza facility at Slough, UK. This section describes a trial in which the ultra scale-down centrifugation technique was used to mimic the performance of an Alfa Laval BTAX 215 continuous-flow, disc-stack centrifuge with an equivalent separating area of 197,900 m^2 and a standard feed zone configuration, which is used in the manufacturing process for the harvesting of a 20,000 L cell culture reactor containing an undisclosed customer CHO cell line.

It was anticipated that this larger scale centrifuge would perform less well than the pilot centrifuge as the tip-velocity of critical structures within the feed zone, where initial contact and acceleration of the process stream occurs, would be relative orders of magnitude higher and hence would dissipate a greater amount of energy into the process fluid. In order to improve clarification performance at the large-scale, experiments were carried out at different bowl speeds, with a view to reducing the tip-speeds and shear rates to which cells and cell debris would be exposed. This study allowed the validation of the ultra scale-down technology at a larger scale and with a different cell line.

3.2 Materials and Methods

The experimental overview and calculations of solids remaining were as detailed in the previous chapter.

3.2.1. Cell Culture Broth: Experiments were carried out using cell culture broth containing a customer Chinese Hamster Ovary (CHO) cell line expressing a monoclonal antibody product. The broth was produced using a 20,000 L fed-batch, stirred-tank manufacturing fermenter. All centrifugation studies were undertaken using broth from the late decline phase of growth, 14 days after inoculation.

3.2.2. Rotating-disc device: The rotating-disc device was operated as detailed in the section 2.2.5 at maximum energy dissipation rates of 1.95×10^4, 1.08×10^5 and 3.67×10^5 W kg^{-1}

3.2.3. Laboratory-scale centrifugation: IEC Centra CL3 laboratory centrifuge with the '243' swing-out rotor (IEC International Equipment Company, Massachusetts, USA). Polypropylene centrifuge tubes, 15 mL, filled with 10 mL of broth were used. Following each centrifuge run the uppermost 5 mL of supernatant was removed by pipette, taking care not to disrupt the sediment at the bottom of the tube. Centrifugation conditions are detailed in section 3.3. Well-spun samples providing solid-free supernatant were prepared by centrifugation at 13 200 rpm for 15 minutes.

3.2.4. Industrial-scale centrifugation: The mammalian cell culture broth was harvested using an Alfa Laval BTAX 215 disc stack centrifuge (Alfa Laval, Lund,

Sweden) by over-pressurizing the vessel with compressed air. The centrifuge was variously run at bowl speeds of 5000, 5500 and 6000rpm and flow rates of 3300, 4800 and 6000 L/h respectively. Supernatant samples were taken once the centrate optical density had stabilized.

3.2.5. Measurement of remaining solids: As described in section 2.2.6.5 the proportion of solids remaining in the supernatant following centrifugation was determined by optical density measurements of feed, supernatant and well-spun samples, using a Shimadzu UV160U UV/Vis spectrophotometer at 550 nm, blanked with phosphate-buffered saline, pH 7.4.

3.3. Results

Figure 3.1 shows that, as the ratio of equivalent flow rate to settling area is increased (using the ultra scale-down technique), the proportion of solids remaining in the centrifuge supernatant increases, as the particles have less opportunity to sediment. This trend is consistent with data presented in Figure 2.8. Prior to centrifugation samples were exposed to four levels of energy dissipation rate in the rotating-disc device.

These results again demonstrate that as the magnitude of these hydrodynamic forces is increased, the proportion of solids failing to sediment increases. From previous results this observation is attributed to the general reduction in particle size and the build up of a small population of fine solids (particle size less than 5 μm) as shown in Figure 2.4.

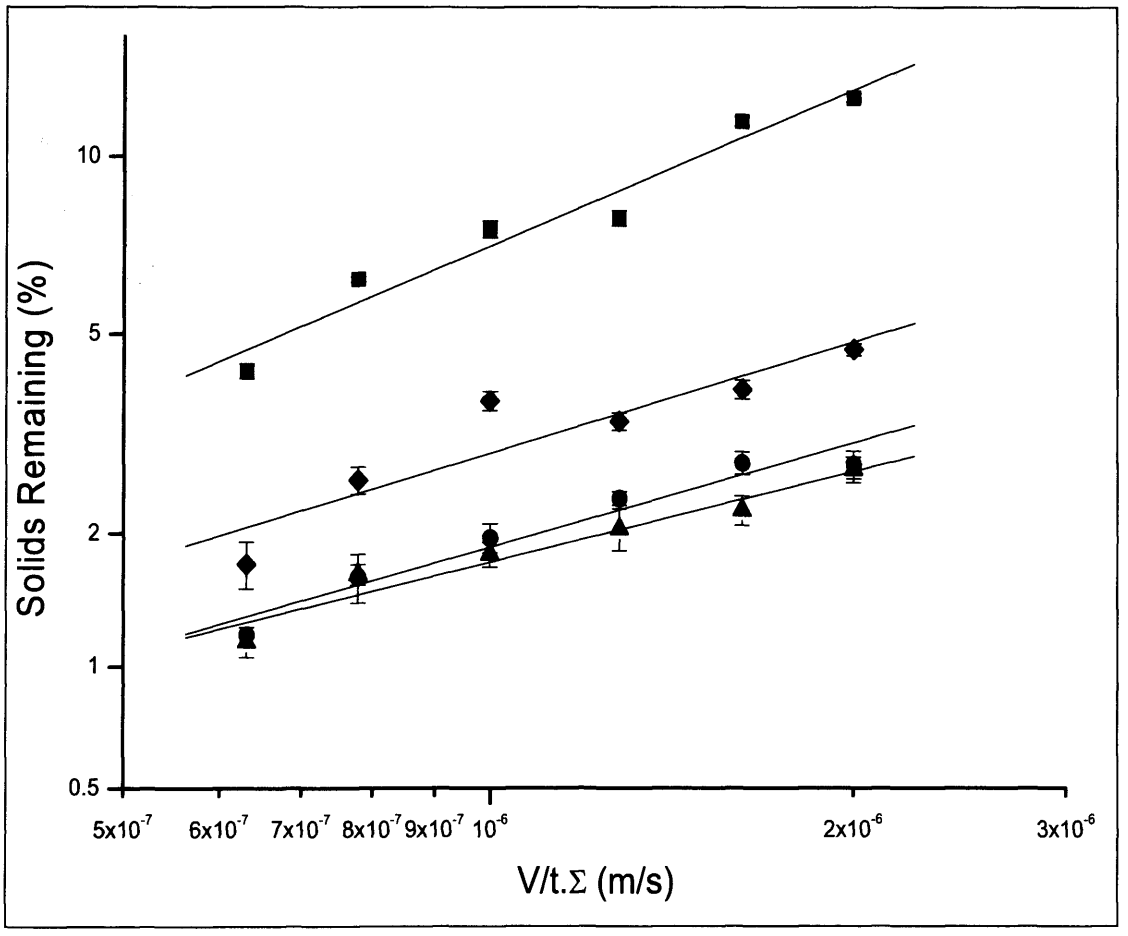

Figure 3.1. Relationship between the % solids remaining and the ratio of equivalent flow rate to centrifuge separation area, plotted on probability-logarithmic axes, for ultra scale-down method. Mammalian cell broth exposed to the following shear conditions in the rotating disc-device: ▲, non-sheared; ●, 1.95 x 10^4 W kg^{-1}; ◆ 1.08 x 10^5 W kg^{-1} ■, 3.67 x 10^5 W kg^{-1}. Symbols represent the means of two measurements and bars represent the range of measurements.

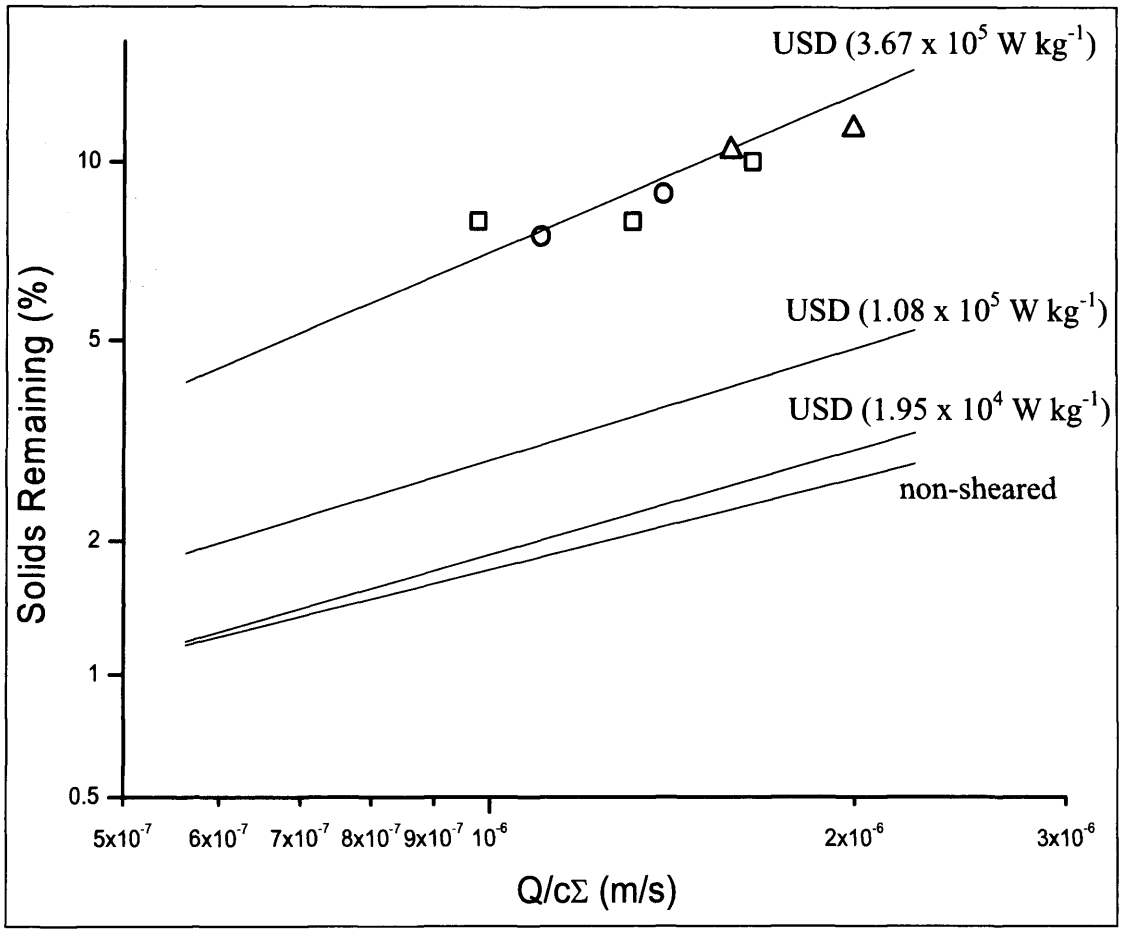

Figure 3.2. Relationship between the % solids remaining and the ratio of equivalent flow rate to centrifuge separation area, plotted on probability-logarithmic axes, for both the ultra scale-down method and the industrial scale, continuous-flow, disc-stack centrifuge. Solid lines represent ultra scale-down predictions from Figure 3.1. Alfa Laval BTAX 205 operated at a bowl speeds of 5000 rpm (△) 5500 rpm (□) and 6000 rpm (○).

Figure 3.2 shows data from the BTAX 205 operated at bowl speeds of 5000 rpm, 5500 rpm and 6000 rpm. The data points at all three bowl speeds approximate the performance of the ultra scale-down centrifugation method in which samples were sheared, prior to centrifugation, at a maximum energy dissipation rate of 3.67×10^5 W kg^{-1}. Figure 2.9 shows that the performance of the Alfa Laval BTAX 205 centrifuge was mimicked by subjecting the cell culture broth to the same shear rate as used for the BTPX 205. This observation was unexpected as the tip velocity of the disc would be greater in the Alfa Laval BTAX 205 centrifuge, even at lower rotational speeds as indicated in Table 3.1. The "critical structure" of the disc stack centrifuge feed zone was taken to be the zone in which fluid flows up, past the lowest disc, into the bowl; CFD analysis has previously shown that this is the region of maximum energy dissipation (Boychyn *et al.,* 2004).

Figure 3.2 shows that the extent of shear damage is not decreased by reducing the bowl speed, as data points from the large-scale centrifuge operated at 5000 rpm, 5500 rpm and 6000 rpm are all in agreement with the ultra scale-down prediction, based on samples pre-sheared at a maximum energy dissipation rate of 3.67×10^5 W kg^1. The explanation for these observations can possibly be found in Figure 2.7 which shows that at high maximum energy dissipation rates, further increases in energy dissipation do not lead to significant increases in solids carry-over; it is postulated that solids susceptible to shear damage are disrupted at lower energy dissipation levels.

	Alfa Laval BTPX 205	Alfa Laval BTAX 205		
Use	Development Pilot Machine	Manufacturing		
Bowl Volume (L)	3.1	52.0		
Bowl Speed (rpm)	9650	5000	5500	6000
Equivalent Settling Area (m^2)	11,350	137,500	166,300	197,900
Disc outer diameter (m)	0.17	0.43	0.43	0.43
Tip velocity ($m\ s^{-1}$)	85	113	124	135

Table 3.1 Comparison of pilot- and large-scale centrifuges, indicating variation in tip speed with scale and bowl speed.

It may be that the hydrodynamic environments in the feed zones of both the BTPX 205 and the BTAX 205 are both sufficiently aggressive to disrupt all susceptible solids and that reducing the tip speed of the BTAX 205 to 5000 rpm fails to reduce maximum energy dissipation in the feed zone to levels that will significantly impact on the recovery of solids in this feed stream. This observation of equivalent levels of cell disruption in the feed zones of the BTPX 205 and the BTAX 205 is significant, in that it suggests that scaling between the two centrifuges will be consistent with sigma theory whereas reduced clarification performance may have been expected at the large-scale at equivalent Q/Σ values due to the effect of increased cell disruption.

3.4 Conclusions

The results presented in this chapter are further evidence that the ultra scale-down centrifugation method can be used to accurately predict the performance of large-scale, continuous-flow, disc-stack centrifuges. Here the approach has been verified using material from a different fermentation carried out with a different cell line and at a ten-fold greater scale than in Chapter 2. The results indicate that the centrifuge used to harvest the 20,000 L bioreactor does not disrupt cells to a greater extent than that used to harvest the 2,000 L bioreactor. However, taking into account the results presented in Chapter 2 it is hypothesized that this is because only a small proportion of the total solids in the bioreactor at the harvest point is shear-sensitive and not that the larger and pilot scale centrifuges generate similar levels of energy dissipation.

Chapter 4 – The use of an ultra scale-down chromatography column for the prediction of product elution profiles and its verification by comparison with an elution profile from a pilot-scale chromatography column.

4.1. Introduction

The volume of buffer required to elute product from a production scale chromatography column is frequently a concern, especially at very large scales. Laboratory experiments are used to predict elution volumes; however, the accuracies of these predictions are often inadequate for the purpose of specifying large-scale facility design. The consequences of this uncertainty in determining elution volumes are severe for a manufacturer. At the large scale, receiving tanks of an appropriate size must be available into which the eluted peak can be collected. As the volume of the elution peak is frequently determined at the point of elution by the absorbance of the column effluent at 280 nm, and not prior to the operation of the production, column, it is conceivable that an unexpectedly large elution volume could exceed the capacity of the tank designated to receive it. In order to prevent associated product loss, processes are developed using excessively large receiving tanks as a contingency measure, but contributing to manufacturing process inefficiencies.

The volume into which the product elutes determines the concentration of the eluted product. Eluted product concentration is an important design variable used to develop subsequent process steps such as membrane operations. Unexpectedly dilute feed streams to membrane operations demand longer processing times, as parameters such as membrane area and flow rates are fixed in advance. Conversely, large-scale chromatographic processes yielding lower elution volumes than expected and

increased maximum product concentrations can be observed upon scale-up despite maintenance of a constant bed height. The reasons for this are poorly understood but the magnitude of the problem is both product- and buffer-specific. High product elution concentrations can, in turn, increase the degree of product aggregation. Two possible hypotheses to explain scale-dependent product aggregation upon elution are (i) that as processes move to larger scales, where extra-column volumes are small relative to the total volume of the system, extra-column dispersion is minimized leading to tall, concentrated elution peaks or (ii) that increasing the column diameter may alter the packing characteristics of the bed due to the loss of wall support (Sofer & Nystrom, 1989). It is thought that columns with diameters of less than 20 mm, which are frequently used in process development, may have less compressed beds and greater void volumes, which may result in reduced product concentrations and aggregation upon elution. Chromatographic aggregation removal steps developed in the laboratory must clear aggregates from the product stream at the large-scale, to pre-specified limits, if not, the batch must be discarded to avoid compromising patient safety.

Predicting the volume and product concentration of the eluate of a chromatographic step at increasing scales is of great importance to biopharmaceutical manufacturers and yet is inadequately covered in the published literature. This chapter describes the use of ultra scale-down methodologies for the prediction of eluate volumes and product concentration from an affinity chromatography step for capturing antibodies from clarified cell culture supernatant.

Theoretical considerations in zone broadening: Differential migration provides the basis for chromatographic separations; however, the effectiveness of

chromatography is also dependent on the degree of zone spreading. Ideally each solute should pass from the column at a different instant in time, however, in practice this does not happen and elution bands spread out so that each solute takes a finite period of time to pass from the column. Zone spreading can occur by axial diffusion, eddy diffusion and local non-equilibrium effects.

Axial diffusion of molecules along the length of the chromatography column broadens the peak by transporting solute upstream and downstream away from the region of greatest concentration at the centre of the zone (Figure 4.1(a)).

Spreading by eddy diffusion is a consequence of the differing lengths of flow paths along which solute molecules will pass while traveling through the packed bed. Those solute molecules taking a more direct path through the column will travel ahead of the average rate of progress, while those taking a more tortuous path will travel more slowly (Figure 4 1(b)).

In chromatography, the local non-equilibrium effect is perhaps the most important cause of zone spreading. As a solute passes through a column, concentration within the zone increases from the front edge and reaches a maximum at the centre before decreasing to zero at the trailing edge (Figure 4.1b). Non-equilibrium effects are caused by delays in mass transport of the product through the boundary layer and the liquid in the pores to the internal surface where adsorption takes place.

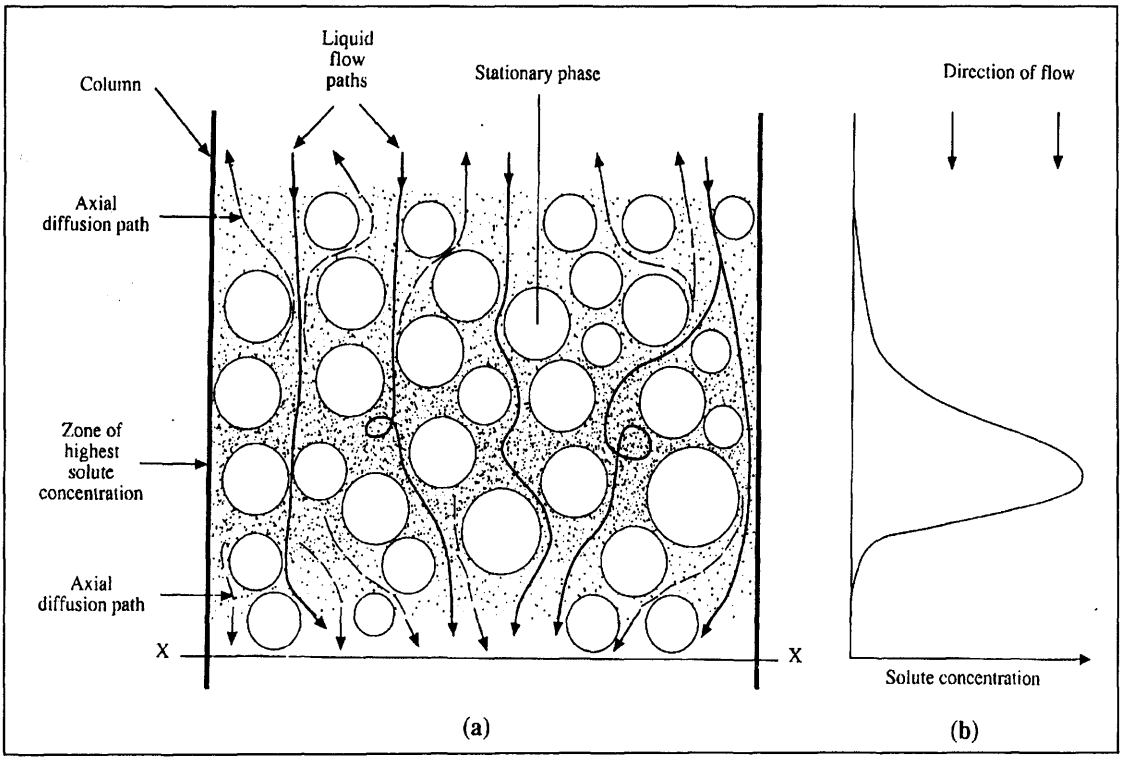

Figure 4.1 showing the axial diffusion path from the zone of highest solute concentration and the differing flow paths that solutes can take contributing to zone spreading. Reproduced from Doran 1994.

This delay prevents equilibration being reached between the liquid and solid phases and consequently the front edge of the pulse will travel down the column more rapidly than that which will follow it while the rear edge of the pulse will continually be stretched out as the solid phase will continue to lose solute molecules once the liquid phase concentration has reached zero (Doran, 1994).

Zone broadening is often analyzed using the concept of theoretical plates (Doran, 1994). A theoretical plate is an equilibrium stage with a magnitude of the same order as a resin particle. Although equilibrium is rarely reached in a chromatography column and thus, the concept is a poor reflection of conditions within the column, it provides a measure of zone spreading. The lower the height equivalent to a theoretical plate (*HETP*) the narrower the solute peak should be. A frequently used expression relating *HETP* to the linear velocity of the liquid (v) is as follows;

$$HETP = (A.v^{-1}) + (B.v) + C \qquad \text{Equation 4.1}$$

where A, B and C are experimentally determined constants. The first term, A, refers to molecular diffusion, B results from mass transfer resistances and C originates from eddy diffusion effects (Doran, 1994). A graphical representation of the expression is given in Figure 4.2.

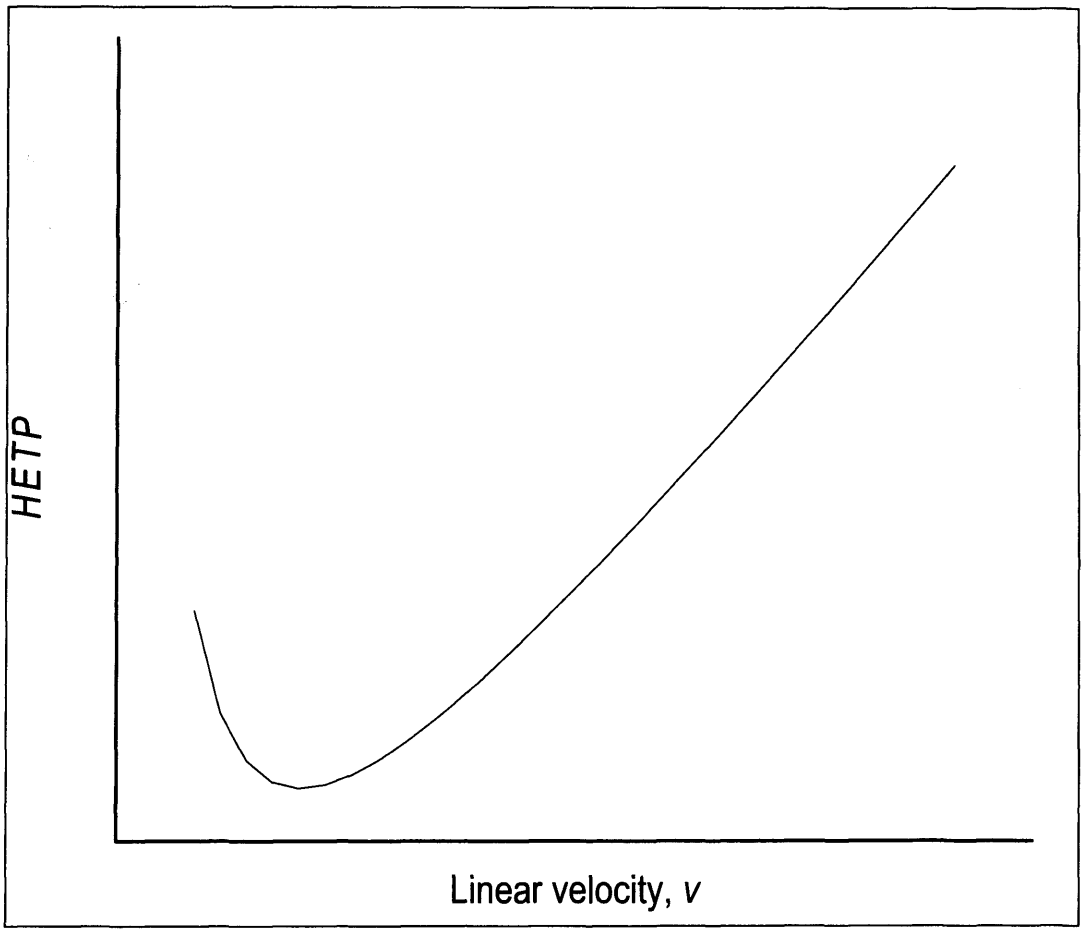

Figure 4.2 The relationship between linear flow rate and *HETP*. At low linear flow rates diffusion effects dominate and *HETP* decreases as the flow rate increases; however, at higher velocities mass transfer effects begin to dominate and HETP increases with increasing flowrate.(Illustrative figure generated using Equation 4.1 and hypothetical values for constants *A, B* and *C*) (Doran, 1994).

Pulsed-input testing of packed chromatography beds is commonly performed in order to estimate the *HETP* as an indication of resin packing efficiency (Hoffman, 1998). A pulse of tracer molecule, equivalent to 1-5% of the total column volume, is applied to the column inlet and the tracer concentration in the column effluent is monitored over time. The variance in the pulse of the tracer at the column outlet, σ^2, is proportional to the distance travelled by the pulse, z. Hence *HETP* is a measure of zone broadening per unit column length, as given by equation 4.2:

$$HETP = \frac{\sigma^2}{z} \qquad \text{Equation 4.2}$$

Alternatively, the number of theoretical plates, N, is often used as a measure of how well a chromatography column is packed and is related to *HETP* as follows:

$$N = \frac{z}{HETP} \qquad \text{Equation 4.3}$$

The distance traveled by the solute pulse is usually substituted by the more easily determined retention volume, V_R, which is the equilibration buffer volume delivered by the pumps, measured from the time when half the sample mass is applied to the column to the time when half the sample mass is eluted from the column. Hence,

$$N = \frac{z}{\left(\sigma^2/z\right)} = \frac{V_R}{\left(\sigma^2/V_R\right)} = \left(\frac{V_R}{\sigma}\right)^2 \qquad \text{Equation 4.4}$$

Hence *HETP* on a chromatography column, of bed height, L, can be described as follows,

$$HETP = \frac{L}{N} = \frac{L}{\left(V_R/\sigma\right)^2} \qquad \text{Equation 4.5}$$

Two simplifications are often applied when determining the solute retention volume. The contribution of the pulse volume to the retention volume is often ignored if the pulse is small; however, if the pulse volume is not negligible the solute retention volume is set when half the sample volume has been injected. Also the contribution to broadening of extra-column volumes, in pipes from the injector to the column and from the column to the detector, is often ignored.

The assumption that zone broadening in extra-column volumes is insignificant is unlikely to be true, especially in the laboratory where standard chromatographic systems are frequently used. Decreasing the column bed height in order to minimize the volume of process material required for chromatography process development will increase the influence of extra-column broadening on the data acquired from such studies. There is a limit to the extent that extra-column volume can be minimized and hence the ratio of extra-column volume to column volume will increase with the degree of scale-down.

Extra-column broadening can be subdivided into dispersion in tubes, contributions of dead volumes, finite detector volume and dynamic behavior of transducers and electronics. Tubing introduces a symmetrical, Gaussian-type broadening (σ_t^2) to the sample, under the combined actions of molecular diffusion and the axial flow velocity profile.

Under laminar flow conditions broadening caused by tubing can be described by

$$\sigma_t^2 = \frac{t_R . r^2}{24 D_M} \qquad \text{Equation 4.6}$$

where t_R is the retention time, r the tube radius and D_M the molecular diffusion coefficient (Kaltenbrunner *et al.,* 1997). Dead volumes introduce an exponential

contribution to the band broadening (τ_{dead}), which is a function of the dead volume (V_{dead}) and the flow rate (Q) as described by(Kaltenbrunner *et al.*, 1997),

$$\tau_{dead} = \frac{V_{dead}}{Q} \qquad \text{Equation 4.7}$$

Additionally the finite sensing volume of a detector introduces an additional symmetrical, rectangular broadening (σ_d) as described by,

$$\sigma_d^2 = \frac{V_d^2}{12Q^2} \qquad \text{Equation 4.8}$$

where V_d is the sensitive detector volume. An exponential contribution to the band broadening is introduced by the finite response rate of the amplifier and recorder (τ_{el}). (Cram & Glenn, 1975). Assuming additivity of the variances, the total extra-column broadening can be written as,

$$\sigma_{ex}^2 = \sigma_s^2 + \sigma_t^2 + \sigma_d^2 + \tau_{dead}^2 + \tau_{el}^2 \qquad \text{Equation 4.9}$$

where σ_{ex}^2 is the lumped extra-column dispersion and σ_s^2 is the variance of the initial injection profile. Assuming that the variances introduced by the electronics and the detector volume are negligible compared to other variances,

$$\sigma_{ex}^2 = \sigma_s^2 + \sigma_t^2 + \tau_{dead}^2 \qquad \text{Equation 4.10}$$

The total broadening (σ_{total}^2) is the sum of column internal broadening (σ_{col}^2) and the extra column broadening (σ_{ex}^2), ie.

$$\sigma_{total}^2 = \sigma_{col}^2 + \sigma_{ex}^2 \qquad \text{Equation 4.11}$$

Defining the plate number, N, for a column, as

$$N = \frac{V_R^2}{\sigma_{col}^2} \qquad \text{Equation 4.12}$$

substitution yields the following expression,

$$\sigma_{total}^2 = \frac{V_R^2}{N} + \sigma_{ex}^2 = \frac{HETP}{L}.V_R^2 + \sigma_{ex}^2 \qquad \text{Equation 4.13}$$

which enables extra-column broadening (σ_{ex}^2) to be determined from a plot of total band broadening (σ_{total}^2) as a function of V_R^2, where V_R is the retention volume (Huber & Rizzi, 1987). The work described in this chapter investigates the possibility of accurately determining the relative contributions of column and extra-column broadening to elution profiles and using this information to make scale-down predictions for a pilot-scale chromatography column with column volume of 18.3 L.

The use of pulse inlet testing, although common for measuring column packing efficiencies, becomes impractical for very small columns (ie. column volumes of a milliliter or smaller) as pumps fitted to standard laboratory chromatography systems would be unable to accurately deliver sufficiently small pulses. Transition analysis provides a suitable alternative to pulse inlet testing for determining zone spreading, by measuring the response at the outlet of a column to a step change at the column inlet. Step changes in optical density, conductivity and pH can be used, with the relevant detector at the column outlet, to assess the condition of the packed bed. During a standard chromatographic cycle numerous transitions occur, allowing the quality of the bed to be easily assessed after each cycle in order to detect changes in bed quality over time (Larson *et al.,* 2003).

4.2 Materials and Methods

4.2.1 Laboratory Studies

4.2.1.1 Packing and transition analysis. Five Tricorn columns, with internal diameter of 5 mm, were packed to bed heights of 20 mm, 53 mm, 102 mm, 145 mm

& 205 mm, respectively, with rmp Protein A Sepharose 4FF (GE Healthcare) chromatography matrix using equilibration buffer at 150% of the operating flowrate of 1.5 m h^{-1}. The experimental set-up is schematically illustrated in Figure 4.3. The columns were equilibrated with 50 mM glycine-glycinate, 250 mM sodium chloride, pH 8.0 before transition to the 100 mM glycine – HCl, pH 3.5, initiated by switching of the pump valve. Effluent conductivity was monitored beyond the outlet of the column, as close to the fraction collector as possible. Once the conductivity transition (from high conductivity to low conductivity) had reached completion the column was re-equilibrated and the experiment repeated.

4.2.1.2 Elution profiles: Elution profiles were generated from 53 mm and 157 mm columns by loading and eluting purified chimeric B72.4 antibody. Table 4.1 shows the operating conditions of the laboratory columns. Column flow rate was varied to maintain a constant column residence time of 0.1 h. Excess buffer was used to ensure that each stage had reached completion; thus buffer volumes are not indicative of volumes required at larger scales. Fractions (100 µL from the 53 mm and 300 µL from the 157 mm column) were collected into a 96-well plate. The fractions were analyzed on the basis of absorbance at 280 nm. Details of the columns used in this chapter are given in Table 4.2

Elution profiles at different flow rates were determined using the column of 53 mm bed height, by repeating the above procedure at elution flow rates, without changing the operating flow rate for any other step.

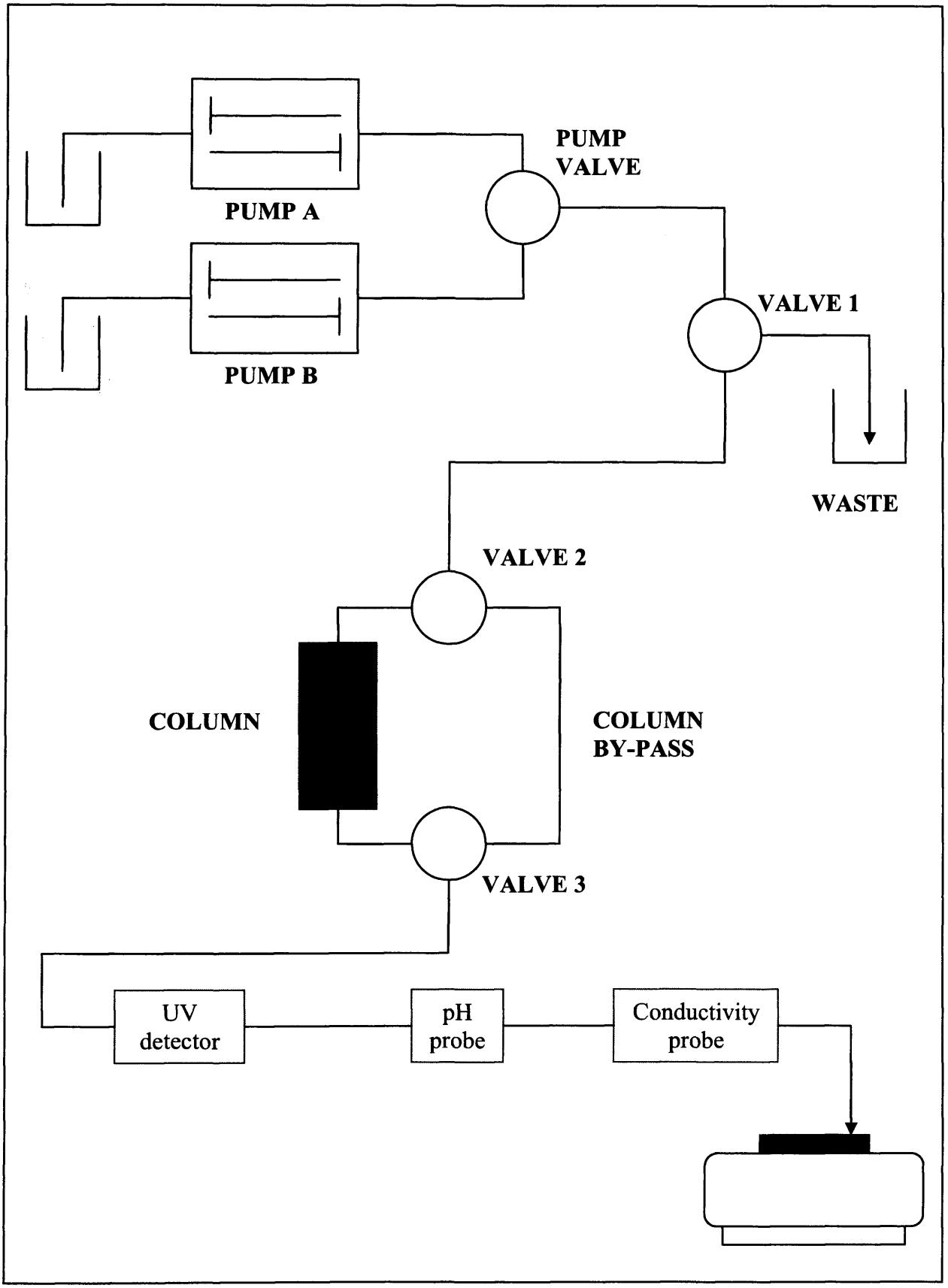

Figure 4.3 Schematic diagram of the chromatography system used in laboratory scale experiments.

Step	Buffer	Column Volumes	Linear Flow Rate (m/h)
Equilibration	50 mM glycine-glycinate/ 250 mM NaCl pH 8.0	6	1.5
Product Load	0.50 mg/mL b72.3 antibody, pH 8.0	20	0.53 & 1.57 for the 5.3 cm and 15.7 cm column bed heights, respectively
Post-Load Wash	50 mM glycine-glycinate/ 250 mM NaCl pH 8.0	6	1.5
Elution	100 mM glycine hydrogen chloride pH 3.5	8	1.5
Strip	50 mM glycine-glycinate/ 1.75 M NaCl, pH 8.0	10	1.5
Sanitization	6 M guanidine hydrogen chloride, pH 3.5	6	0.52
Re-equilibration	50 mM glycine-glycinate/ 250 mM NaCl pH 8.0	6	1.5

Table 4.1. Operating conditions for the 0.5 cm diameter Tricorn columns with bed heights of 53 mm and 157 mm. The linear flow rate during the product loading phase was varied to give constant residence time.

Bed height (cm)	Diameter (cm)	Volume (mL)	Aspect Ratio	Use
2	0.5	0.4	4.0	Transition analysis
5	0.5	1.0	10.0	USD
10	0.5	2.0	20.0	Transition analysis
15	0.5	2.9	30.0	Transition analysis
20	0.5	3.9	40.0	Transition analysis
15	40	18849.6	0.4	Pilot

Table 4.2. Summary of columns used in this chapter.

4.2.2 Pilot Studies

4.2.2.1. Packing and transition analysis. A pilot-scale chromatography column, with internal diameter of 400 mm, was packed to a bed height of 146 mm with rmp Protein A Sepharose 4FF chromatography matrix (GE Healthcare) using equilibration buffer at 150% of the operating flowrate of 1.5 m h^{-1}. As with the laboratory-scale columns, the pilot-scale column was equilibrated with 50 mM glycine-glycinate, 250 mM sodium chloride, pH 8.0, before a transition to the 100 mM glycine – HCl, pH 3.5 was initiated. The effluent conductivity was monitored beyond the outlet of the column; once the downwards conductivity transition had reached completion the column was re-equilibrated and the experiment repeated.

4.2.2.2. Elution profiles: The elution profile from the pilot-scale column was generated by loading and eluting purified chimeric B72.4 antibody. Loading of the columns to a level consistent with the laboratory columns was achieved by maintaining a constant column residence time of 0.1 h and an equal feed-to-column volume ratio. Equilibration, post-load wash, elution, column strip and re-equilibration stages were carried out at 1.50 $m.h^{-1}$ while the sanitization step was carried out at 0.52 $m.h^{-1}$. During elution 15 mL samples of the eluate were collected at 2 L intervals and the absorbance (at 280 nm) determined to measure MAb concentration. Buffers used at the pilot-scale were as those used for the laboratory experiments with the exception of the strip buffer, which was replaced with 100 mM citric Acid, pH 2.1.

4.2.3. Transition Calculation Methodology

Conductivity transition data were normalized by finding the maximum and minimum conductivity values over the course of the transition volume, subtracting the minimum from each value of the solute signal and dividing each of these values by the difference between the maximum and minimum values. dR/dV, the first derivative of the normalized conductivity response data array, R, and the totalized volume data paired with R, V, was estimated numerically using a moving average of the slope. Calculating dR/dV using a moving average interval produces a smooth transition shape and increases the accuracy of subsequent calculations (for sample calculation see Appendex 1).

Moment analysis of the transitions allows values for *HETP* and dispersion to be obtained from the entire solute response curve, without making any assumptions about the distribution of the curve, as follows,

$$HETP_N = \frac{\sigma^2 L}{\left(\frac{M_1}{M_0}\right)^2} \qquad \text{Equation 4.15}$$

where σ^2 is the variance as expressed as follows,

$$\sigma^2 = \frac{M_2}{M_0} - \left(\frac{M_1}{M_0}\right)^2 \qquad \text{Equation 4.16}$$

and M_0, M_1 and M_2 are the zeroth, first and second moments, respectively, with the integrals estimated by trapezoidal approximation according to equation 4.17, where R is the solute step response and k is the moment number (for sample calculation see Appendix 1)

$$M_k = \int V^k \frac{dR}{dV} dV \qquad \text{Equation 4.17}$$

4.3 Results

4.3.1 Transition analysis of ultra scale columns

Conductivity transitions (A) for the five columns, plotted on a volume basis, and the first derivative (B) of the conductivity transitions are shown in Figure 4.4. In each case the conductivity drops from approximately 25 mS/cm to 0.5 mS/cm as the equilibration buffer (50 mM glycine-glycinate, 250 mM sodium chloride) is replaced by the elution buffer (100 mM glyine hydrogen chloride). This particular transition is part of the generic Protein A affinity chromatography step at Lonza Biologics. As the column heights and volumes increase, the transition residence volume also increases, as the distance between the pump valve (where the transition starts its course through the system) and the conductivity meter (where the transition is measured) increases. Furthermore, it can be seen that the gradients of the conductivity transitions become less steep, the height of the first derivative peak decreases and the peak width of the first derivative increases. The increase in the transition broadening with column length is attributable to the effects of axial and eddy diffusion, both of which will increase as the distance over which the transition passes increases. It can be seen that the first derivatives of the 145 mm and 205 mm bed height columns are less smooth than the others. This indicates that the moving average filter applied during the calculation did not include sufficient data.

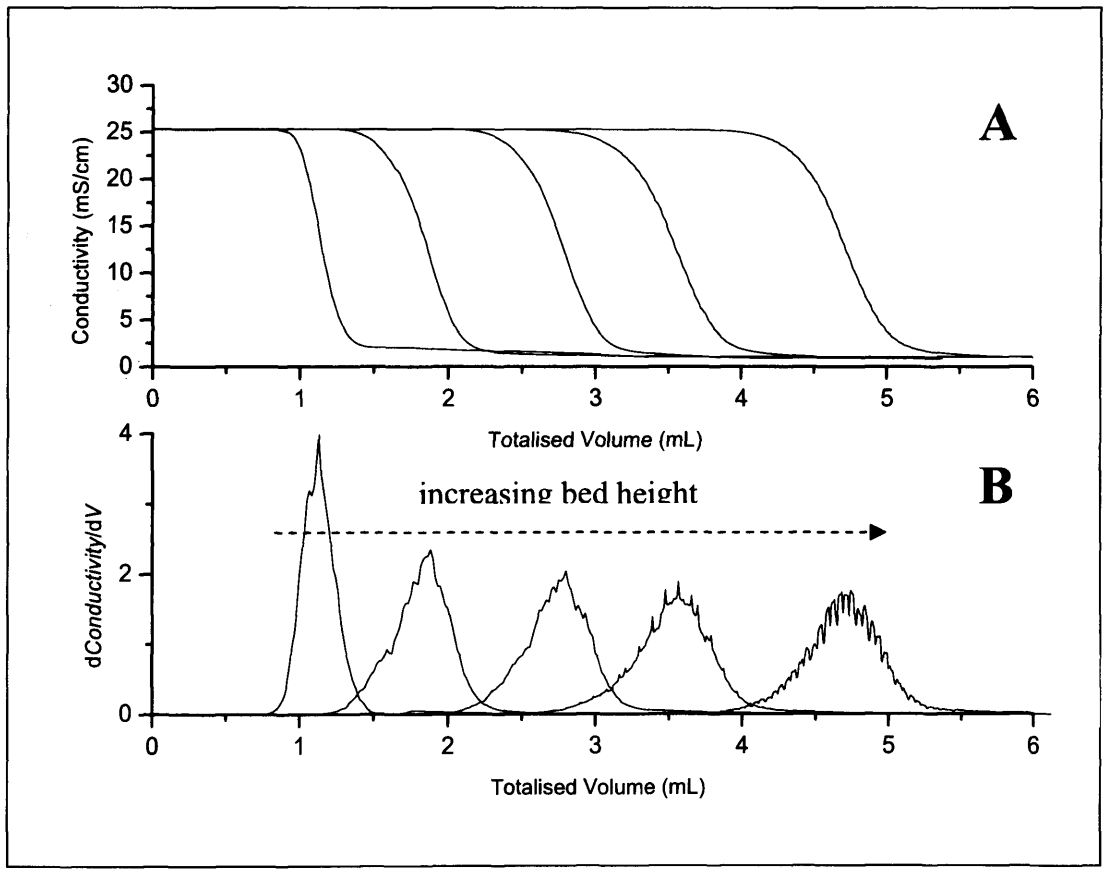

Figure 4.4. Regime analysis of laboratory chromatography systems, showing the effect of decreasing bed height on the retention volume and dispersion of the conductivity transition. From left to right curves correspond to bed heights of 20, 53, 102, 145, 205 mm respectively. Each column had a bed diameter of 5 mm, was packed with Protein A Sepharose 4 FF resin and was attached to the same AKTA FPLC system with identical connecting tubing. A: conductivity data; B: first derivative of the conductivity data with respect to totalized volume, giving an insight into the maximum rate of change and dispersion associated with each curve.

The data presented in Figure 4.4 are again presented in Figure 4.5, but plotted on the basis of column volumes. Thus presented the results show that the transition residence volumes increase with decreasing column height when normalized by column volume. This occurs because the extra-column volume, constant for all columns, constitutes a greater proportion of the total system volume for smaller columns. For the same reason, the transition gradients decrease and the width of the first derivatives increase with decreasing column size. The dispersion caused by the transition flowing through the extra-column volume makes up a larger proportion of total system dispersion for a smaller column.

Figure 4.6 shows the positive linear relationship between the column volume, V_C, and the retention volume, V_R, of the transition, as determined by moment analysis of the transition curves presented in Figure 4.4. The relationship can be described as follows,

$$V_R = \varepsilon . V_C + V_{ex} \qquad \text{Equation 4.18}$$

where ε is the average column void fraction and V_{ex} is the extra-column volume. From the intercept with the y-axis the extra-column volume was determined to be 0.81 mL which represents a significant contribution to the total system volume particularly when operating the smallest column with a column volume of 0.4 mL. This value can also be determined by connecting the upper and lower column adapters; however, this was not technically possible with the particular columns used in this experiment. The gradient of the line is equal to the column void fraction which in this case was determined to be 0.97 which although quite high, may not be unrealistic since the solute was small ionic species and the matrix is highly porous.

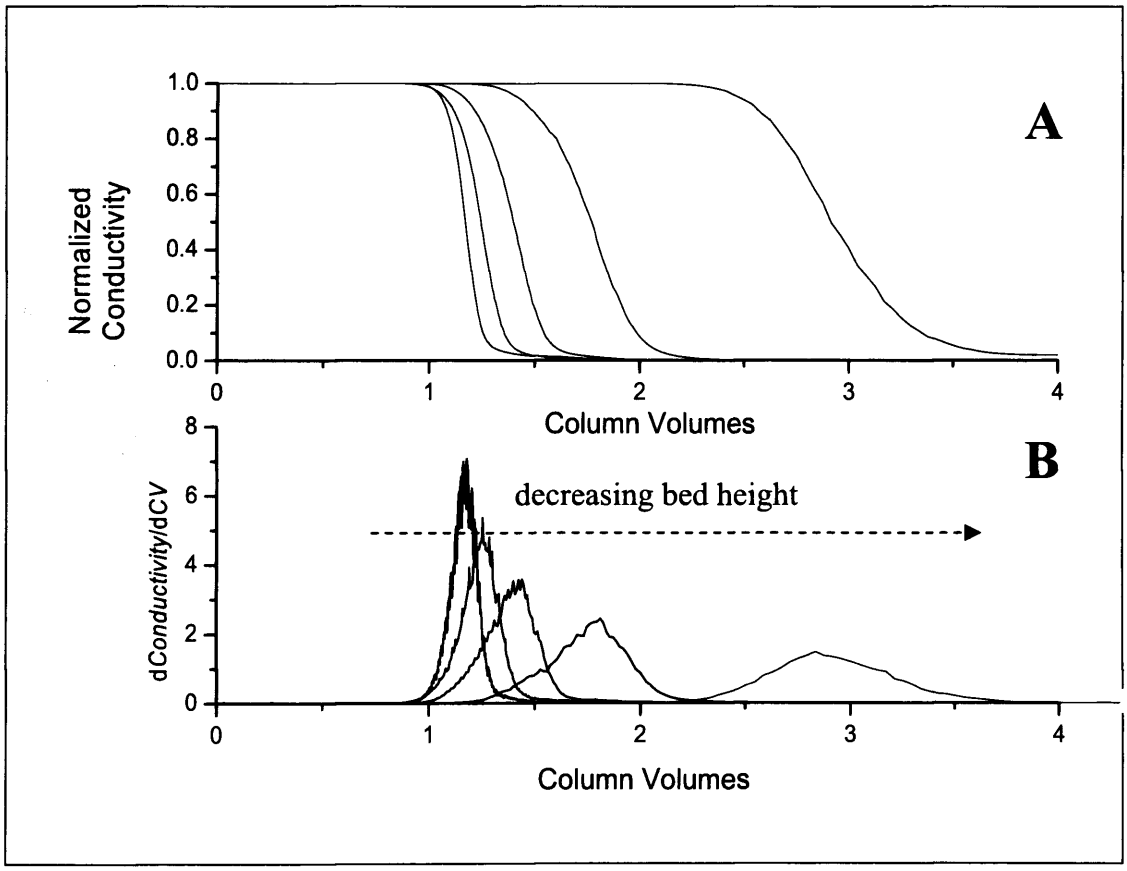

Figure 4.5. Regime analysis of laboratory chromatography systems showing the effect of decreasing bed height on the retention volume and dispersion of the conductivity transition. Data as for Figure 4.4 but using column volumes rather than total volume to compare performances. Curves from left to right are, respectively, bed heights of 205, 145, 102, 53, 20 mm. Each column had a bed diameter of 5 mm, was packed with Protein A Sepharose 4 FF resin and was attached to the same AKTA FPLC system with identical connecting tubing. A: normalized conductivity data; B: the first derivative of the conductivity data with respect to column volumes.

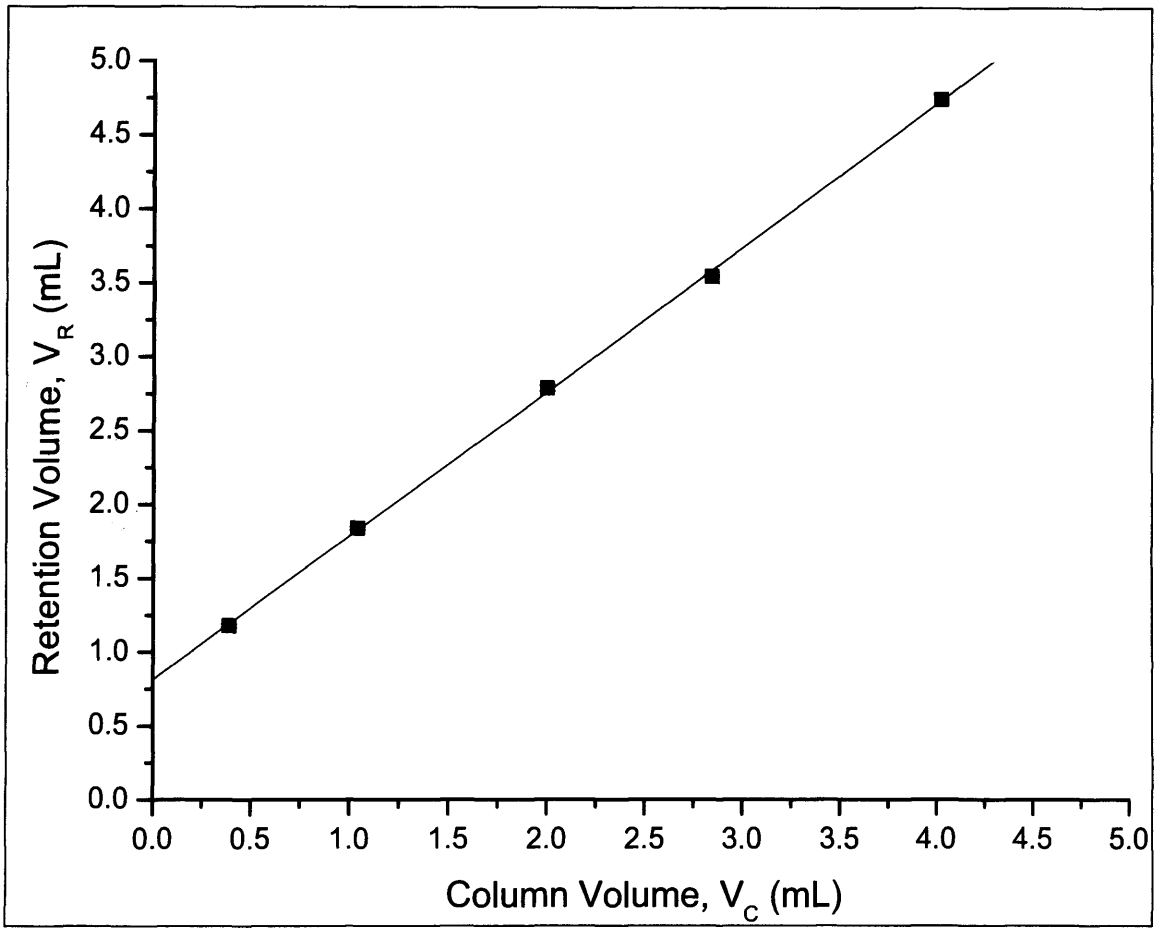

Figure 4.6 – Experimentally-determined relationship between retention volumes, V_R and total column volumes, V_C. Linear regression analysis yields $V_R = 0.81 + 0.97V_C$ corresponding to a void fraction of 0.97 and the extra-column volume of 0.81 mL

The result contrasts with that published by Kaltenbrunner *et al.* (1997) in which the system extra-column volume was determined to be 0.32 mL with a void fraction of 0.47. Kaltenbrunner *et al.* used a different chromatography resin (Q-HyperD) in their experiments and a protein pulse under non-binding conditions.

An alternative figure can be plotted using the same transition analysis data. If the retention volume of a transition is normalised with respect to the column volume as described in equation 4.19,

$$V_R^* = \frac{V_R}{V_C} \qquad \text{Equation 4.19}$$

where V_R^* is the normalised retention volume of a transition, then equation 4.18 can be re-written as,

$$V_R^* = \varepsilon + \left(\frac{V_{ex}}{\pi r_C^2}\right)\frac{1}{L} \qquad \text{Equation 4.20}$$

where r_C is the column radius and L is the chromatography bed height.

A plot of normalized retention volume (V_R^*) against reciprocal chromatography bed height (L^{-1}) is shown in Figure 4.7. It should be reiterated that Figure 4.7 provides no additional information to that presented in Figure 4.6. However, it usefully summarizes the findings of Figure 4.5, showing that scaling-down by reducing column bed height increases the normalized retention volume, because the extra-column volume constitutes a greater proportion of the total system volume. The relationship between retention volume and transition dispersion, described by equation 4.13, is shown in Figure 4.8. The gradient of the line is equal to the number of plates per unit length of column (1/N = 0.0236). From the equation of the line σ^2 can be determined for the retention volume equal to that of the void volume. Using equation 4.13 dispersion attributable to flow through the extra-column volume for this system can be calculated to be 0.028 mL^2. For small scale-down columns, the band broadening which occurs in the extra-column volume can dominate over total band broadening in the system.

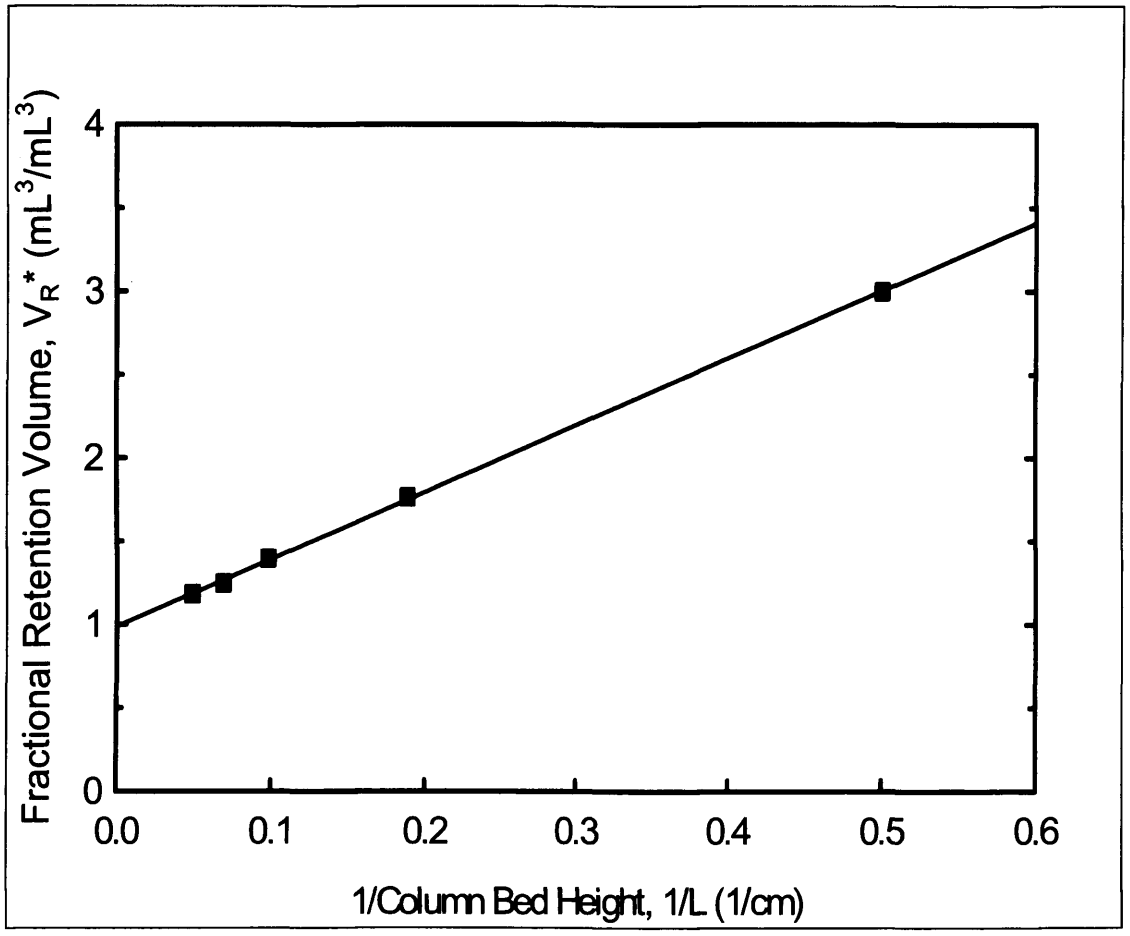

Figure 4.7. Fractional retention volume for columns of varying heights, determined from the conductivity transitions shown in Figure 4.6. The least squares best fit line ($R^2 > 0.99$) has a slope of 4.1 cm, giving an extra column volume for the system of 0.81 mL and an intercept of 0.97, equivalent to the void fraction of the bed, according to equation 4.20.

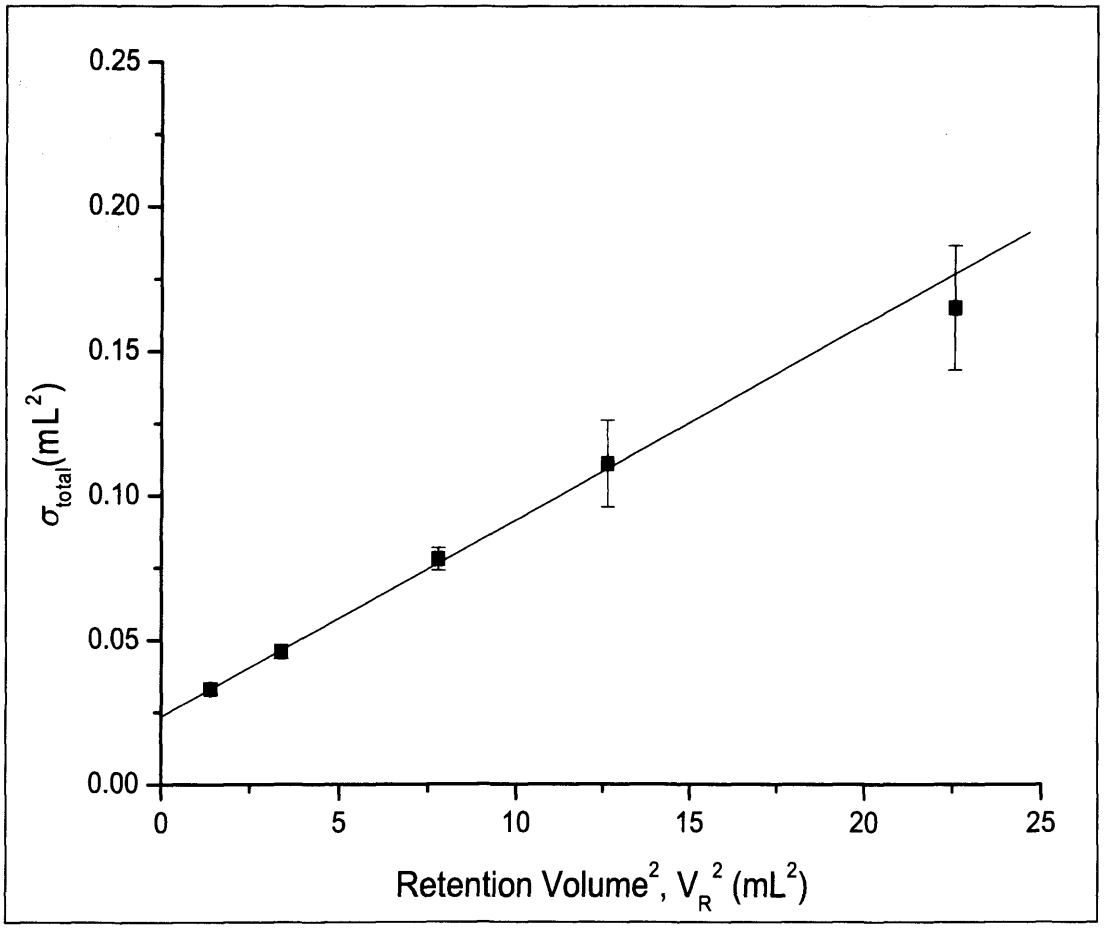

Figure 4.8. Plot of total band broadening versus retention volume. Equation of line, $\sigma^2_{total} = 0.02355 + 0.00679\ V_R^2$ ($R^2 > 0.99$) From equation 4.13 the extra-column volume determined to be 0.81 mL.

Total dispersion can be normalized by column volume and related to the normalized retention volume as follows,

$$\sigma_{total}^{2}{}^{*} = \frac{V_R^{2}{}^{*}}{N} + \frac{\sigma_{ex}^{2}}{V_C{}^{2}} \qquad \text{Equation 4.21}$$

where V_C is the chromatography bed volume ($V_C = \pi r_C{}^2 L$). Substitution of equation 4.20 and rearrangement expresses the normalized total dispersion as a function of the chromatography bed height, allowing the prediction of the total band broadening occurring in a column of any length on the same chromatography system:

$$\sigma_{total}^{2}{}^{*} = \frac{\varepsilon^2}{N} + \left(\frac{2\varepsilon V_{ex}}{N\pi r_C{}^2}\right)L^{-1} + \pi^{-2} r_C{}^{-4}\left(\frac{V_{ex}^2}{N} + \sigma_{ex}^2\right)L^{-2} \qquad \text{Equation 4.22}$$

The data from Figure 4.8 are plotted according to Equation 4.22 as shown in Figure 4.9. The figure illustrates how decreasing the bed height of the column significantly increases the zone spreading relative, to the size of the column.

The proportion of the total dispersion that is attributable to flow through the extra-column volume, for columns of different heights is shown in Figure 4.10. The figure shows that this proportion increases from 17%, for a column with a bed height of 205 mm, to 86%, for a column with a bed height of 20 mm, illustrating the importance of accounting for extra-column broadening when making predictions of large-scale chromatography operations using very small volume columns.

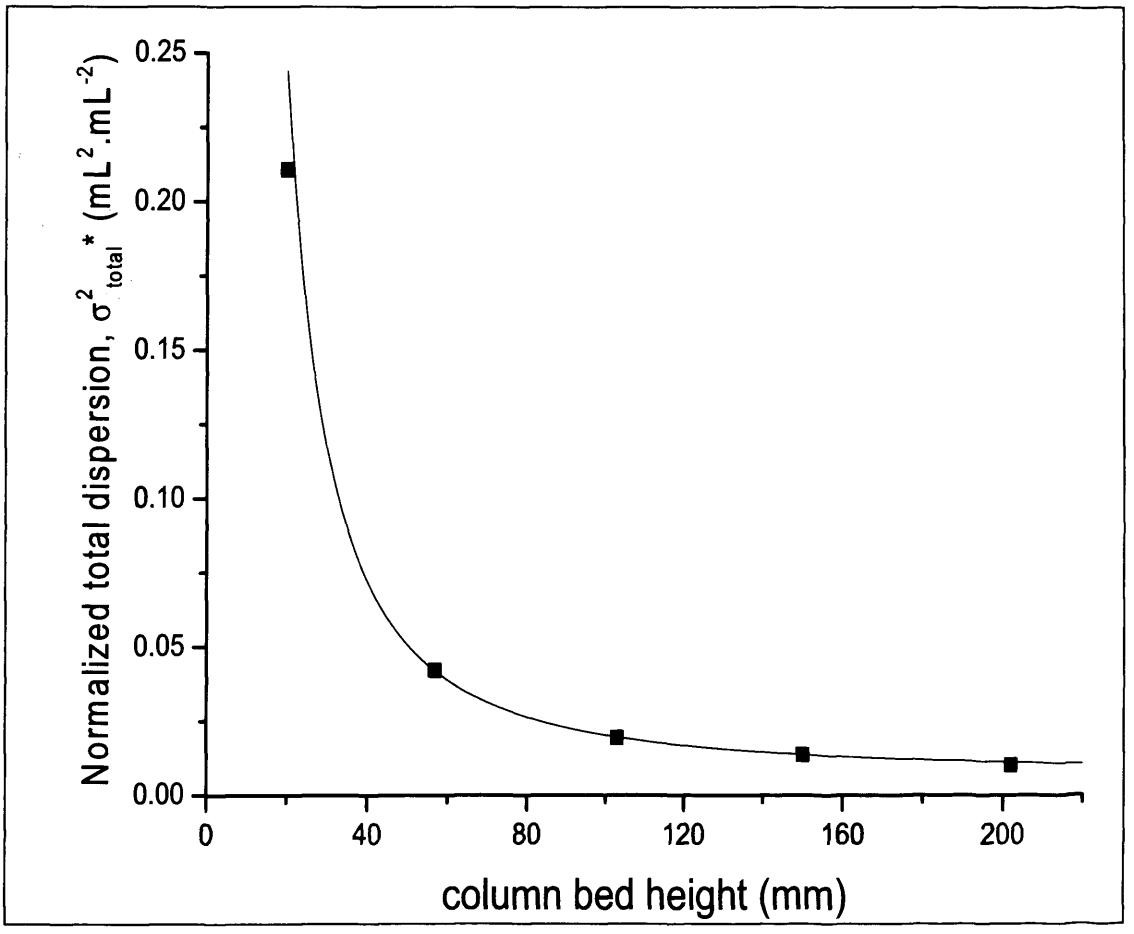

Figure 4.9. Normalized total dispersion for columns of varying bed height, showing increasing importance of dispersion at reduced bed heights. In the form of Equation 4.22, the equation of the non-linear curve fit is

$$\sigma^2_{total}* = 6.39\times10^{-3} + 5.43\times10^{-2}L^{-1} + 0.842L^{-2} \quad (R^2 > 0.99)$$

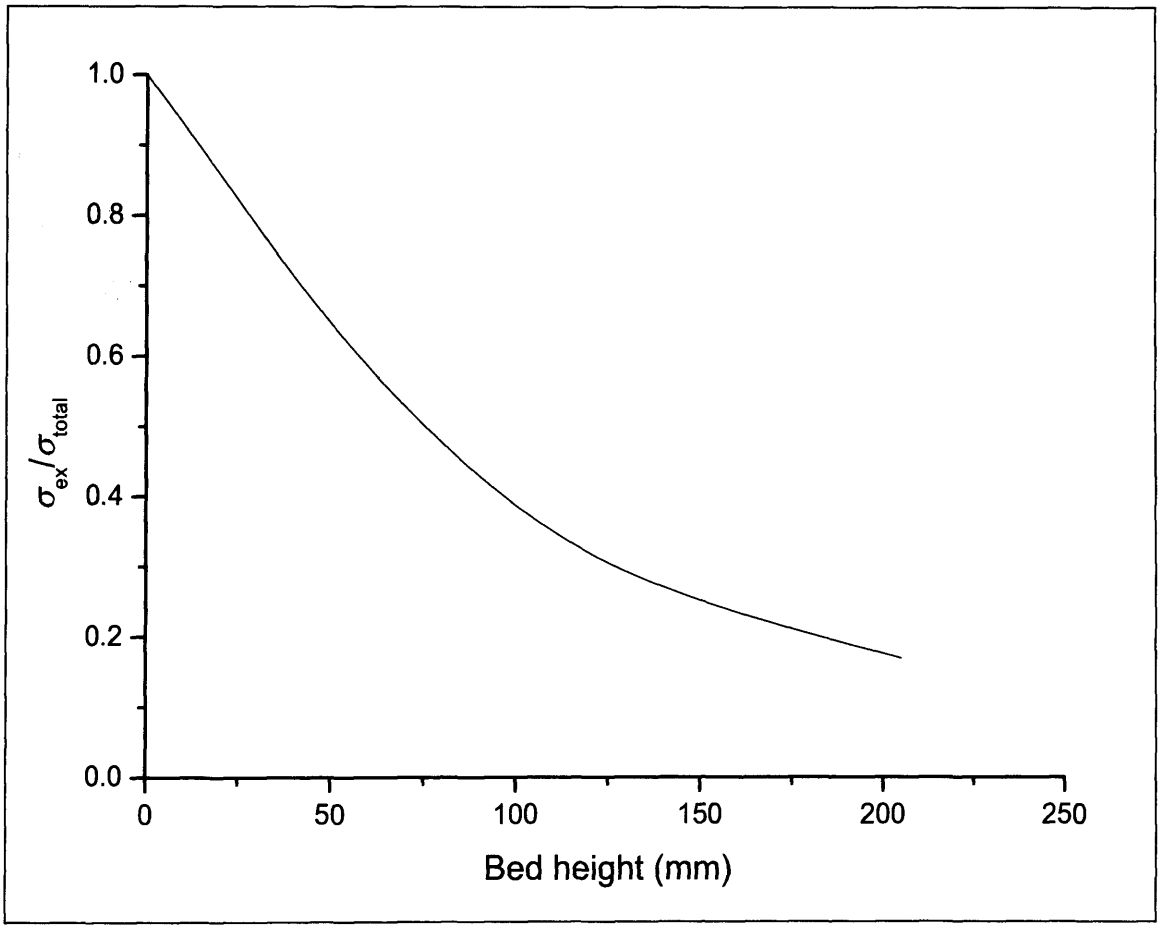

Figure 4.10. Ratio of extra column broadening to total broadening, as a function of the column bed height, calculated using the regression lines from Figures 4.6 and 4.8.

4.3.2 Comparison of ultra scale-down columns with laboratory-scale columns

Developing the ultra scale-down approach for predicting elution volumes was performed in two phases. Firstly, a method to predict the performance of a laboratory column with an ultra scale-down was developed and then the approach extended to allow predictions of a pilot-scale column. Scaling-down the laboratory column by reducing the bed height represents only a small decrease in scale, however, it requires changing the parameter that along with linear flow velocity is traditionally kept constant during scaling and hence represents a considerable challenge. Figures 4.11 and 4.12 show the elution profiles from the 53 mm and 157 mm bed height columns. Data points represent the mean product concentrations in each fraction based on replicate measurements and error bars represent one standard deviation from this mean. To further reduce the feed volume, it would have been preferable to use the 20 mm column to predict the product elution volume and concentration for large-scale columns; however, it was not possible to collect sufficient fractions to plot an elution profile from the smaller column. It was necessary to collect fractions, rather than use the on-line UV detector because the protein concentration during elution was sufficiently high to saturate the detector. The 157 mm column was used for the ultra scale-down column comparison as this is within the validated range of column bed heights used in this process at the manufacturing scale (150 mm ± 10 %).

Figure 4.11 shows the concentration of product in collected fractions on a volume basis while Figure 4.12 shows the same data normalized for column volumes. There are similar trends to those observed for the conductivity transitions presented in

Figures 4.4 and 4.5: the elution peak for the 1 mL column elutes before that of the 3 mL column, as the distance between the pump valve and the fraction collector is smaller; with both columns loaded with 10 mg of antibody per millitre of chromatography resin. the area under the elution profile for the 53 mm bed is approximately one third of that of the column 157 mm bed echoing the column volume ratio. Figure 4.12 shows that the bound product for a small volume column with reduced bed height elutes in a greater number of column volumes than the taller column due to the large effect of the extra-column dispersion relative to the column volume. Furthermore, the residence volume of the elution peak is greater for the ultra scale-down column. As discussed previously, with respect to the conductivity traces (Figure 4.4 & 4.5), this is because the extra-column volume is more significant relative to column volume at the smaller scale. In Figure 4.12 the areas under the elution curves are approximately the same (± 2%) as the eluted product concentration per column volume must be constant. Figure 4.12 shows that an ultra scale-down column cannot be used to predict the elution volume and concentration of the larger column simply by normalizing the elution profiles with respect to column volume.

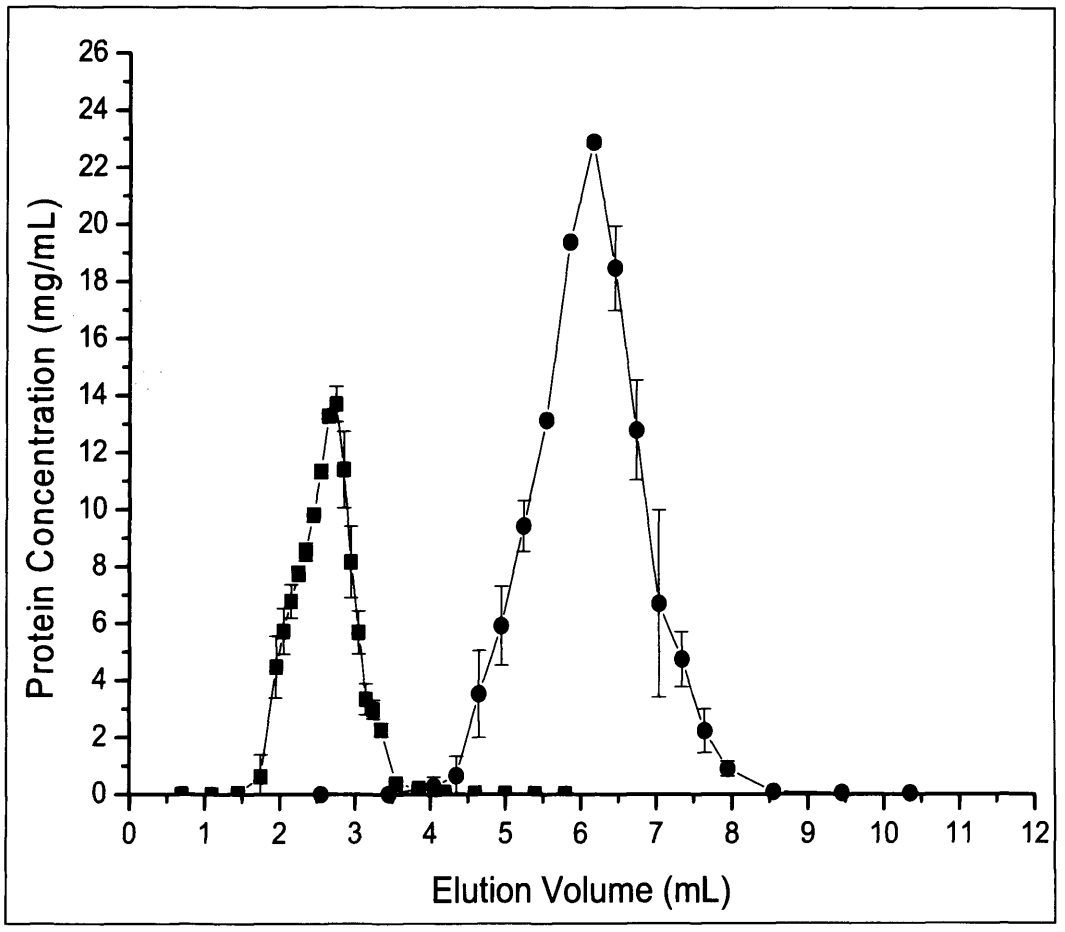

Figure 4.11. Elution profiles for the 53 mm column (■) and 157 mm column (●). Error bars represent the range of duplicate measurements.

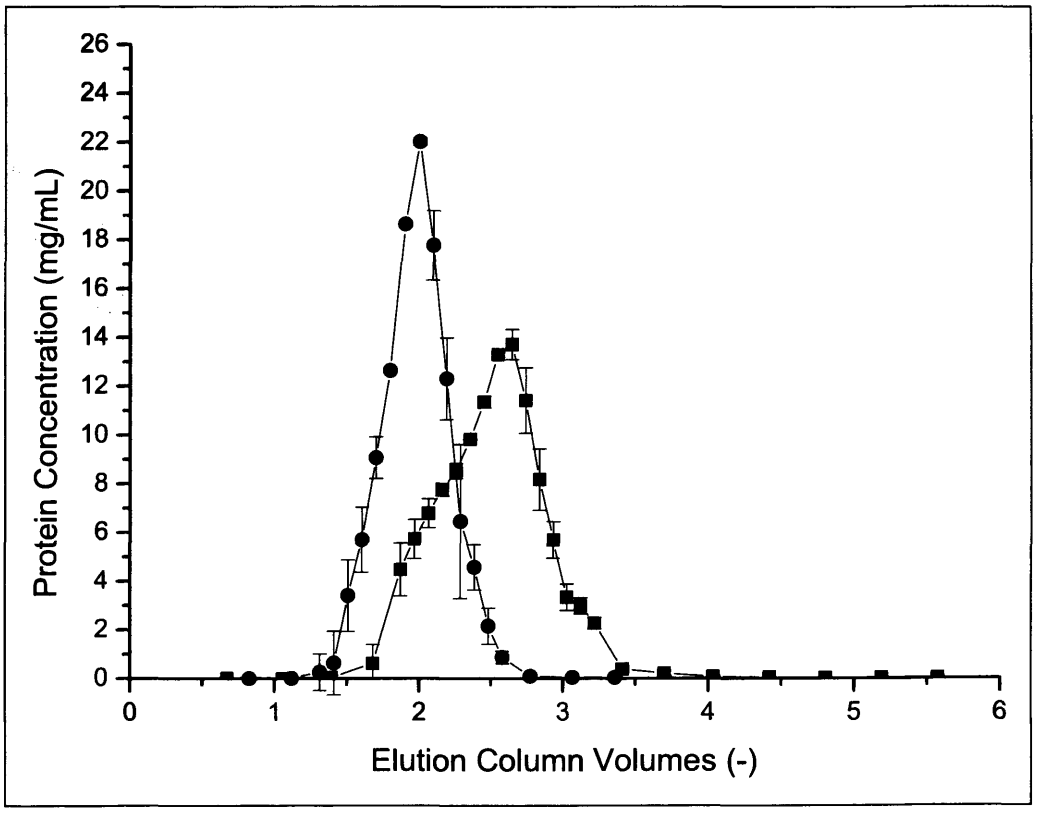

Figure 4.12. Elution profiles for the 53 mm column (■) and 157 mm column (●); data as for Figure 4.11 but normalized using column volumes.

The elution profile obtained with the ultra scale-down column of 5.3 cm bed height and column volume of 1.04 mL was corrected to make a prediction of the elution profile expected from a laboratory-scale column of the same diameter but increased bed height of 157 cm. The prediction was formulated by correcting the ultra scale-down elution profile, on a volume basis, to account for additional zone spreading and increased residence time (Figure 4.5). The correction factors were determined from the transition analysis data. Unlike the conductivity transition that disperses from the pump valve to the conductivity detector (Figure 4.3) the protein sample becomes more concentrated as it binds to the and then becomes more dispersed as it elutes and travels to the fraction collector. Although it might appear that to use data from the conductivity transitions would lead to over-correcting of dispersion effects on the protein sample, it should be considered that the elution buffer front will also become more disperse as it travels from the pump valve to the column inlet. This will lead to a more gradual drop in the pH of the column which will cause spreading of the proteins sample and which must also be accounted for. Although this is a simplification of the changing engineering environments in the chromatography system, the correction process offers a pragmatic approach to improving the predictions of elution profiles derived from ultra scale-down columns.

According to equation 4.22, the variance of the peak of the ultra scale-down column must be adjusted according to $\left(\sigma^2_{total}\ast\right)_{L=15.7}/\left(\sigma^2_{total}\ast\right)_{L=5.3} = 0.31$. In order to maintain the characteristic shape (e.g. shoulders) of the ultra scale-down column elution peak, the width of the peak was reduced by the ratio of the standard deviations or $\sqrt{0.31}$ about V_R^*. The height of the peak was increased by an appropriate factor in order to maintain the area of the peak (Figure 4.13). The resulting peak profile was narrower

and had a significantly higher maximum concentration than the uncorrected profile (Table 4.3). Further improvement in the prediction was achieved by applying a correction factor $\left(V_R^*\right)_{L=15.7}/\left(V_R^*\right)_{L=5.3} = 0.72$ to the normalized peak retention volume as determined from Equation. 4.20, shifting the peak to earlier elution times (Figure. 4.14). (See Appendix 2 for more details)

Since the transition analysis was performed using ionic species which diffuse easily into the matrix pores compared to a large protein molecule such as an antibody, this correction factor is likely to be an underestimation of the actual correction required. The final prediction, taking into account differences in both in residence time and degree of dispersion per column volume, gives a significantly better prediction of the elution profile than the uncorrected ultra scale-down data (Table 4.3). To use the spreading of transitions of ionic species to account for the dispersion of the elution buffer front upstream of the column and the protein pulse on and downstream of the column is a practical approach. Finding more representative ways to correct for the dispersion of both the pH front, which leads to product elution, and the protein sample as it travels from the column to the fraction collector, warrants further investigation. Such work may in future lead to even better predictions of larger-scale columns.

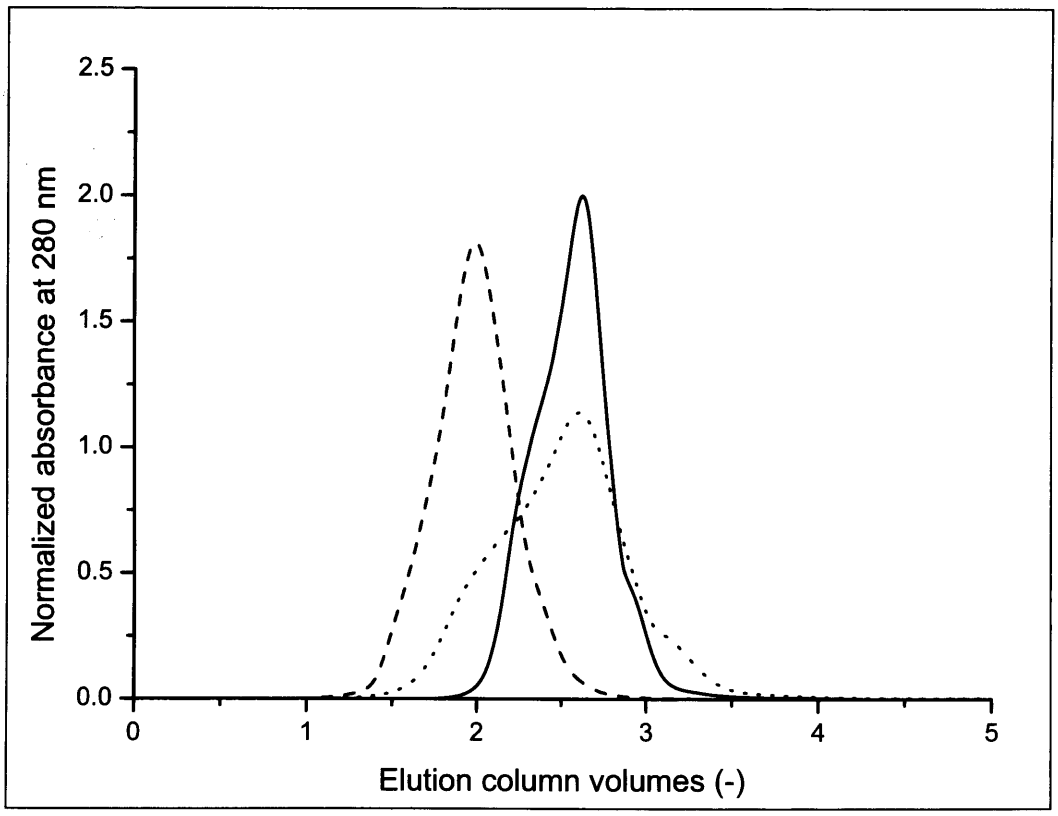

Figure 4.13. MAb elution profiles obtained at different scales and after correction for scale effects: Elution profiles obtained with an ultra scale-down column of 5.3 cm bed height and 0.5 cm diameter (dotted line), and a standard, laboratory-scale column of 15.7 cm bed height and 0.5 cm diameter (dashed line). The data from the ultra scale-down column were corrected (solid line) for extra-axial dispersion effects arising from greater relative extra-column volume.

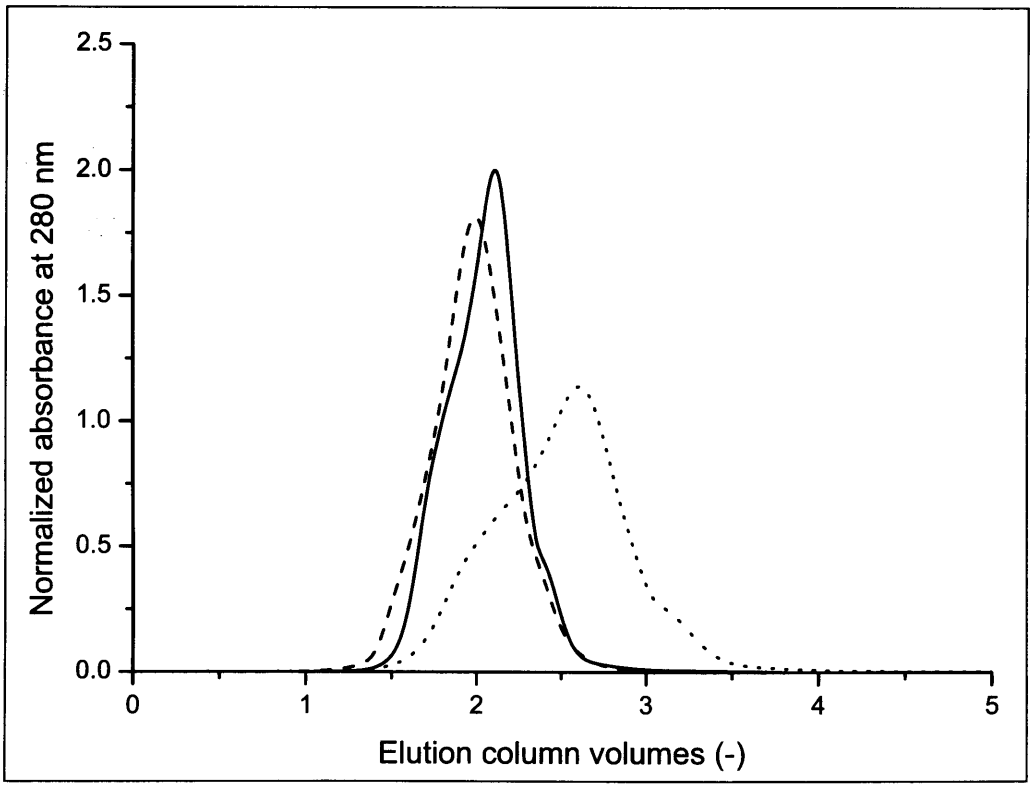

Figure 4.14. MAb elution profiles obtained at different scales and after correction for scale effects: Elution profiles obtained with an ultra scale-down column of 5.3 cm bed height and 0.5 cm diameter (dotted line), and a standard, laboratory scale column of 15.7 cm bed height and 0.5 cm diameter (dashed line). Prediction of laboratory scale peak profile (solid line) after further correction of the ultra scale-down peak for contribution of extra-column volume to retention volume.

Column	Column bed volume (mL)	Retention volume (Column Volumes)	Volume of elution peak (Column Volumes)
USD 1 5.3 cm x 0.5 cm *uncorrected*	1.0	2.6	2.3
USD 1 5.3 cm x 0.5 cm *corrected*	1.0	2.1	1.5
Lab scale 15.7 cm x 0.5 cm	3.1	2.0	1.5
USD 2 5.7 cm x 0.5 cm *uncorrected*	1.1	2.7	2.4
USD 2 5.7 cm x 0.5 cm *corrected*	1.1	2.1	1.7
Pilot scale 14.6 cm x 40.0 cm	18,346	2.1	1.6

Table 4.3. Separation performance at different scales, based on MAb elution profiles. The separation performance characteristics of the ultra scale-down (USD) columns are given before and after correction for scale effects. USD 2 and Pilot-scale elution profiles are given in Figure 4.18

Figure 4.15 shows the effect of increasing the linear flow rate (v) on the normalized total dispersion (σ^2_{total} *). The positive linear correlation over the flow rates investigated is in accordance with the Equation 4.1 in the region where mass transfer kinetics of the solute through the pores of the solid phase dominate in their contribution to band- or transition-broadening, in contrast to the effects of molecular diffusion or bed tortuosity. The p-value of less than 0.05 shows that the positive relationship is significant; however the low R^2 value indicates that, alone the linear flow rate variable explains only a small proportion of the variation in the normalized total dispersion.

The impact of increasing the linear flow rate from 61 cm/h to 150 cm/h on the elution profiles from the ultra scale-down column is shown in Figure 4.16. Making use of the linear correlation obtained from Figure 4.15, the expected elution profile for operation at 150 cm/h was predicted from the elution profile obtained at 61 cm/h, by applying a correction factor of 0.93 to reduce the variance of the peak dispersion. The results indicate that the use of the conductivity transition analysis method under-predicts the degree of elution peak broadening that occurs as a consequence of increasing flow rate. This may be due to the significantly different mass transfer characteristics used for low molecular weight ionic species of the conductivity measurements and the antibody macromolecules. The gradient of the least-squares best fit line is an inverse function of the molecular diffusivity of the analyte. As the low molecular weight buffer components have a high molecular diffusivity coefficient the increase in transition-broadening with flow rate is relatively small; however, as the antibody macromolecules have a significantly lower molecular diffusivity coefficient, broadening will be a stronger function of flow rate. Improved

predictions are likely to be observed should correction factors be determined by pulse experiments, at different flow rates, using non-interacting proteins or antibodies under non-binding conditions However, such experiments are significantly less convenient to run and are not part of a normal chromatography run.

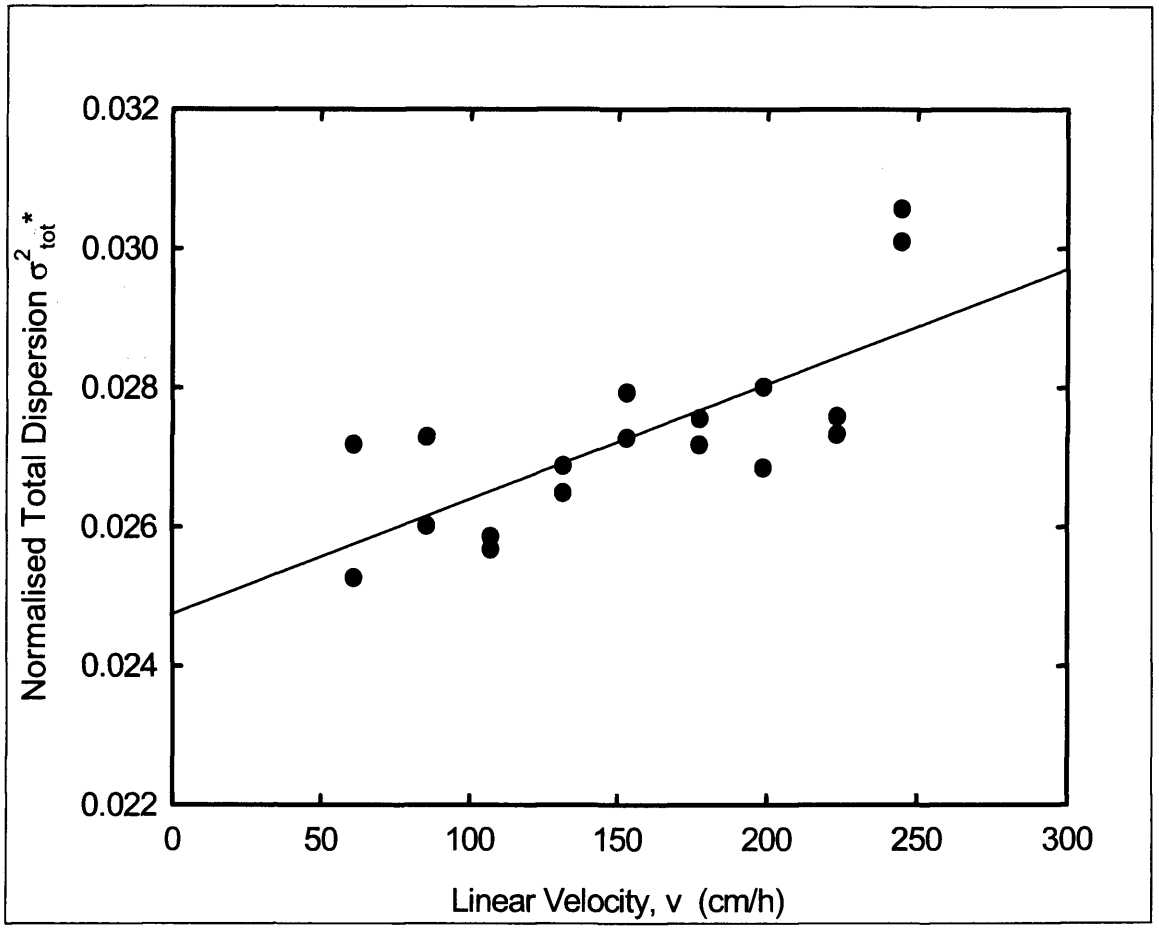

Figure 4.15 – Change in the normalized dispersion of the conductivity transition with linear flow rate. Data were obtained with the ultra scale-down column (5.3 x 0.5 cm) packed with rmp Protein A Sepharose 4 FF. The line is obtained from linear regression of data. The least-squares best fit line is defined by the equation, $\sigma^2_{total}* = 1.6x10^{-5}v + 0.025$, over the range of flow rates tested (R^2 = 0.40 , p = 0.009)

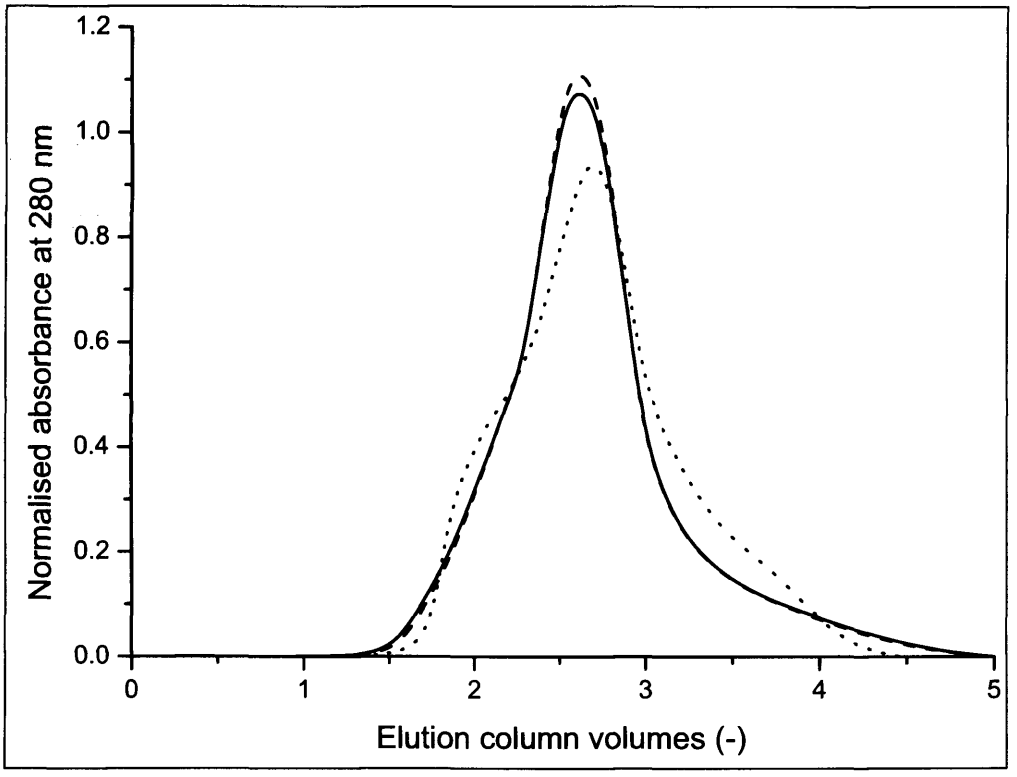

Figure 4.16. Correction of elution profile for the change in dispersion which occurs with change in flow rate. MAb elution profiles obtained with USD column 2 operated at 61 cm/h (dashed line) and 150 cm/h (dotted line). Prediction (solid line) of the elution profile at 150 cm/h, made by correcting the profile obtained at 61 cm/h by a factor of 0.93 determined using the data shown in Figure 4.15.

4.3.4 Comparison of ultra scale-down column with pilot-scale column

Normalized conductivity transitions obtained with an ultra scale-down column (column volume of 1.1 mL) and with a pilot scale column (18.3 L bed volume) are shown in Figure 4.17. The total normalized dispersion (σ^2_{total} *) for the ultra scale-down column was determined as 0.042 while that of the pilot-scale column was 0.009. The use of equation 4.22 to predict the total normalized dispersion for a laboratory column with bed height equivalent to that of the pilot-scale column, would give a total normalized dispersion of 0.014, 1.6-fold greater than that obtained experimentally. This highlights the need to take into account discrepancies between the relative extra-column volumes of two chromatography systems when scaling-up, and suggests that characterization of the chromatography system should be done directly on the relevant large-scale system. Figure 4.18 shows the effect of applying a correction factor to reduce the dispersion of the elution profile from the ultra scale-down column by 0.21, according to the ratio of the normalized total dispersion acquired from the transition analysis at the two scales (Figure 4.17). Further correction of the ultra scale-down column elution profile for the effect of the extra-column volume on retention volume was made, based on the transition data, reducing the retention volume by a factor of 0.74 (Figure 4.19).

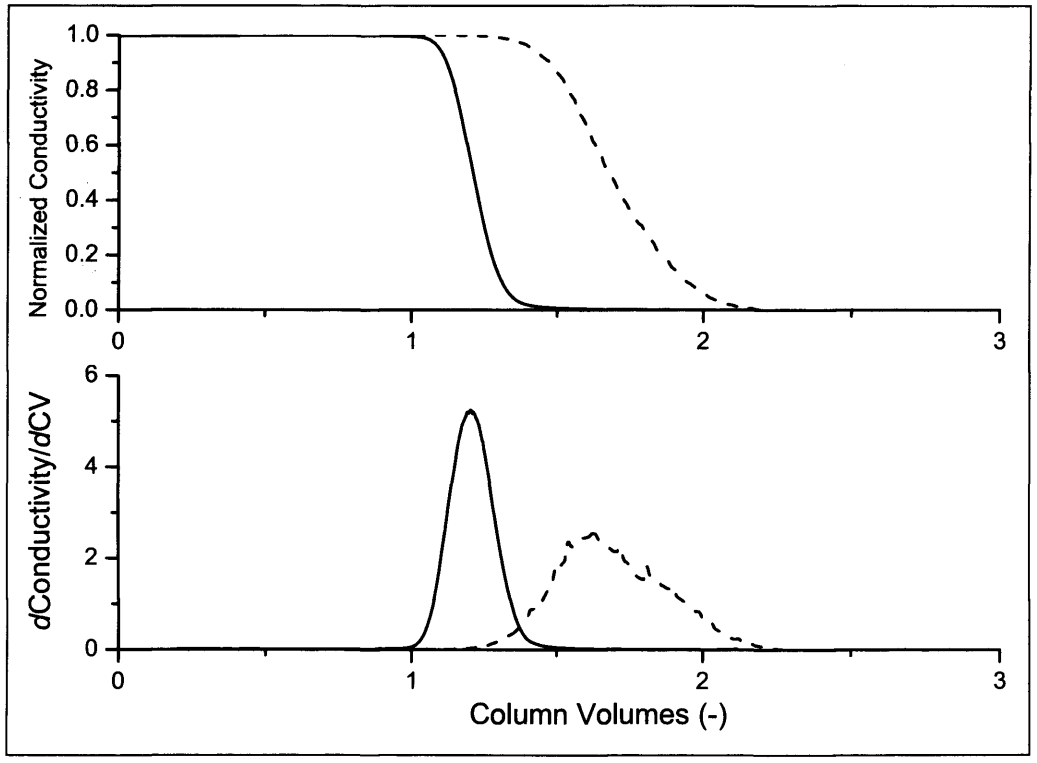

Figure 4.17. Conductivity transitions obtained from an ultra scale-down column (dashed line) (5.7 cm height, 0.5 cm diameter, 1.12 mL volume) and a pilot scale column (solid line) (14.6 cm height, 40.0 cm diameter, 18.3 L bed volume). Both columns were packed with Protein A sepharose 4 FF. The normalized total dispersion variance (σ^2_{total} *) of the transition are 0.042 and 0.009, for the ultra scale-down and pilot columns, respectively. A: normalized conductivity data; B: the first derivative of the conductivity data with respect to column volumes, giving an insight into the maximum rate of change and dispersion associated with each curve.

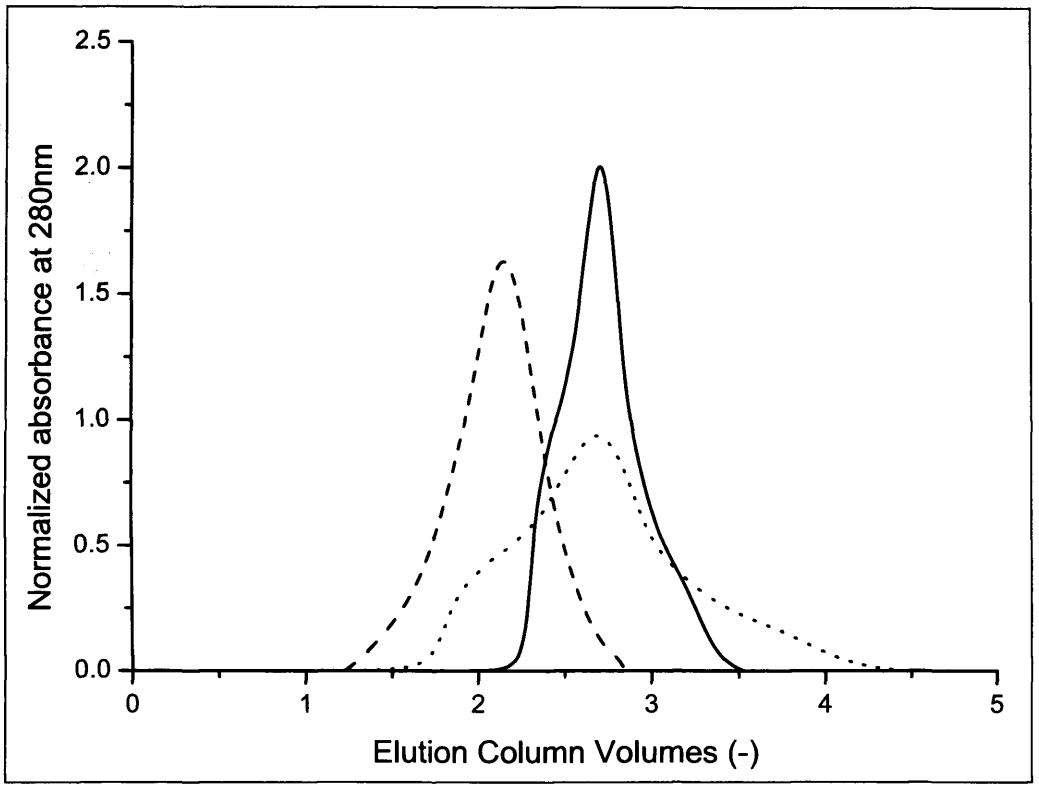

Figure 4.18. Prediction of pilot-scale antibody elution peak from elution data obtained with an ultra scale-down column. Elution profiles obtained with ultra scale-down column of 1.1 mL bed volume (5.7 cm height, 0.5 cm diameter) (dotted line), and a pilot-scale column of 18.3 L bed volume (14.6 cm height, 40.0 cm diameter) (dashed line). The ultra scale-down elution profile was corrected for dispersion effects to give prediction of pilot scale peak (solid line).

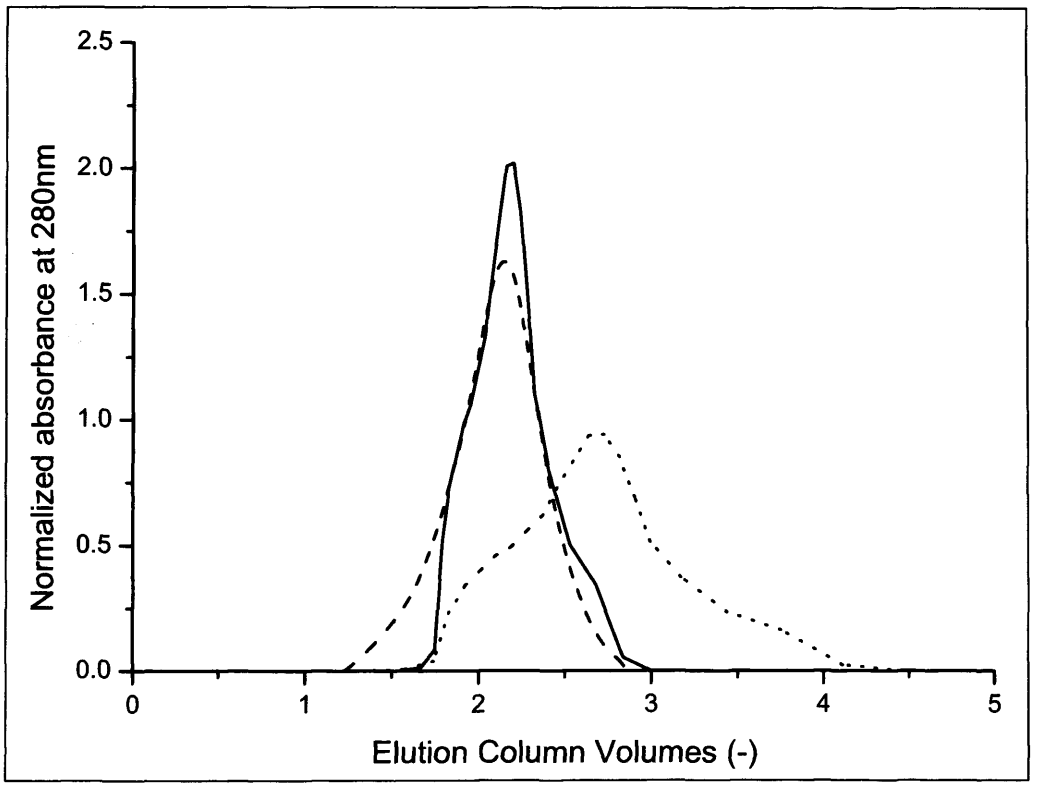

Figure 4.19. Prediction of pilot-scale antibody elution peak from elution data obtained with an ultra scale-down column. Elution profiles obtained with ultra scale-down column of 1.1 mL bed volume (5.7 cm height, 0.5 cm diameter) (dotted line), and a pilot-scale column of 18.3 L bed volume (14.6 cm height, 40.0 cm diameter) (dashed line). Ultra scale-down elution profile corrected for extra-column volume effects on residence time (solid line).

4.4 Conclusions

It has been shown, in this chapter, that it is possible to predict the elution profile of a monoclonal antibody from a pilot scale protein A chromatography column (18 L bed volume) based on data obtained with an ultra scale-down column (1 mL bed volume). Correction of peak profiles, to account for increased axial dispersion and solute retention times due to higher relative extra-column volumes in small columns, is necessary for accurate predictions. Conductivity transition tests can be used on columns at both scales to determine the necessary correction factors. If these corrections are not applied, lower maximum and average pooled product concentrations could be predicted for the elution peak at large-scale, with unexpected and undesirable consequences in large-scale operation, such as product instability at high concentrations.

The concern when using columns with narrow diameters such as the ultra scale-down column described in this chapter, is that the bed resin particles are supported by the column wall and therefore the bed does not undergo compression to the same extent as at the large-scale. For this reason, high flow rates achieved in a column with a narrow diameter can often not be used in a wide diameter column, because the hydrodynamic pressure drop across the bed would be excessively large and lead to equipment failure. A method by which flow rates proposed for the large-scale can be assessed prior to operation of the large-scale column is described in the next chapter.

Chapter 5 – The construction and use of a semi-empirical model for predicting scale-dependent chromatography bed compression and its use with ultra scale-down chromatography.

5.1 Introduction

Determining optimum elution flow rates, to maximize productivity without exceeding elution volume constraints (imposed by the capacity of the elution fraction collection vessel) is an important part of chromatography process development. In Chapter 4 the use of ultra scale-down chromatography techniques to predict the elution profiles from large scale chromatography columns over a range of flow rates was demonstrated. Operating flow rates determined at the laboratory-scale are frequently unachievable at the large scale due to the compressible nature of the highly porous agarose resins commonly used in preparative chromatography media. Increases in column diameter and the resultant loss in wall support lead to both greater resin compression and hydrodynamic pressure drops across the bed.

To make use of the ultra scale-down chromatography technique for predicting elution profiles, a method for identifying which elution flow rates are achievable at the large-scale is required. The work described in this chapter focuses on the use of a published semi-empirical model that can be used in conjunction with ultra scale-down chromatography techniques, to ensure that operating parameters determined with the small-scale column will be achievable at the large scale.

The compression of packed beds is affected by friction between the wall and the bed particles and internal friction between particles in the bed. In the past, models to predict bed compression have been based on force balances, while

accounting for the varying contributions of friction; however, the number of variables to be defined makes their application complicated (Colby *et al.*, 1996; Soriano *et al.*, 1997). Empirically derived models exist and are easier to use; however, many empirical models cannot predict the effect of decreasing bed height with flow-induced compression (Mohammad *et al.*, 1992). The objective of this study was to experimentally determine the parameters required for the use of an empirical model to predict the pressure drop in compressible packed beds, at varying scales. The research uses a semi-empirical method to predict decreasing bed height with compression, which is less complex than non-empirical solutions (Stickel and Fotopoulos, 2001).

The parameters of linear flow velocity, pressure drop and bed height are co-dependent. For the purpose of constructing this model it was assumed that linear flow velocity is an independent variable. Increases in linear flow velocity lead to an increase in the fluid drag on the packed particles and cause bed compression (λ). Bed compression is defined by the equations:

$$\lambda = \frac{V_{co} - V_c}{V_{co}}$$

$$\lambda = \frac{L_o - L}{L_o} \qquad \text{Equation 5.1}$$

where V_c is the packed bed volume at bed height L, V_{co} is the gravity-settled bed volume and L_o is the gravity-settled bed height. Bed compression must lead to a decrease in interstitial bed porosity (ε) and reduced permeability, as defined by the following relationship (Stickel and Fotopoulos, 2001):

$$\varepsilon = \frac{\varepsilon_o - \lambda}{1 - \lambda} \qquad \text{Equation 5.2}$$

where ε_o is the gravity settled bed porosity. The observed increase in pressure drop is a result of both increased fluid velocity and reduced bed permeability. At a critical flow velocity (u_{cri}), an increase in pump speed leads to an increase in bed compression but no increase in linear flow velocity. Hence, the critical bed compression (λ_{cri}) is defined by the formula:

$$\lambda_{cri} = \frac{L_o - L_{cri}}{L_o} \qquad \text{Equation 5.3}$$

where L_{cri} is the bed height at the critical point. Increases in pressure drop beyond the critical point are as a result of decreasing permeability alone, as the linear flow velocity does not increase. It has been observed that bed compression plotted as a function of linear flow velocity shows an approximately linear relationship, described by the following equation (Stickel and Fotopoulos, 2001):

$$\frac{\lambda}{\lambda_{cri}} = \frac{u}{u_{cri}} \qquad \text{Equation 5.4}$$

It has also been observed that λ_{cri} does not vary significantly with aspect ratio, implying that this parameter is material-specific and unaffected by wall support. λ_{cri}, therefore, provides an indication of the magnitude of change in bed height that a packed bed undergoes as the critical velocity is approached (Stickel & Fotopoulos, 2001).

5.1.1. Correlation between column aspect ratio and medium compressibility: It has been previously shown (Stickel & Fotopoulos, 2001) that the critical velocity can be correlated with bed height and column diameter by plotting the term $u_{cri}L_o$ as a

function of the column aspect ratio (L_o/D) and that the relationship is linear (Stickel & Fotopoulos, 2001). This permits the use of the empirical correlation:

$$u_{cri}L_o = m\left(\frac{L_o}{D}\right) + b \qquad \text{Equation 5.5}$$

where m and b are empirical constants, determined by linear regression. The empirical constant b is the value of $u_{cri}L_o$ for an infinite diameter column and provides, therefore, a numerical indication of the compressibility of the medium under a given set of operating conditions. The slope m indicates the changing wall support with scale.

5.1.2 Modeling Pressure-Flow Profiles. The Blake-Kozeny equation can be used to describe the pressure drop across packed beds of rigid particles under laminar flow (Geankoplis, 1993):

$$\Delta P = \mu \frac{K_o}{d_p{}^2} \frac{(1-\varepsilon)^2}{\varepsilon^3} L.u \qquad \text{Equation 5.6}$$

where μ is fluid viscosity, d_p is the particle diameter and K_o is an empirical constant. The model assumes both constant bed height and porosity which is not the case for systems involving compressible media. The use of Blake-Kozeny equation is, however, justified as bed height and porosity can be correlated to the linear flow velocity. Of the material properties, particle diameter and critical bed compression were found experimentally whilst porosity values were obtained from the literature (Stickel & Fotopoulos, 2001).

5.1.3. Calculation Methodology. For a given column geometry the critical velocity, u_{cri}, is determined using Equation 5.5. During packing at any given linear flow rate the bed compression can be calculated using Equation 5.4. Subsequently, this value

can be used in Equations 5.1 and 5. 2 to determine values for bed height and bed porosity at that flow velocity. These values, along with the structural properties of the media and the viscosity of the liquid phase, can be used in the Blake-Kozeny equation (equation 5.6) to predict the pressure drop for a given linear flow velocity. A predicted pressure-flow curve can be generated by repeating the procedure over a range of linear flow velocities, until the critical velocity is reached, beyond which the empirical correlation for compression as a function of fluid velocity is no longer valid.

5.2 Materials and Methods

5.2.1. Equipment. A transparent laboratory-scale column (model XK26, Amersham Biosciences, Piscataway, NJ) with adjustable length and an inner column diameter of 26 mm, was used. Analogue pressure gauges mounted on the column inlet and outlet, were used to measure pressure drops across the bed. Either (i) the peristaltic pump and pulse dampener of an AKTA Prime system were used to pump buffer through the column in order to achieve stable pressure and flow rate readings or (ii) compressed air was used to overpressure buffer from a 10 L pressure canister through the column. A 25 mL measuring cylinder and a stop watch were used to measure column effluent flow rates and a ruler used to measure packed bed heights (Figure 5.1).

A particle size analyzer (Mastersizer, Malvern Instruments, Southborough, MA) was used to verify the particle size distribution of the chromatography media.

5.2.2. Chromatography Media. The resin used in this study was rmp Protein A Sepharose 4 Fast Flow (Amersham Biosciences, Sweden).

5.2.3. Procedures. 20% ethanol, 50 mM glycine-glycinate, 250 mM sodium chloride, pH 8.0 and 6 M guanidine hydrogen chloride were used as mobile phases and recycled through the column during packing and operation. In each case the buffers were allowed to equilibrate to room temperature (22 °C) prior to the commencement of experiments. A pressure-flow rate profile was generated for the empty column and associated equipment prior to packing (Figure 5.2). This curve was subsequently used to subtract equipment pressure drop from the total pressure drop to determine the pressure drop across the packed bed alone. All pressure-flow profiles shown have been corrected for the equipment pressure drop.

Prior to packing, the slurry concentration, in terms of gravity-settled medium, was determined by centrifuging 10 mL samples of slurry for 5 minutes at 4000rpm in an ALC centrifuge PK120 with soft acceleration and deceleration.

For each experiment, a measured volume of slurry was poured into the column and allowed to settle under gravity. To generate a packing pressure-flow curve, the top adapter was left fully raised and an initial pressure drop of less than 4 x 10^4 Pa was maintained across the column for a minimum of 0.5 h to allow the flow rate and bed height to equilibrate, before inlet pressure, outlet pressure, flow rate and bed height were recorded. The pump speed or air pressure (as appropriate) was then increased to achieve an incrementally greater pressure drop and a further 0.5 h allowed before measurements were retaken. This process was repeated until a very large change in pressure resulted from a small change in pump speed or until consistent flow rates were observed despite an incremental increase in air pressure to

the pressure canister. A summary of all columns discussed in this chapter is given in Table 5.1.

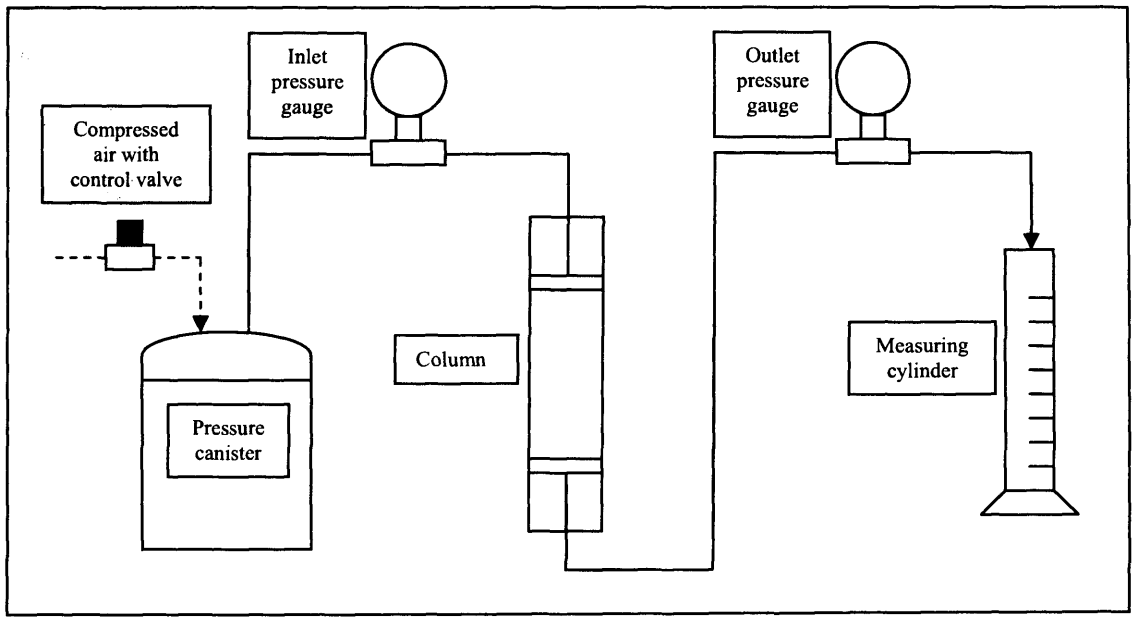

Figure 5.1. Schematic diagram of the experimental set-up for generating the pressure-flow curves.

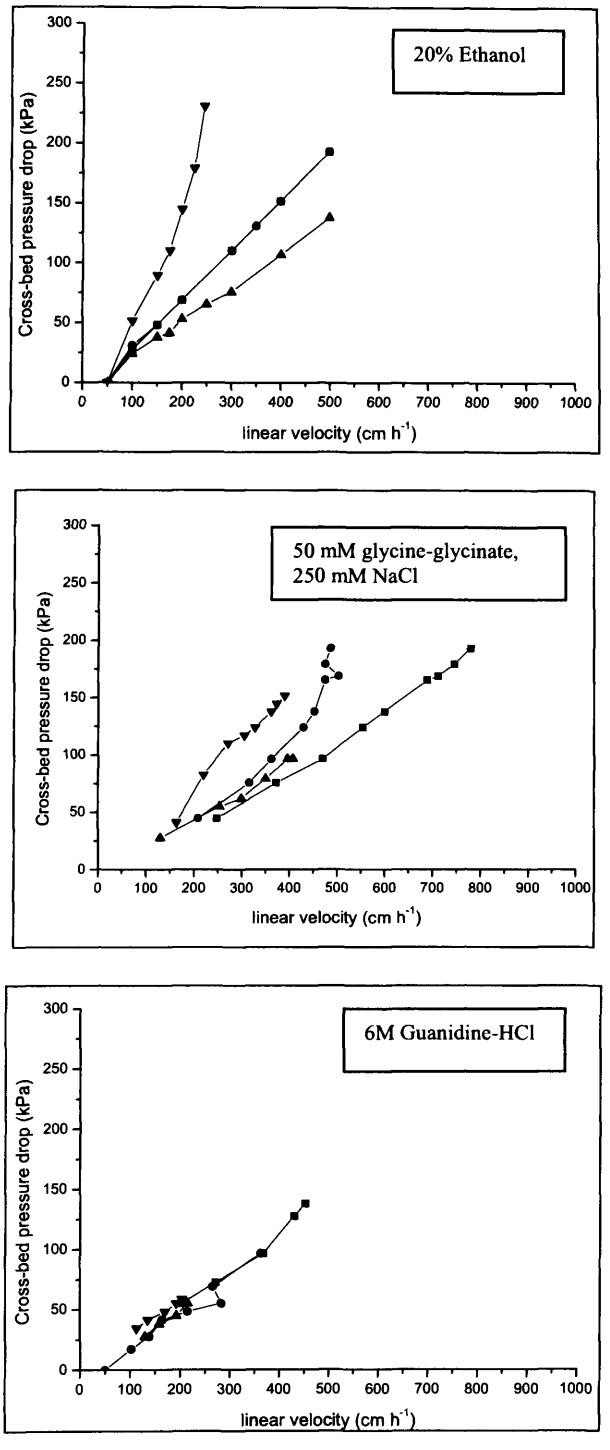

Figure 5.2. Equipment pressure-flow profiles for four different initial bed heights. Column diameter is 26 mm. Packing buffers are indicated on the figure annotation. (■) 80 mm bed height; (●) 150 mm bed height; (▲) 300 mm bed height; (▼) 450 mm bed height.

Bed height (cm)	Diameter (cm)	Volume (mL)	Aspect Ratio	Use
8	2.6	42.5	3.1	Emperical constant determination
15	2.6	79.6	5.8	Emperical constant determination
30	2.6	159.3	11.5	Emperical constant determination
45	2.6	238.9	17.3	Emperical constant determination
5	0.5	1.0	10.0	USD - model prediction
15	40	18,849.6	0.4	Pilot - model prediction
15	200	471,238.9	0.1	Production - model predition

Table 5.1. Summary of columns used in this chapter

5.3 Results

Figures 5.3, 5.4 and 5.5 show pressure-flow profiles for the three different liquid phases for packed beds of the same diameter but different heights. The non-linear profiles are characteristic of compressible media. The linear flow velocities were increased beyond the upper limits shown; however, this led to increases in cross-bed pressure drop above 4.2×10^5 Pa at which point the matrix permanently deforms. As the pressure across the bed did not reach equilibrium, a pressure reading could not be taken and hence the data are not shown. The linear flow velocity at which the slope of the curve becomes infinite is defined as the critical velocity and is the highest achievable steady-state flow velocity for a packed bed under a given set of conditions. Lower critical velocities imply greater compression and the data confirm observations that shallow beds are more stable than tall beds (Soriano *et al.*, 1997).

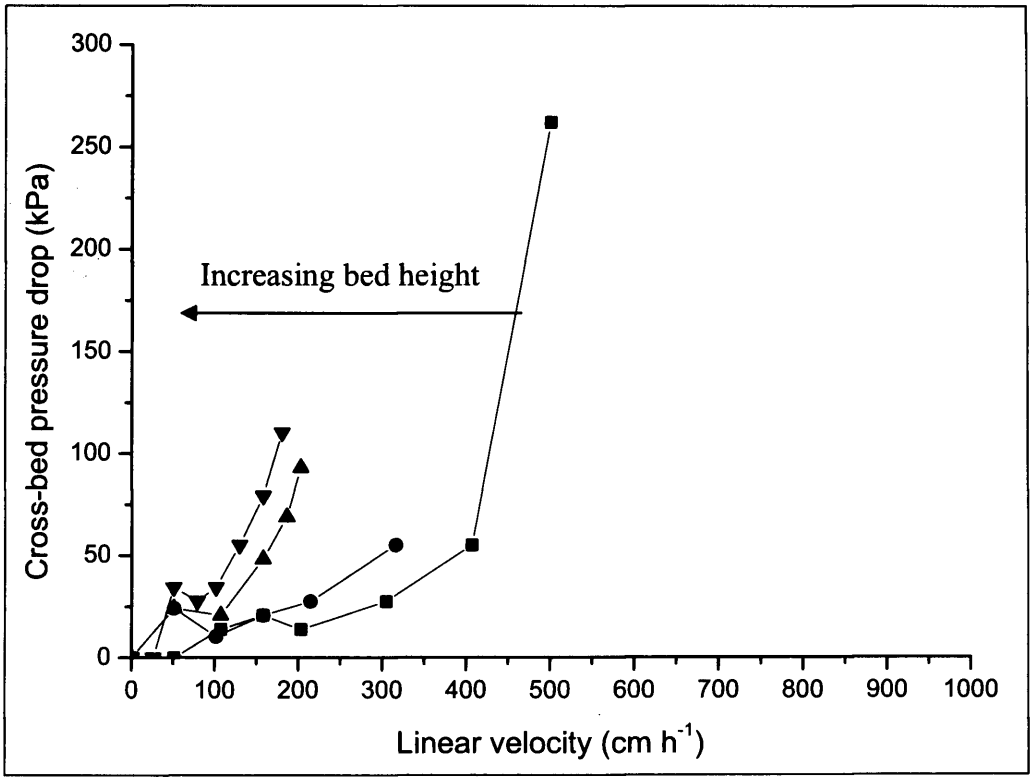

Figure 5.3. Pressure-flow profiles for four different initial bed heights. Column diameter is 26 mm. Packing buffer is 20% ethanol at 22°C. (■) 80 mm bed height; (●) 147 mm bed height; (▲) 306 mm bed height; (▼) 444 mm bed height.

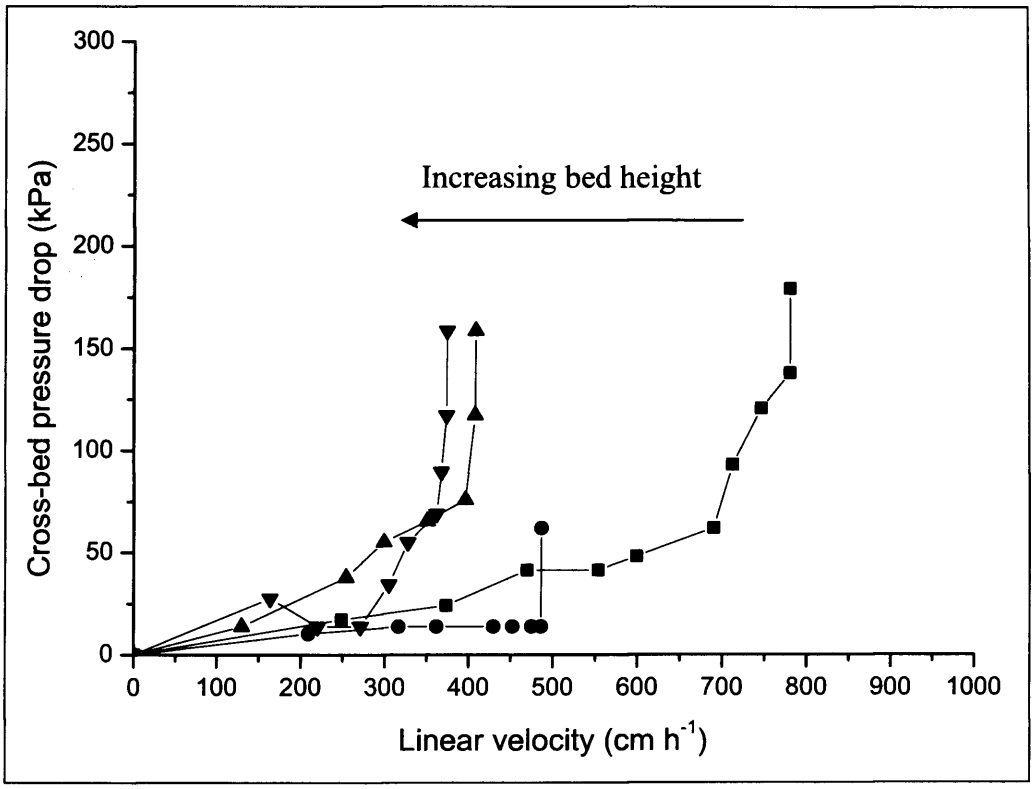

Figure 5.4. Pressure-flow profiles for four different initial bed heights. Column diameter is 26 mm. Packing buffer is 50 mM glycine-glycinate, 250mM sodium chloride, pH 8.0 at 22°C. (■) 79 mm bed height; (●) 147 mm bed height; (▲) 290 mm bed height; (▼) 455 mm bed height.

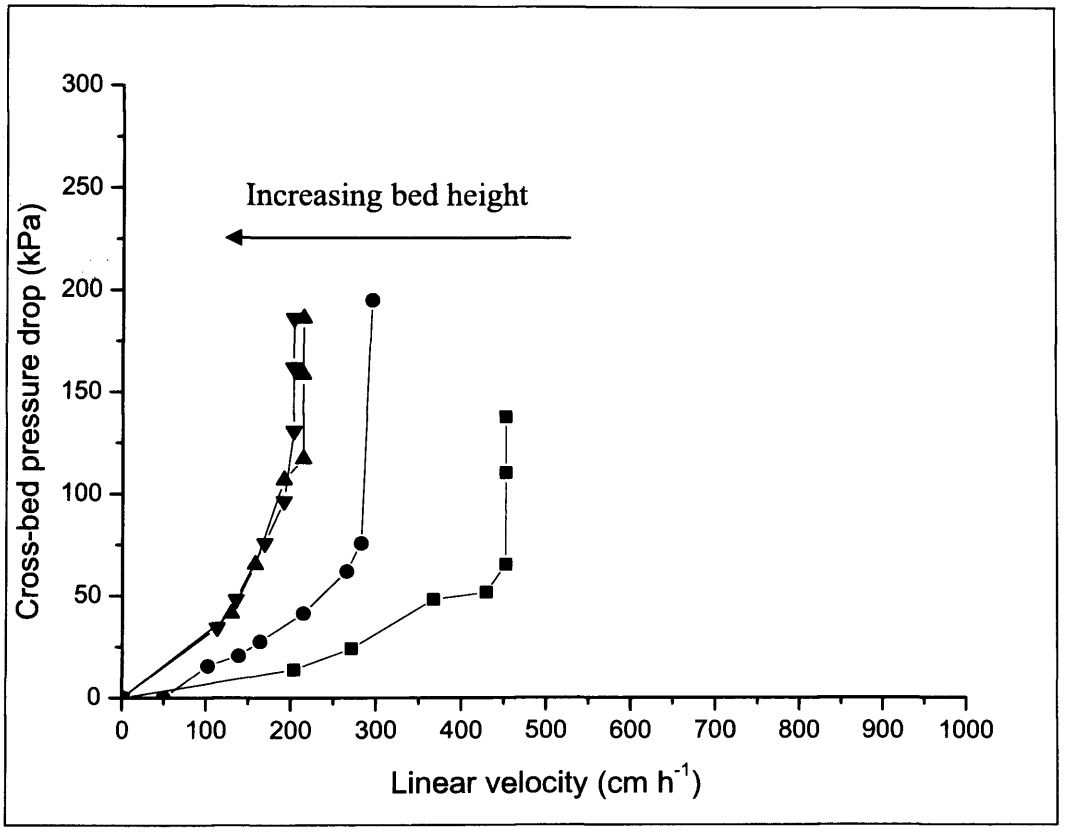

Figure 5.5. Pressure-flow profiles for four different initial bed heights. Column diameter is 26 mm. Packing buffer is 6M guanidine hydrogen chloride at 22°C. (■) 78 mm bed height; (●) 150 mm bed height; (▲) 305 mm bed height; (▼) 445mm bed height.

The variations in critical velocities over the range of bed heights studied for each of the liquid phases can be seen in Figure 5.6. The critical velocities for 50 mM glycine-glycinate, 250 mM sodium chloride, pH 8.0, at different bed heights, are greater than those for both 6M guanidine hydrogen chloride and 20% ethanol primarily due to the lower viscosity of the glycine-glycinate, sodium chloride (see Table 5.2). 20 % ethanol has a higher viscosity than the 6M Guanidine-HCl yet the model predicts higher critical velocities at the same flow rate. The difference in the viscosities of the two fluids is not sufficiently great to be detected by the accuracy of the analogue pressure gauges using only the single measurements taken during these experiments. Figure 5.6 demonstrates that care must be taken when using columns with reduced bed heights for developing purification processes as taller columns used in manufacturing cannot be operated at similarly high flow rates.

The method of determining the empirical constants for the model by linear regression is illustrated in Figure 5.7. The empirical constant b shown in Table 5.2 is the value of $u_{cri}L_o$ for an infinite diameter column; hence, large values indicate that the mobile phase will compress the chromatography bed to a lesser extent. It may be expected that as the viscosity increases, $u_{cri}L_o$ decreases due to viscous drag. It should be noted that all experiments were performed with columns of the same diameter and that the column aspect ratio (L_0/D) was varied by changing the bed height, L_0. However, the slope m implies changing wall support with scale and the shallow gradient suggests that the shift in pressure-flow profiles between columns with different diameters may not be particularly pronounced. Table 5.2 also shows the R^2 values for the least squares best fit line. All values are greater than 0.99

indicating that almost all the variation in the independent variable is described by the regression model.

Figure 5.8 shows that the model predicts different bed structures for the ultra scale-down and large-scale column. The model used for these predictions was constructed using the empirical constants determined for 50 mM glycine-glycinate, 250 mM sodium chloride. The figure shows that both large-scale columns are more compressed at the same linear flow rates than the ultra scale-down column and that the bed void fractions are lower. This is a consequence of the different bed heights and reduced wall support for the matrix. It may be imagined that such differences in bed structure would lead to differences in column performance between the ultra- and the large-scales. For example, if the resin particles are more densely packed in the large-scale columns, it would seem likely that the capacity of the column per unit volume would be higher as more ligand per unit volume must be present. A reduced column void fraction might also imply greater interstitial linear velocities and, in turn, altered mass transfer characteristics in chromatography beds at the large-scale. Determining if such changes in bed structure with scale affect column performance is a subject for future investigations. The results of such investigations may even allow for a greater refinement of the process for correcting data from the ultra-scale to predict performance at the large-scale.

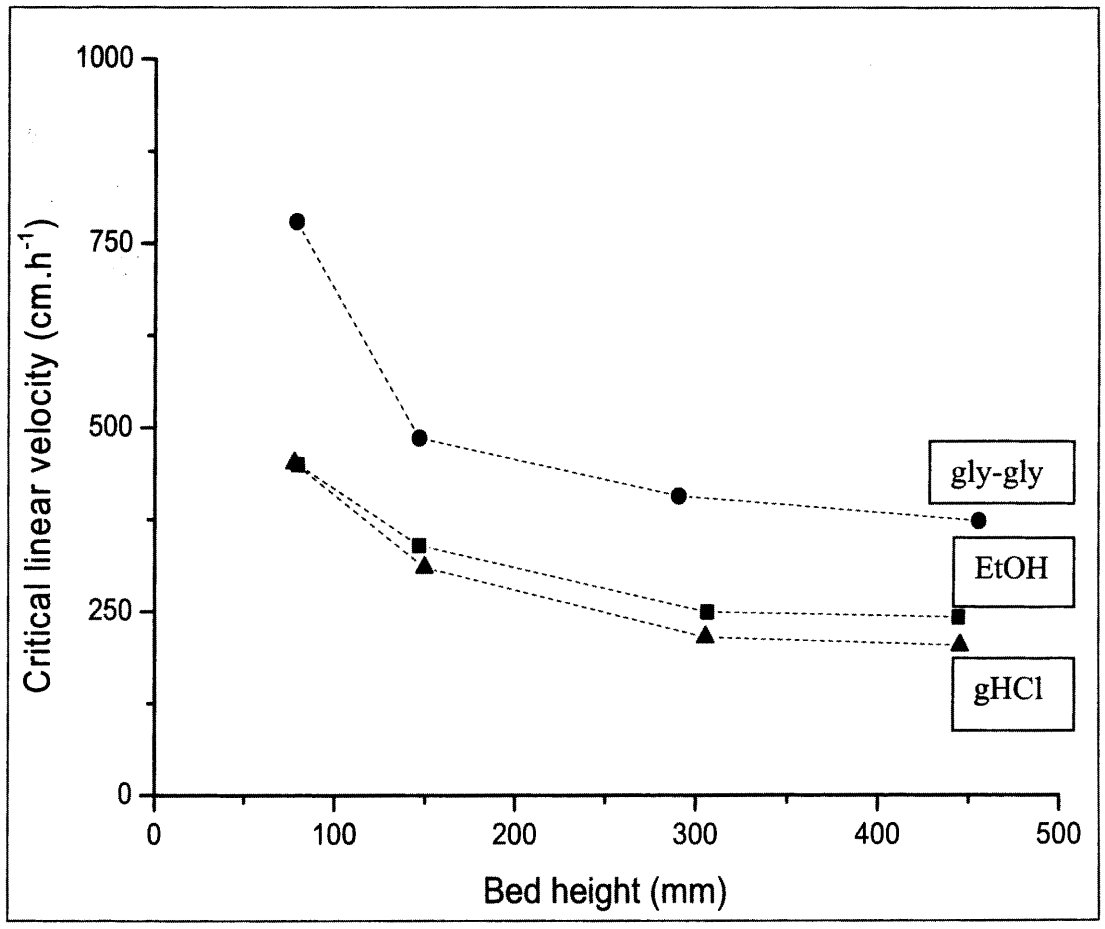

Figure 5.6. Critical linear velocities for four different bed heights in a 26 mm diameter column at 22 ^{0}C, for three different buffers, (■) 20% ethanol, (●) 50 mM glycine-glycinate, 250mM sodium chloride, pH 8.0, (▲) 6 M guanidine hydrogen chloride.

Medium	Mobile Phase	viscosity (*cP*) at 23 ^{0}C	*m* (cm^2/h)	*B* (cm^2/h)	R^2
Sepharose 4FF	20% ethanol	2.24	500	2050	0.99
Sepharose 4FF	50mM glycine-glycinate, 250mM sodium chloride, pH 8.0	1.40	770	3320	0.99
Sepharose 4FF	6M guanidine hydrogen chloride	2.02	383	2350	0.99

Table 5.2 Mobile phase viscosity values and empirical constants for critical velocity correlation. The slope, *m*, intercept, *b*, and coefficient of determination, R^2, refer to the linear regressions shown in Figure 5.6.

Medium	d_p (μm)	ε_o	λ_{cri}
Sepharose 4FF	96	0.41	0.21

Table 5.3. Structural properties of Sepharose 4FF

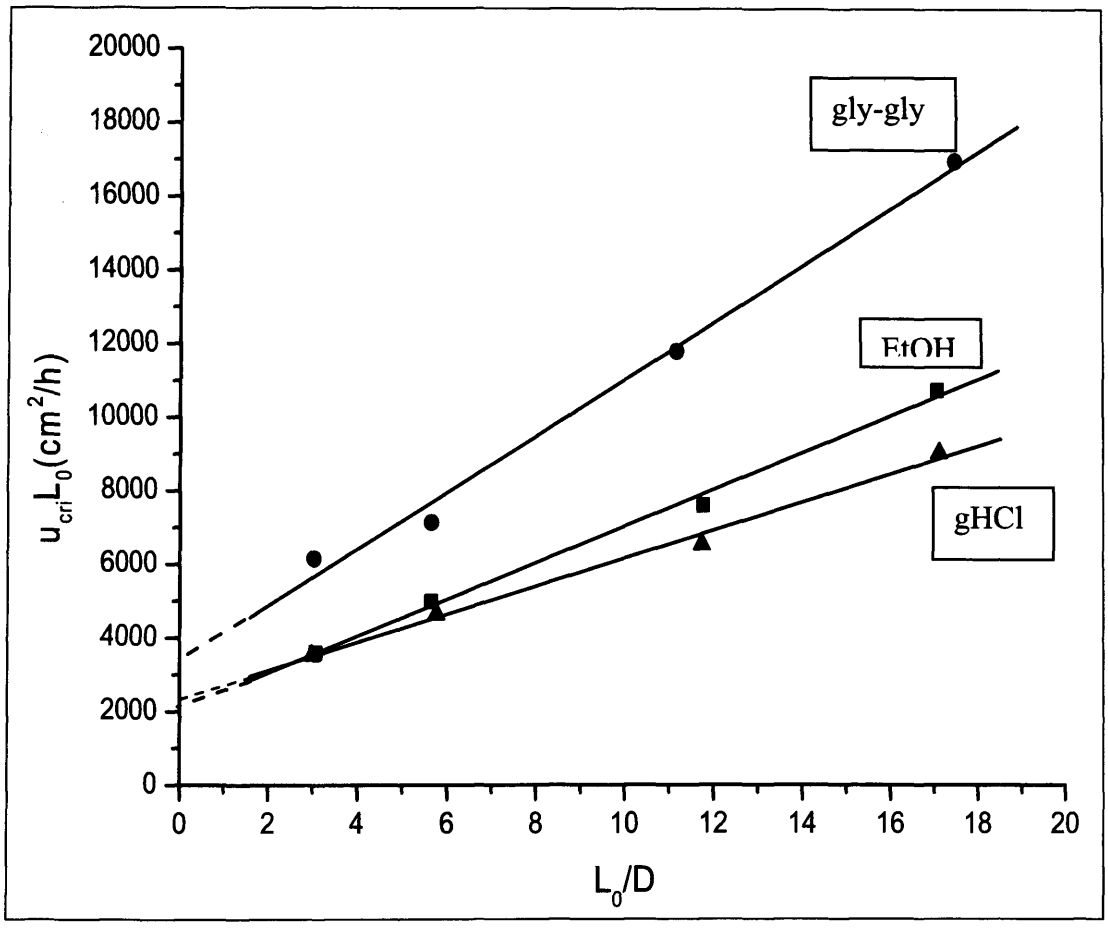

Figure 5.7. Experimental data for determining the empirical constants *m* and *b* (see Table 5.2) for Sepharose 4FF matrix at 22 ^{0}C with three different buffers, (■) 20% ethanol, (●) 50 mM glycine-glycinate, 250 mM sodium chloride, pH 8.0, (▲) 6 M guanidine hydrogen chloride according to equation 5.5.

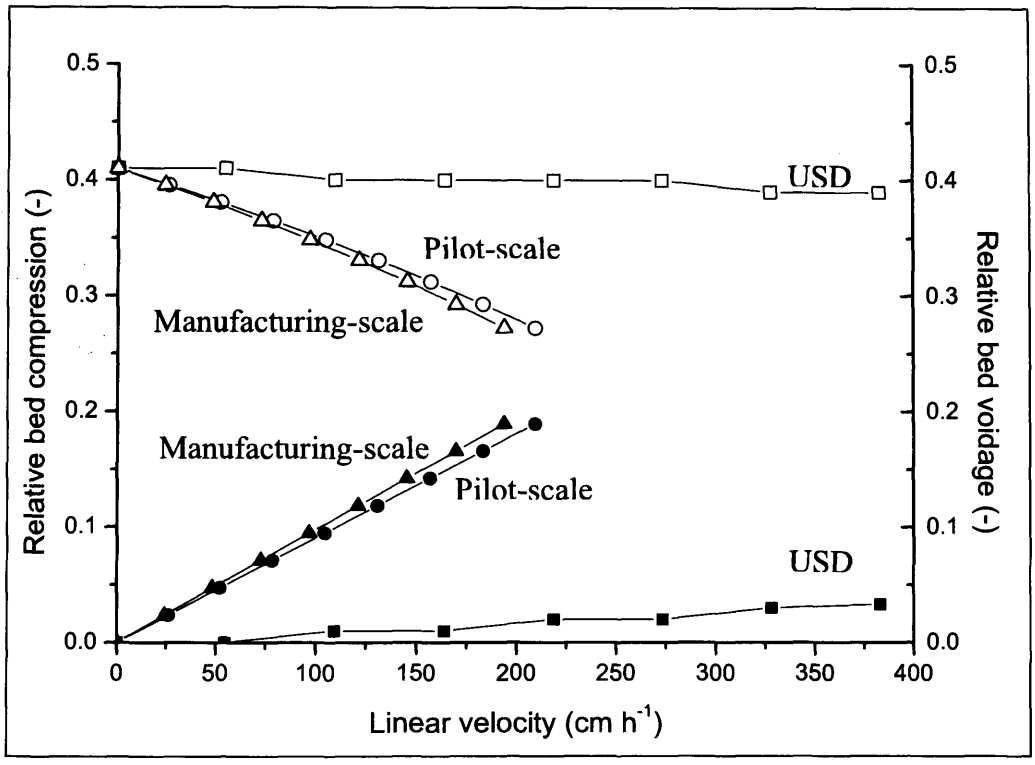

Figure 5.8. The effect of changing scale on the structure of the chromatography bed packed with Sepharose 4FF. Model predictions of the degree of bed compression over a range of linear flow rates for; (■) the ultra scale-down column (0.5 x 5 cm); (●) 400 mm diameter pilot column; (▲) 2000 mm diameter manufacturing scale column. The bed voidage as a function of flow rate is given by; (□) ultra scale-down column; (○) 400 mm diameter pilot column; (△) 2000 mm diameter manufacturing scale column. Both pilot and manufacturing columns have a bed height of 15 cm. The model used to generate the predictions was constructed using the empirical constants *m* and *b* determined for 50mM glycine-glycinate, 250mM sodium chloride (Table 5.2.)

Model predictions for bed heights and cross column pressure drops over a range of linear flow rates, for the ultra scale-down column, the 400 mm diameter pilot column and a 2000 mm diameter manufacturing scale column are shown in Figure 5.9. Greater cross-column pressure drops are predicted for the large-scale columns due in part to the taller beds but also significantly from the loss in wall support for the bed as the diameter is increased. It might have been expected that the influence of decreasing wall support would be negligible above a diameter of 400 mm and therefore it is of interest that the model predicts a slightly lower pressure-flow profile and higher bed height for the pilot than for the industrial-column, at equivalent linear flow rates. It is also noteworthy that the decrease in bed height with increasing linear flow rate in the two large scale columns is greater than that of the ultra scale-down column. The results show the potential danger of using an ultra scale-down column for the development of large scale processes. It is evident from the predictions that an ultra scale-down column can be operated at significantly higher flow rates than either the pilot- or manufacturing-scale columns. The predictions show that an ultra scale-down column can be operated at linear flow rates beyond 350 cm h^{-1} with no significant increase in cross-column pressure drop or decrease in bed height. Both the pilot and manufacturing columns would be inoperable above a linear flow rate of 250 cm h^{-1} because the pressure drops across the beds would be too great and would lead to equipment failure. This would not have been predicted by the ultra scale-down column highlighting the need for a 'toolbox' of methodologies and equipment including mathematical models for the development of processes at the ultra-scale.

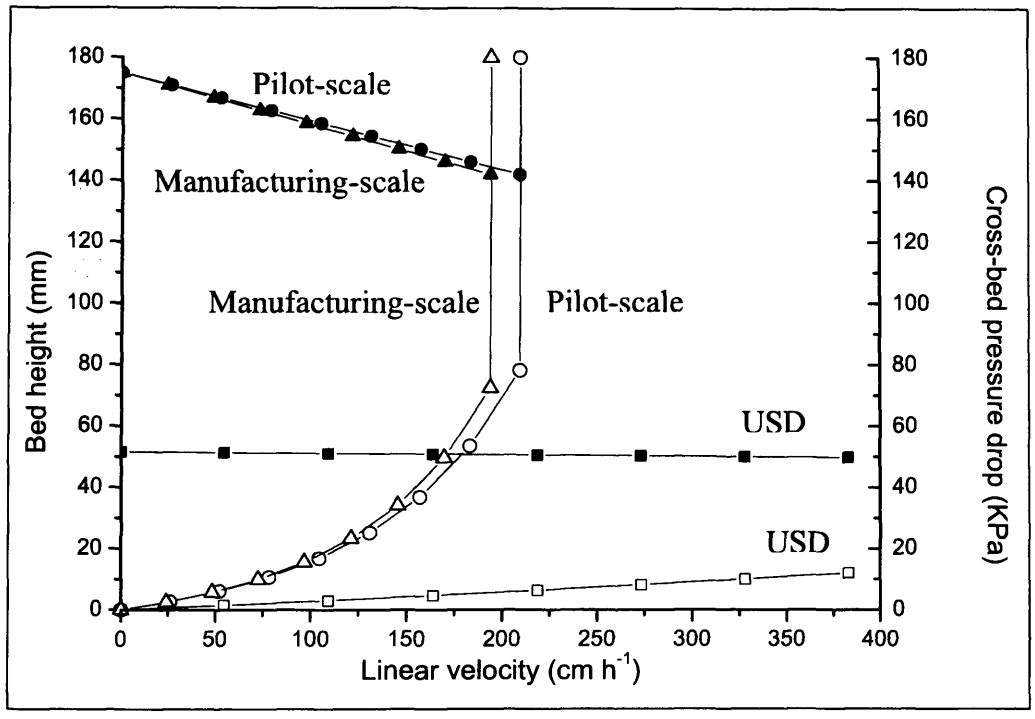

Figure 5.9. The impact of increasing scale, from the ultra scale-down to the pilot-scale and industrial-scale, on the operability of chromatography columns packed with Sepharose 4FF. Model predictions of bed heights over a range of linear flow rates for (■) the ultra scale-down column; (●) 400 mm diameter pilot column; (▲) 2000 mm diameter manufacturing-scale column; and the cross-bed pressure drops for (□) the ultra scale-down column; (○) 400 mm diameter pilot column; (△) 2000 mm diameter manufacturing scale column, over the same linear flow rates. The model used to generate the predictions was constructed using the empirical constants *m* and *b* determined for 50mM glycine-glycinate, 250mM sodium chloride (Table 5.2).

5.4 Conclusions

Relationships have been determined that allow pressure drops to be predicted in columns of different heights and diameters packed with Sepharose 4FF. The model has been used with three different chromatography buffers. At any given flow rate the degree of bed compression, bed height and bed porosity can be predicted. Verification of the model is provided in the literature and so has not been included in this study (Stickel & Fotopoulos, 2001).

Results from the model show that the bed structure of ultra scale-down columns and large-scale columns will be different at equivalent linear flow rates. Structural differences may lead to differences in separation performance and will require further investigation. The results of studies on the effects of bed compression on column performance may further enhance our ability to accurately predict chromatographic behaviour at the large-scale from data derived from the ultra-scale.

Significantly, it has been shown that high flow rates accessible at the ultra-scale can not be applied at the large-scale due to matrix compression caused by the loss of wall support at increased column diameters. The model generated by this work is a useful tool that must be used alongside the ultra scale-down column to allow the development of operable chromatography processes capable of delivering the required performance.

Chapter 6 –Discussion

6.1. Conclusions

Laboratory-scale experiments are likely to play an important role in the development of large-scale bioprocesses. Conventional scaling rules (Doran, 1994), such as increasing chromatography column diameter while maintaining bed height and linear flow rate, impose a limit both on the amount of data that can be collected (and, hence on the degree to which a process can be optimized in the limited time available) and on the minimum amount of material required to conduct such studies. Novel techniques allowing more rapid process development with small volumes of process material are required. To this aim the following have been reported in this thesis,

- mimicking the clarification performance of continuous, pilot-scale centrifuges using an ultra scale-down technique requiring a few hundred millilitres of process material. Results showed that the performance of both a soft- and normal-feed centrifuge could be predicted by adjusting the conditions within a rotating-disc device designed to mimic the hydrodynamic environment of the continuous centrifuge feed-zone.
- demonstration of the comparability between the large- and ultra scale-down centrifuge supernatant and product.
- development of a centrifugation, windows of operation visualisation tool to allow process design decisions to be made readily from ultra scale-down data.

- verification of the ultra scale-down centrifugation technology by comparison of predictions with the performance of a manufacturing-scale, disc-stack centrifuge, used to harvest a 20,000 litre cell culture bioreactor.
- development of a technique to adjust elution profiles for extra-column zone broadening when using scaled-down columns with reduced bed heights.
- addition of an existing model to the scaled-down chromatography toolbox to facilitate their scale-up and suggest future investigations to improve predictions.

6.2 Discussion and recommendations for future work

6.2.1. Ultra scale-down centrifugation

In this thesis the ultra scale-down centrifuge methodology in which the rotating-disc device mimics hydrodynamic conditions in the feed zone of the large-scale centrifuge has been successfully applied to the development of centrifugation processes, for the clarification of mammalian cells from two therapeutic monoclonal antibody processes, at two different scales (Chapters 2 & 3). On the basis of this success it is worth considering issues governing the uptake of the technology. The design of the rotating-disc device is now at the point where it can be developed beyond a prototype. For use in a commercial environment a reliable and reproducible method for charging the chamber with liquid, while ensuring the exclusion of air is required; robust sealing of the chamber at the point at the impeller shaft bearing is also essential. In addition, software would be needed for the relatively complex calculations required to determine the operating conditions of the laboratory

centrifuge and the rotating-disc device. More trials would be required to help verify that the technique can be used to predict accurately centrifuge performance with different cell lines and cell culture processes.

6.2.1.1. Future uses of ultra scale-down centrifuge technology

The biopharmaceutical industry seeks to invest in research aimed at increasing cell culture product titres, to give increasingly productive manufacturing processes. Ultra scale-down methods can be used to evaluate the effect of associated cell culture changes on product recovery. Although the economic value of using ultra scale-down methods is difficult to determine and outside the scope of this thesis, an ultra scale-down centrifuge tool can be utilized to yield a real a benefit. For example, shortening the duration of cell culture by early harvesting could be effective if product quality deteriorates towards the end of a fermentation. Ultra scale-down centrifugation would be ideal for assessing the impact of this change on clarification processes, and without the need for expensive large-scale cell culture fermentations of varying dilutions; samples could be harvested from a single fermentation at different times and run in the scaled-down centrifuge.

In the time between the centrifuge experiments reported here which were carried out on the NS0 cell line 6A1(100)3 and the completion of this thesis the proportion of processes utilizing NS0 cell lines has decreased and the proportion using CHO cell lines has increased. CHO fermentations typically maintain and are harvested at higher cell viabilities than NS0 fermentations. Although the data presented in Table 2.1 showed that there was no significant shear-related release of impurities from NS0 cells this could be due to the low cell viability at the point of

harvest, which would have lead to significant impurity release prior to harvest. This is unlikely to apply with a CHO cell line harvested at higher cell viability where impurity release during harvesting may be much more significant. Testing this hypothesis with the ultra scale-down centrifuge tool would be of great industrial interest as selection of low-shear harvesting operations could relieve downstream bottlenecks caused by increased product titres. A reduction in cellular impurities entering purification processes could allow the use of high-throughput (although currently low-capacity) alternatives to chromatography, such as membrane adsorbers.

Increasing cell culture titres combined with successful large-scale cell cultivation are creating urgent development targets downstream of the bioreactor to facilitate capture and purification of increasingly large masses of product. Manufacturers are actively seeking novel alternatives to chromatographic purification methods to alleviate mammalian cell protein purification bottlenecks. Operations based on precipitation and crystallization, for example, may require solid-liquid separations that could be performed using centrifuges. The ultra-scale centrifuge protocols, combined with operating windows, would provide an ideal technique for evaluating the integration of such new steps and would allow equipment specification at an early stage in process development. The shear sensitivity of solid particles could be determined at the bench-scale to allow identification of the most suitable separation technology. If the decision to use a centrifugal separator at the large-scale was taken, then the size and flow rates could be specified long before pilot-scale studies commenced. Contract manufacturers may find that new separation techniques are less generic than existing technologies;

process development at the ultra-scale could be routinely used to specify product-specific processes.

Further research is required to assess the impact of hydrodynamic forces on glycosylated proteins (Qvist *et al.,* 2006). Although the results presented in this thesis indicate no gross effects on the antibody studied (Section 2.3.3.), more subtle alterations to the molecular structure may have occurred requiring investigated using advance analytical techniques such as mass spectroscopy. Proteins other than antibodies such as hormones may have complex multi-subunit structures making them more fragile and sensitive to shear; product comparability studies need to be carried out for each new product.

6.2.1.2. Microscale centrifugation

Ultra scale-down centrifugation, using a few hundred milliliters of material, need not be the smallest scale for centrifuge process development. Laboratory centrifuges such as the IEC Centra manufactured by Thermo Electron are available that hold microwell plates. Preliminary studies, conducted during the course of this research, though not presented as part of the thesis, showed that 96-well plates with a capacity of 350 μL of fluid per well could be used to clarify cell culture supernatant (Tylka, 2003). Different equivalent flow rates could be achieved by varying the volume of process fluid in the well; dimishing clarification performance was observed with increasing equivalent flow rate. The method was significantly quicker than the ultra scale-down centrifuge method, because the particle settling distance was very small, and in particular, because many equivalent flow rates could be studied in a single centrifuge. Further, the micro-well centrifugation technique could be automated

using liquid-handling robots: microwell plates could be charged with process material, centrifuged and supernatant withdrawn and loaded into a second microwell plate for optical density determination at the appropriate wavelength using, the liquid-handling system. The use of liquid-handling systems should lead to a highly reproducible technique, which is of particular importance when dealing with microlitre volumes of material. Initial trials of this technology showed that the clarification results from the microwell plate and the ultra scale-down centrifuge were similar, although the microwell plate technique consistently failed to clarify the cell culture broth to the same extent as the ultra scale-down protocol at the same equivalent flow rates(Tylka, 2003). This discrepancy requires further investigation.

6.2.2. Ultra scale-down chromatography

Considerable resources are allocated to the development of chromatographic processes in the biopharmaceutical industry due to their complex nature. A large number of factors need to be considered, including appropriate resin selection, buffer composition, flow rates and bed height. The pressure to progress to clinical trials in the shortest time possible permits only limited process optimization. This can lead to inefficiencies in manufacturing product batches at the large-scale. Rapid techniques, requiring very small volumes of process material but allowing reliable prediction of the performance of large-scale columns would be of considerable use. Such techniques would allow testing of a greater number of process alternatives than is currently possible for short development projects. Despite being frequently overlooked in published literature, intermediate product volumes are also an important and frequently poorly predicted variable. For example, variations in

elution volumes affect product concentrations entering subsequent operations and can contribute to product instability. The presence of large intermediate product volumes leads to inefficient use of a manufacturing facility; the ability to predict these volumes would allow operating managers to efficiently plan the processing of such volumes.

6.2.2.1. Applicability of ultra scale-down column to anion- and cation-exchange chromatography development.

Elution volumes from affinity chromatography columns were studied in this thesis (Chapter 4). Both anion- and cation-exchange columns are also frequently utilized in the manufacture of therapeutic recombinant proteins such as monoclonal antibodies. Determining the applicability of the method of elution volume correction would be to these two methods of chromatography is of interest and could be investigated in future. In monoclonal antibody processing anion-exchange chromatography is typically operated as an impurity capture step, during which the product does not bind to the resin. Determining the elution volume of the product as it flows through the column would be of interest. During a well-operated anion-exchange step, the product and captured impurities should be separated within the chromatography system by a large volume of wash buffer, as occurs during affinity chromatography. Hence, the additional zone-spreading experienced at the ultra-scale should have little impact on the product purity achieved by this step and, thus, loading and wash buffer conditions specified at the ultra scale-down should be applicable to larger-scale columns.

Unfortunately the opposite is true during cation-exchange chromatography when the accurate prediction of elution volumes is most important. The purpose of the cation exchange step is to separate monomer product from aggregated product. The similarities between these molecules means that they frequently have similar elution residence times and overlapping elution profiles (Bonnerjea, 2006). Development of a robust cation-exchange step typically requires the identification of a cation concentration that will separate the monomer from the impurities without causing the product to elute in an unacceptably large volume. As material available for such studies is often especially valuable and limited, due to the number of steps required to generate it, the use of the ultra scale-down column for such studies would be of great use. At the production scale, more highly optimized steps are likely to lead to large reductions in the cost of goods, as small improvements in yield are significant at this stage when the product has had considerable value added to it. Although the ultra scale-down column would be a very valuable tool in the development of cation-exchange chromatography steps, similarities between the retention times of the product and impurity would require the additional complexity of correcting for the effect of extra-column mixing on product purity to be considered.

6.2.2.2. Dynamic binding capacity determination using ultra scale-down chromatography methods

The dynamic binding capacity of a resin under a given set of conditions is an important design variable. Determining the capacity of the resin for the product using an ultra scale-down column would be of great value as it would minimize the

amount of material required for such a study. It is likely, however, that the dynamic binding capacity of the small scale column would over predict the capacity of a large scale column because of the way in which bound product is distributed on a loaded column. At the column inlet the concentration of the product in the mobile phase is at a maximum and hence there exists the maximum concentration gradient between that and the stationary phase that will drive the diffusion of product molecules through the stagnant layer of fluid that surrounds resin particles and onto the resin. As the fluid flows down through the column the concentration of the product in the mobile phase and hence the concentration gradient between the mobile and stationary phases decreases due to binding of product to resin close to the inlet. For this reason matrix close to the outlet is less efficiently utilized than the resin at the top of the column. The total dynamic binding capacity of a column with a reduced bed height will be greater than that of a large-scale column because it mimics the performance of the top of the large scale column only.

6.2.2.3. Micro-scale chromatography

The use of ultra scale-down columns would allow a greater number of process alternatives to be tested using the same amount of material. However, the total number of variables is extremely large and a full screen of these variables would be resource intensive. As has been proposed for the development of centrifugation processes (Section 6.2.1.2.) the use of microwell plate technology could allow the screening of even more variables in a shorter space of time than could be achieved at the ultra-scale. One method of achieving a screen of chromatography conditions in a microwell plate format would be to use 100 μL

volumes of resin in a microfilter plate which can be equilibrated, loaded and eluted using a vacuum manifold capable of sucking the appropriate solution (previously loaded into the well) through the resin bed and discharging it into a collection plate. Using this technique many different combinations of resins and buffers could be tested, to determine those most useful for given purposes. For evaluation of elution buffers resin could be pre-equilibrated and loaded with product prior to being aliquoted into wells to maximize experimental throughput. Up to 96 different process combinations could be studied on a single plate and the process could be readily automated using liquid-handling robots. It is unlikely that either the ultra scale-down method (Chapter 4) or the proposed microwell method used in isolation would form an entire strategy for developing chromatography processes, but that together, along with the appropriate mathematical models they would form a "toolbox" for the complete characterization of separation processes. It should, however, be remembered that this type of high-throughput chromatography development work would generate large numbers of samples for analysis. It is easy to conceive that sample analysis could then become the limiting factor. Although analytical capacity can be increased with few technological obstacles it would add significantly to the cost of the process development. Increasing analytical throughput to support bioprocess development is a major technological challenge for scientists working in that field.

6.2.3. Whole bioprocess scale-down

This thesis has focused on two unit operations used in the purification of monoclonal antibodies; however, ultra scale-down techniques are required for every

unit operation in the process, including normal flow filters and tangential flow membranes. Once this has been achieved then material from scale-down of one unit operation can be fed into subsequent process steps for the development of entire bioprocesses. Considerable progress has been made in recent years in the use of scale-down bioreactors for the development of cell culture processes (De Jesus *et al.* 2004). Such miniature bioreactors will not yield sufficient volume of material or mass of product to permit downstream process development using conventional techniques. Only ultra-scale and micro-scale process development methods can generate useful data with limited process material. Furthermore, by linking ultra scale-down operations together it will be possible to investigate the complex interactions between processing steps. For example, the relationships between the clarifying performance of operations such as centrifuges and filters and the degree of fouling of purification operations such as packed bed chromatography columns or the generation of product aggregates during cell cultivation and the removal of the aggregates by cation-exchange chromatography. Currently, performing experiments to investigate such interactions would be too expensive even at pilot or laboratory-scales; however, they could be performed rapidly and inexpensively at an ultra- or micro-scale. The ability to run entire bioprocess at these scales fully representative of the large-scale, could be included into process validation protocols during which process control limits are set and tested. Availability of scale-down techniques would allow simultaneous testing of a large combination of process limits to ensure safe and effective operation.

The development and operation of manufacturing process for the production of safe recombinant protein therapeutics continues to require a combination of skill and experience, even though this class of pharmaceutical has been approved for

marketing for twenty years (eg. Muromonab-CD3 for transplant rejection) (Guru, 2002). Prices of this category of drug will be driven down by the inevitable and imminent loss of patent protection for currently marketed products and the introduction of generic biopharmaceuticals such as has occurred outside the USA with generic forms of erythropoietin (ie Eprex (Johnson & Johnson), NeoRecorman. (Roche) and Dynepo (Shire)). Manufacturers of products under patent protection need to maximize their monopoly on the market by getting products to the market as rapidly as possible, thus reducing costs and prices and minimizing the impact of generic products when the monopoly comes to an end. Increased competition will force manufacturers to ensure that their processes operate as efficiently as possible; enabling technology will be even more essential than at the current time. There is every reason to believe that empirical approaches to process development, providing industrially applicable data with minimal amounts of process material, will significantly contribute to improvements in process efficiencies.

Appendix 1 - Transition analysis sample calculations

Columns 1 & 2 of Table A.1.1. show data from the conductivity transition paired with the respective volume data. The conductivity data is normalized using the maximum and minimum response data given in Table A.1.2.and Equation A.1.1.,

$$R = \frac{value - \min imum\ response}{\max imum - \min imum\ response} \qquad \text{Equation A.1.1}$$

1	2	3	4	5
Response (Conductivity) ($mS.cm^{-1}$)	Volume *V* (mL)	Normalised Conductivity *R* (-)	*dR/dV*	Moving average *dR/dV*
17.701	4.586	0.692	2.190	
17.476	4.590	0.683	2.270	2.068
17.303	4.594	0.676	1.746	1.729
17.187	4.598	0.671	1.170	1.366
17.07	4.602	0.667	1.181	1.181
16.952	4.606	0.662	1.191	1.191
16.833	4.61	0.657	1.201	1.204
16.712	4.614	0.652	1.221	1.214
16.591	4.618	0.647	1.221	1.185
16.453	4.623	0.642	1.114	1.609
16.206	4.627	0.632	2.492	2.033
15.959	4.631	0.622	2.492	

Table A.1.2 Sample calculation of the transition analysis

Max response	25.33
Min response	0.553

Table A.1.2 Maximum and minimum conductivity data

An example of the calculation of the rate of change of the response with volume (*dR/dV*) is given in Equation A.1.2 using the values in Table A.1.1 highlighted in blue.

$$\frac{dR}{dV} = 2.270 = \frac{0.692 - 0.683}{4.590 - 4.586} \qquad \text{Equation A.1.2.}$$

An example of a moving average calculation is given in Equation A.1.3 using data from Table A.1.1. highlighted in grey.

$$moving\ average = 1.364 = \frac{1.746 + 1.170 + 1.181}{3} \qquad \text{Equation A.1.4}$$

Each moment is calculated as follows

$$M_0 = 1.00 = \int V^0 \frac{dR}{dV} dV \qquad \text{Equation A.1.5}$$

$$M_1 = 4.75 = \int V^1 \frac{dR}{dV} dV \qquad \text{Equation A.1.5}$$

$$M_2 = 22.65 = \int V^2 \frac{dR}{dV} dV \qquad \text{Equation A.1.6}$$

The variance, σ^2, is calculated from moments 1,2 & 3 as follows.

$$\sigma^2 = \frac{M_2}{M_0} - \left(\frac{M_1}{M_0}\right)^2 = \frac{22.65}{1.00} - \left(\frac{4.75}{1.00}\right)^2 = 0.150 \qquad \text{Equation A.1.7}$$

Appendix 2 – Elution profile correction process sample calculations

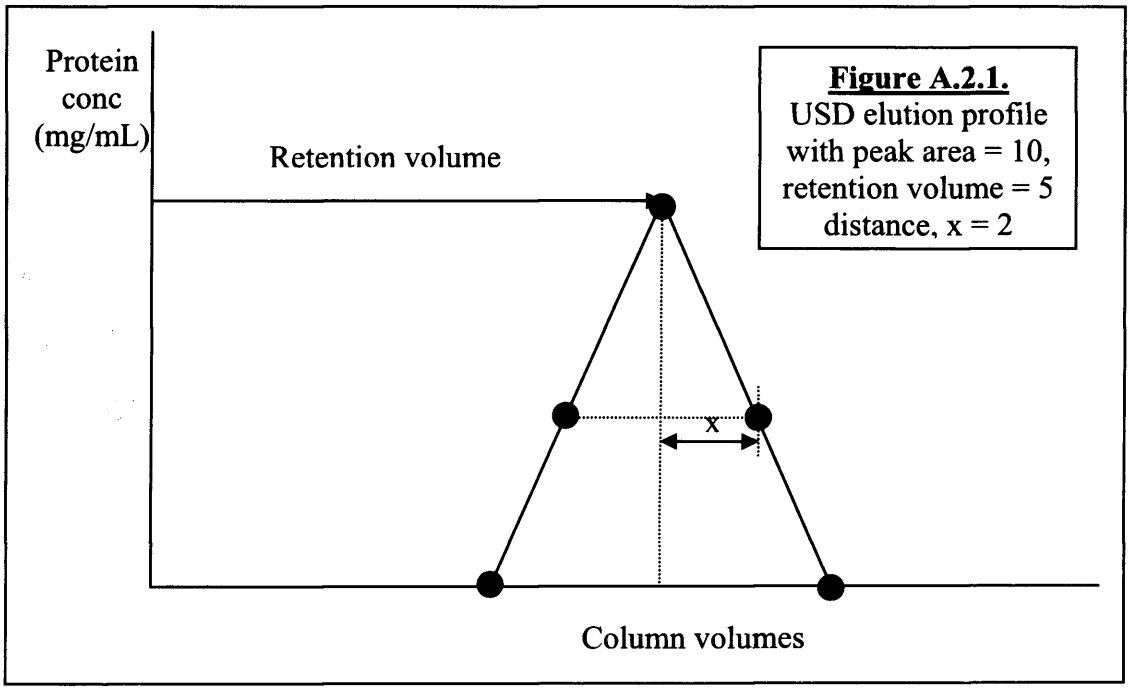

Figure A.2.1 – Original elution profile generated by USD column

The following ratio from the conductivity transitions is then used to correct the data points around the retention volume,

normalized variance from large-scale : normalized variance from USD scale

In this example, this ratio would be

7.11:1

The distance each data point to the retention volume would, therefore, be decreased by a factor of $\sqrt{7.11} = 2.66$ from 2 to 0.75 as shown in Figure A.2.2.

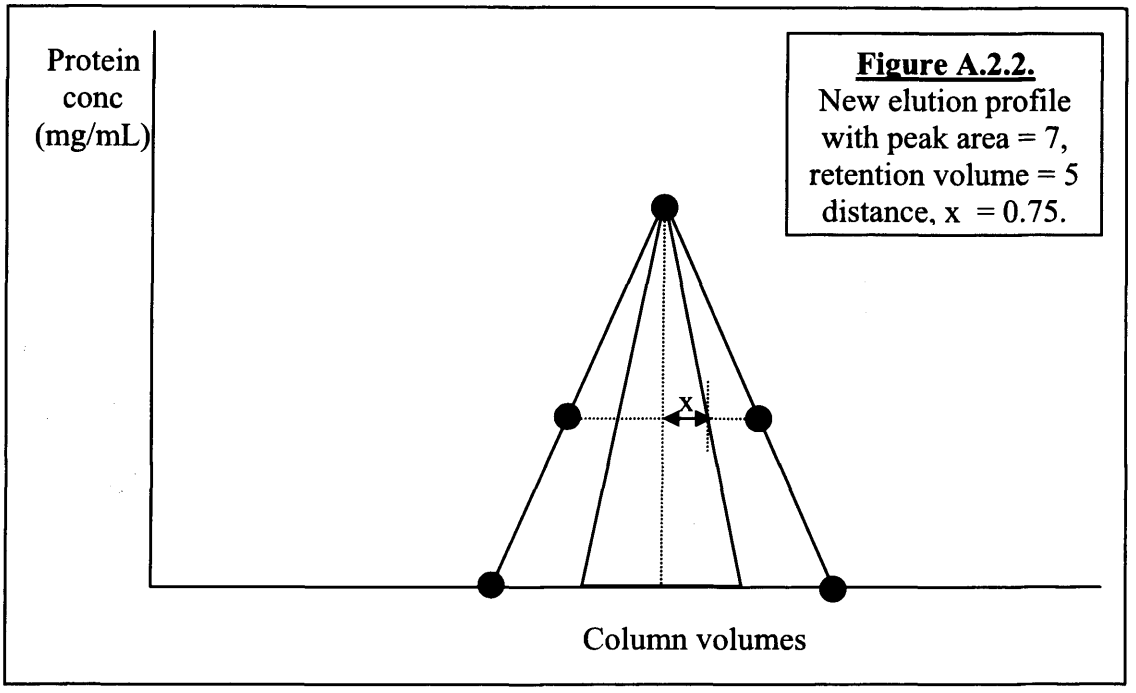

Figure A.2.2. Correction for additional zone broadening

Correction in this way leads to a decrease in the elution peak area. The area must be maintained so while the peak shape is maintained the area is increased as shown in Figure A.2.3.

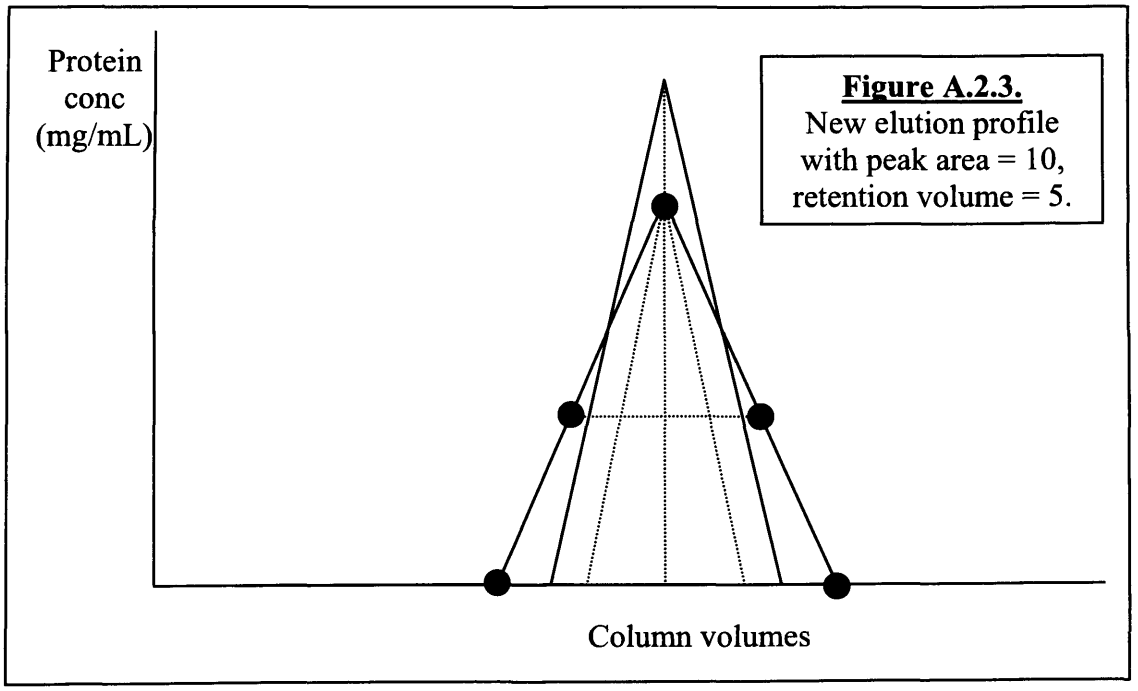

Figure A.2.3. Maintaining peak area.

It is easy to see from Figure A.2.3 how this can be achieved by looking at either half of the elution peak around the retention volume. The area under the curve, determined by integration, is increased until it matches that of the original elution profile. The angle between the vertical line down the centre of the modified elution profile (representing the retention volume) and each data point is maintained as the area of the corrected peak is increased.

The final correction is the adjustment of the peak retention volume using the ratio from the transition analysis,

normalized retention volume (large-scale):normalized retention volume (USD scale)

In this example, this ratio would be

1.25:1

The retention volume of each data point is then reduced by a factor of 1.25 as shown in Figure A.2.4.

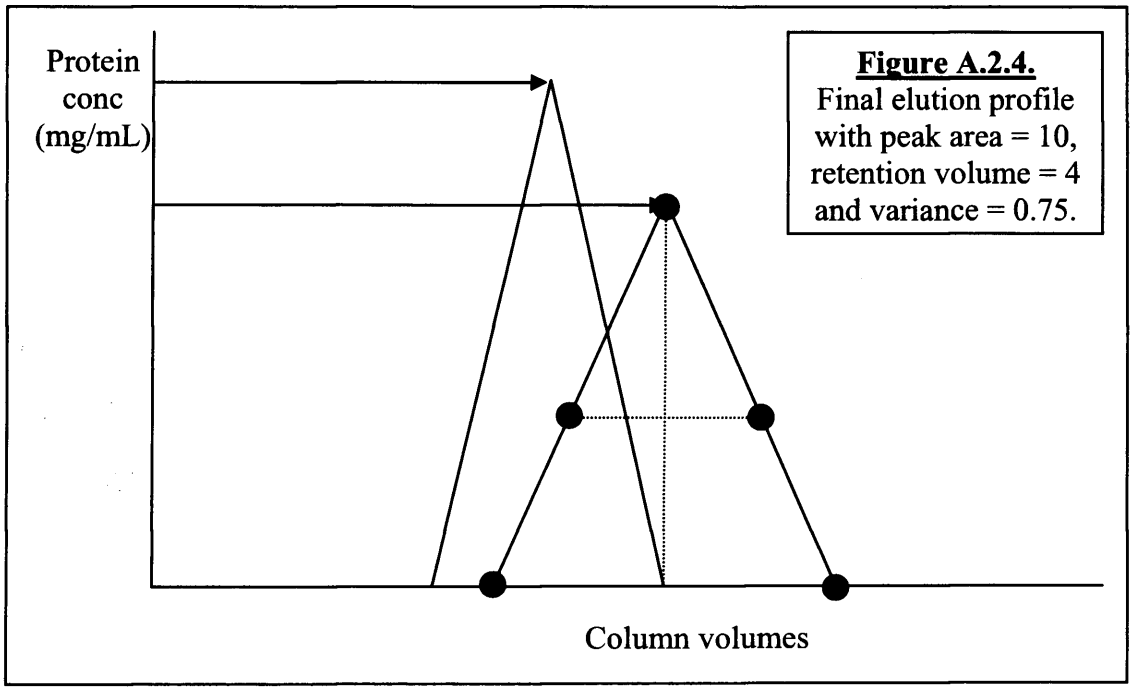

Figure A.2.4 Correction of retention volume.

Nomenclature

Chapter 1

θ (rads) disc half conical angle

ω (s^{-1}) angular velocity

Σ_{ds}(m^2) equivalent centrifuge settling area of the disc stack centrifuge

Σ_{lab} (m^2) equivalent centrifuge settling area of the laboratory centrifuge

$\Delta\rho$ (kg m^{-3}) fluid/solid density difference

μ (Pa s) dynamic viscosity

C_{ds} (-) correction factor for disc stack centrifuge

C_{lab} (-) correction factor for laboratory centrifuge

d (m) particle diameter

Q (m^3/s) flow rate through continuous centrifuge

r (m) settling radius

r_1 (m) disc inner radius

R_1 (m) inner radius

r_2 (m) disc outer radius

R_2 (m) outer radius

$t_{(lab)}$ (s) time of laboratory centrifuge run

u (m s^{-1}) linear fluid velocity

V (m^3) volume of process fluid in centrifuge tube

$v_c(r)$ (m s^{-1}) settling velocity of a particle

x (-) fraction of overall centrifugation time for deceleration

y (-) fraction of overall centrifugation time for acceleration

z (-) number of active discs

Chapter 2

c correction factor for non-ideal flow patterns

OD_0 optical density of a well-spun sample at 550nm

OD_f optical density of the feed at 550nm

OD_s optical density of the supernatant at 550nm

Chapter 3

Chapter 4

ε (-) bed void fraction

σ^2 (m^2) band broadening

σ_{col}^2 (m^2) column internal broadening

σ_d (m^2) band broadeneing due to finite sensing volume of a detector

σ_{ex}^2 (m^2) extra column broadening

σ_t (m^2) tubing band broadening

σ_{total}^2 * (-) total normalized band broadening, $\sigma_{total}^2 * = \sigma_{total}^2 / V_C^2$

σ_{total}^2 (m^2) total band broadening,

τ_{dead} (m^2) exponential contribution of dead volumes to band broadening

τ_{el} (m^2) exponential contribution of the amplifier and recorder to band broadening

D_M ($mm^2\ s^{-1}$) molecular diffusion coefficient

HETP (μm) Height equivalent to a theoretical plate

k (-) moment number

L (m) bed length

M (-) moment

N (-) number of plates

Q (m^3 s^{-1}) volumetric flow rate

r (m) column radius

R (-) response signal

t_R (s) retention time

v (m s^{-1}) linear flow rate

V_C (m^3) column volume

V_d (m^3) detector volume

V_{dead}. (m^3) dead volume

V_{ex} (m^3) extra-column volume

V_R (m^3) retention volume

V_R^* (-) normalised retention volume, $V_R^* = V_R / V_C$

z (m) distance traveled by solute

Chapter 5

ε (-) interstitial bed porosity

ε_o (-) gravity settled bed porosity.

λ (-) bed compression.

λ_{cri} (-) critical bed compression.

μ (Pa s) dynamic viscosity

d_p (μm) resin particle diameter

K_o (-) empirical constant (Blake-Kozeny equation).

L_o (m) is the gravity settled bed height

L_{cri} (m) critical bed height

u_{cri} (cm h^{-1}) critical flow velocity

V_c (mL) column bed volume

V_{co} (mL) gravity settled bed volume

List of Abbreviations

BSA – Bovine Serum Albumin

CFD – Computational Fluid Dynamics

CHO – Chinese Hamster Ovary cells

CV – Column Volume

DHFR – Dihydrofolate Reductase

ELISA – Enzyme Linked Immuno Sorbent Assay

FDA – Food and Drug Administration

GS – Glutamine Synthatase

HAMA – Human Anti-Murine Antibodies

HPLC – High Performance Liquid Chromatography

IEF – Isoelectric Focussing

MAb – Monoclonal antibody

MSX – Methionine Sulphoximine

MTX – Methotrexate

OD – Optical Density

RPM – Rotations Per Minute

TNF – Tissue Necrosis Factor

USD – Ultra scale-down

References

Aalberse RC, Schuurman J. 2002. IgG4 breaking the rules. Immunology. 105:9-19.

Abraham S, Bingham N, Green K, Kenworthy J. 2003. Strategies for improving mammalian cell clarification. Abstr Pap Am Chem Soc. 225:119-BIOT.

Allen T. 1975. Particle size measurement. London: Chapman and Hall.

Ambler CM. 1959. The theory of scaling up laboratory data for the sedimentation type centrifuge. J Biochem Microbiol Tech & Eng 1:185

Anderson DC, Reilly DE. 2004. Production technologies for monoclonal antibodies and their fragments. Curr Opin Biotech 15:456-462.

Axelsson H. 1999. Cell separation, centrifugation. In: Flickinger MC, Drew SW, editors. Encyclopedia of bioprocess technology. 513-531 Wiley. New York.

Bakker H, Bardor M, Molthoff JW, Gomord V, Elbers I, Stevens LH, Jordi W, Lommen A, Faye L, Lerouge P, Bosch D. Galactose-extended glycans of antibodies produced by transgenic plants. Proc Natl Acad Sci USA. 98:2899-2904.

Barnes LM, Bentley CM, Dickson AJ. 2000. Advances in animal cell recombinant protein production: GS-NS0 expression system. Cytotechnology. 32:109-123.

Bernard BA, Yamada KM, Olden K. 1982. Carbohydrates selectively protect a specific domain of firbonectin against proteases. J Biol Chem 257:8549-8554.

Bi J-X, Shuttleworth J, Al-Rueai M. 2004. Uncoupling of cell growth and proliferation results in enhancement of productivity in p21cip-arrested CHO cells. Biotech Bioeng. 85: 741-749.

Blank GS, Zapata G, Fahrner R, Milton M, Yedinak C, Knudsen H, Schmelzer C. 2001. Expanded bed adsorption in the purification of monoclonal antibodies: a comparison of process alternatives. Bioseparations 10:65-71.

Bonnerjea J. 2006. Direct discussion with Head of Purification at Lonza Biologics.

Boulianne GL, Hozumi N, Shulman MJ. 1984. Production of functional chimaeric mouse/human antibody. Nature. 312:643-6.

Boychyn M, Doyle W, Bulmer M, More J, Hoare M. 2000. Laboratory scaledown of a protein purification process involving fractional precipitation and centrifugation recovery. Biotech Bioeng 69:1-10.

Boychyn M, Yim SSS, Bulmer M, More J, Bracewell DG Hoare M. 2004. Performance prediction of industrial centrifuge using scale-down models. Bioprocess Biosyst Eng. 26:385-391.

Boychyn M, Yim SSS, Shamlou PA, Bulmer M, More J, Hoare M. 2001. Characterisation of flow intensity in continuous centrifuges for the development of laboratory mimics. Chem Eng Sci 56:4759-4770.

Bradford M. 1976. A Rapid and Sensitive Method for the Quantitation of Microgram Quantities of Protein Utilizing the Principle of Protein-Dye Binding. Anal Biochem. 72:248-254.

Brose D, Dosmar M, Cates S, Hutchison F. 1996. Studies on the scale-up of crossflow filtration devices. J Pharm Sci and Technol. 50: 252-260.

Brown ME, Renner G, Field RP, Hassell. 1992. Process development for the production of recombinant antibodies using the glutamine synthetase (GS) system. Cytotechnology. 9:231-236.

Cartron G, Dacheux L, Salles G, Solal-Geligney P, Bardos P, Colombat P, Watier H. 2002. Therapeutic activity of humanized anti-CD20 monoclonal antibody and polymorphism in IgG Fc receptor Fc-γRIIIa gene. Blood. 99:754-758.

Charlton HR, Relton JM, Slater NKH. 1999. Characterisation of a generic monoclonal antibody harvesting system for adsorption of DNA by depth filters and various membranes. Bioseparation 8:281-291.

Charlton HR, Relton JM, Slater NKH. 2000. Filter life after cell death:impact of viable, non-viable apoptotic and necrotic mammalian cells on depth filter blinding. Trans IChemE. 78:133-138.

Chiang GG, Sisk WP. 2005. Bcl-x_L mediates increased production of humanized monoclonal antibodies in Chinese Hamster Ovary cells. Biotech Bioeng. 91:779-792.

Chirino AJ, Mire-Sluis A. 2004. Characterizing biological products and assessing comparability following manufacturing changes. Nature Biotechnol. 22: 1383-1391.

Chu L, Robinson DK. 2001. Industrial choices for protein production by large-scale cell culture. Curr Opin Biotech 12:180-187.

Cleland JL, Lam X, Kendrick B, Yang J, Yang TH, Overcashier D, Brooks D, Hsu C, Carpenter JF. 2001. A specific molar ratio of stabilizer to protein is required for storage and stability of a lyophilized monoclonal antibody. J Pharm Sci. 90:310-321.

Clynes RA, Towers TL, Presta LG, Ravetch JV. 2000. Inhibitory Fc receptors modulate *in vivo* cytotoxicity against tumour targets. Nat Med 6:443-446.

Colby CB, O'Neill BK, More J. 1996. A modified version of the volume-averaged continuum theory to predict pressure drop across compressible packed beds of Sepharose Big-Beads SP. Biotechnol. Prog. 12: 92-99.

Cram SP, Glenn TH. 1975. Instrumental contributions to band broadening in gas chromatography: I. Development of a model. J Chrom. 112: 329-341.

Dalm MCF, Jansen M, Keijzer TMP, van Grunsven WMJ, Oudshoorn A, Tramper J, Martens DE. 2005. Stable hybridoma cultivation in a pilot-scale acoustic perfusion system: long-term process performance and effect of recirculation rate. Biotech Bioeng. 91:894-900.

De Jesus MJ, Girard P, Bourgeois M, Baumgartner G, Jacko B, Amstutz H, Wurm FM. 2004. TubeSpin satellites: a fast track approach for process development with animal cells using shaking technology. Biochem Eng J. 17:217–223.

Doran P. 1994. Bioprocess Engineering Principles. 1st Edition. Academic press limited. London.

Fahrner RL, Whitney DH, Vanderlaan M, Blank GS. 1999. Performance comparison of Protein A affinity-chromatography sorbents for purifying recombinant monoclonal antibodies. Biotechnol Appl Biochem. 30:121-128.

Farid S, Novais JL, Karri S, Washbrook J, Titchener-Hooker NJ. 2000. A tool for modelling strategic decisions in cell culture manufacturing. Biotechnol Prog, 16: 829-836.

Filipe CDM, Ghosh R. 2005. Effects of protein-protein interaction in ultrafiltration based fractionation processes. BiotechBioeng. 91:678-687.

Fishwild DM, O'Donnell SL, Bengoechea T, Hudson DV, Harding F, Bernhard SL, Jones D, Kay RM, Higgins KM, Schramm SR, Lonberg N. 1996. High-avidity human IgG_K monoclonal antibodies from a novel strain of minilocus transgenic mice Nature Biotech. 14:845-851.

Gandor C, Leist C, Fiechter A, Asselbergs FA. 1995. Amplification and expression of recombinant genes in serum-independent Chinese Hamster Ovary cells. FEBS Lett. 377:290-294.

Geankoplis CJ. 1993. In Transport Processes and Unit Operations. 3rd Ed. 120 Prentice Hall, Englewood Cliffs, NJ.

Gu T, Tsai G-J, Tsao GT. 1993. Modeling of nonlinear multicomponent chromatography. In: Advances in biochemical engineering biotechnology. Vol 49. Editor Fiechter A. Springer-Verlag. Berlin

Guru T. 2002 Magic bullets hit the target. Nature. 417:584-586.

Hamilton SR, Bobrowicz P, Bobrowicz B, Davidson RC, Li H, Mitchell T, Nett JH, Rausch S, Stadheim TA, Wischnewski H, Wildt S, Gerngross TU. 2003. Production of human glycoproteins in yeast. Science 301:1244-1246.

Hamilton WG & Ham RG. 1997. Clonal growth of Chinese hamster cell lines in protein-free media. In Vitro. 13:537-547.

Hanle DD. 1999. Centrifuges, animal. In: Flickinger MC, Drew SW, editors. Encyclopedia of bioprocess technology. 553-559.Wiley. New York.

Harris RJ, Shire SJ, Winter C. 2004. Commercial manufacturing scale formulation and analytical characterization of therapeutic recombinant antibodies. Drug Dev Res. 61:137-154.

Hoffmann M. 1998. A novel technology for packing and unpacking pilot and production scale columns. J Chrom A. 796: 75-80.

Huber JFK, Rizzi A. 1987. Influence of the accuracy of the extra-column peak-width determination on the verification of theoretical plate-height equations. J Chrom. 387: 337-348.

Ibarra N, Watanabe S, Bi J-X, Shuttleworth J, Al-Rubeai M. 2003. Modulation of cell cycle for enhancement of antibody productivity in perfusion culture of NS0 cells. Biotech Prog. 19:224-228.

ICH. 1998. Guidance for industry. Q5A Viral safety evaluation of biotechnology products derived from cell lines of human or animal origin. CBER. FDA. ICH.

Idling K, Lutkemeyer D, Fraune E, Gerlach K, Lehmann J. 2000. Influence of alterations in culture conditions and changes in perfusion parameters on the retention performance of a 20 micron spinfilter during a perfusion cultivation of a recombinant CHO cell line in pilot scale. Cytotechnology 34:141-150.

Jackson NB, Liddell JM, Lye GJ. 2006. An automated microscale technique for the quantitative and parallel analysis of microfiltration operations. J Mem Sci. 276: 31-41.

Jain M, Paranandi M, Roush D, Goklen K, Kelly WJ. 2005. Using CFD to understand how flow patterns affect retention of cell-sized particles in a tubular bowl centrifuge. Ind Eng Chem Res 44, 7876-7884.

Joh LD, Wroblewski T, Ewing NN, VanderGheynst JS. 2005. High-level transient expression of recombinant protein in lettuce. Biotech Bioeng. 91:861-871.

Johnson VG, Schlom J, Paterson AJ, Bennet D, Magnani JL, Colcher D. 1986. Analysis of a human tumor-associated glycoprotein (TAG-72) identified by monoclonal antibody B72.3. Cancer Res. 46: 3118-3124.

Jones PT, Dear PH, Foote J, Neuberger MS, Winter G. 1986. Replacing the complementarity-determining regions in a human antibody with those from a mouse. Nature 321:522-525.

Kaltenbrunner O, Jungbauer A, Yamamoto S. 1997. Predicion of the preparative chromatography performance with a very small column. J Chrom A 760:41-55.

Karpas A., Dremucheva A.& Czepulkowski B.H. 2001 A human myeloma cell line suitable for the generation of human monoclonal antibodies. Proc Natl Acad Sci, 98:1799-1804.

Köhler G, Milstein C. 1975. Continuous cultures of fused cells secreting antibody of predefined specificity. Nature 256:495-497.

Krapp S. Mimura Y, Jefferis R, Huber R, Sondermann P. 2003. Structural analysis of human IgG-Fc glycoforms reveals a correlation between glycosylation and structural integrity. J Mol Biol. 325:979-898.

Kroon DJ, Baldwin-Ferro A, Lalan P. 1992. Identification of sites of degradation in a therapeutic monoclonal antibody by peptide mapping. Pharm Res 9:1386-1393.

Kurnik RT, Yu AW, Blank GS, Burton AR, Smith D, Athalye AM, van Reis R. 1995. Buffer exchange using size exclusion chromatography, countercurrent dialysis, and tangential flow filtration: Models, development, and industrial application. Biotechnol Bioeng. 45:149-157.

Larson TM, Davies J, Lam M, Cacia J. 2003. Use of process data to assess chromatographic performance in production-scale protein purification columns. Biotech Prog 19: 485-492.

Leung WW-F. 1998. Industrial centrifugation technology. McGraw Hill. New York.

Lonza Biologics plc. website (http://www.lonza.com/) accessed 2005.

Mannweiler K, Hoare M. 1992. The scale-down of an industrial disc stack centrifuge. Bioproc Eng 8:18-25.

Maybury JP, Hoare M, Dunnill P. 2000. The use of laboratory centrifugation studies to predict performance of industrial machines: studies of shear-insensitive and shear-sensitive materials. Biotechnol Bioeng 67:265-273.

Maybury JP, Mannweiler K, Titchener-Hooker NJ, Hoare M, Dunnill P. 1998. The performance of a scaled down industrial disc stack centrifuge with a reduced feed material requirement. Bioprocess Eng 18:191-199.

Mercille S, Massie B. 1994. Induction of apoptosis in nutrient-deprived cultures of hybridoma and myeloma cells. Biotech Bioeng. 44:1140-1154.

Mohammad AW, Stevenson DG, Wankat PC. 1992 Pressure drop correlations and scale-up of size exclusion chromatography with compressible packings. Ind Eng Chem Res. 31:549-561.

Molowa D. 2001. Industry analysis: The state of biologics manufacturing. JP Morgan securities. New York.

Moran EB, McGowan ST, McGuire JM, Frankland JE, Oyebade IA, Waller W, Archer LC, Morris LO, Pandya J, Nathan SR, Smith L, Cadette ML, Michalowski JT. 2000. A systematic approach to the validation of process control parameters for monoclonal antibody production in fed-batch culture of a murine myeloma. Biotech Bioeng. 69:242-255.

Morrison SL, Johnson MJ, Herzenberg LA, Oi VT. 1984. Chimeric human antibody molecules: mouse antigen-binding domains with human constant region domains. 81: 6851-6855.

Newcombe A, Cresswell C, Davies S, Watson K, Harris G, O'Donovan K, Francis R. 2005. Optimised affinity purification of polyclonal antibodies from hyper immunized ovine serum using a synthetic Protein A adsorbant, MAbsoerbent® A2P. J Chrom B. 814:209-215.

Osman J, Khan M, Valentine D, Davies M, Mainwaring D, Knevelman C, Rendall M, Maxwell A, Onadipe K. 2004. Stirred tanks and airlift bioreactors are interchangeable systems for mammalian cell culture. IBC Antibody Conference. San Diego, 25th February.

Peakman TC, Worden J, Harris RH, Cooper JS, Tite J, Page MJ, Gewert DR, Bartholemew M, Crowe JS, Brett S. 1994. Comparison of expression of a humanized

monoclonal antibody in mouse NS0 myeloma cells and Chinese hamster ovary cells. Hum Antibody Hybridomas 5:65-74.

Pinheiro H, Cabral JMS. 1993. Centrifugation. In Kennedy JF, Cabral JMS editors. Recovery processes for biological materials. 145: John Wiley & Sons Ltd. Chichester.

Protherics plc. website. (http://www.protherics.com/) accessed 2005

Qvist C, Baldascini H, Hutchinson N, Bracewell D, Smales M, Hoare M. 2006. Impact of cell bioprocessing on antibody structure and recovery. ESACT-UK, 16th Annual Meeting in Cell Technology, Leicester, UK. 9-10th January.

Reichert JM. 2001. Monoclonal antibodies in the clinic. Nat Biotech. 19:819-822.

Reynolds T, Boychyn M, Sanderson T, Bulmer M, More J, Hoare, M. 2003. Scale-down of continuous filtration for rapid bioprocess design: recovery and dewatering of protein precipitate suspension. Biotech Bioeng. 83: 454-464.

Runkel L, Meier W, Pepinsky RB, Karpusas M, Whitty A, Kimball K, Brickelmaier M, Muldowney C, Jones W, Goelz SE. 1998. Structural and functional differences between glycosylated and non-glycosylated forms of human interferon-beta (IFN-beta). Pharm Res. 15:641-649.

Schenerman MA, Hope JN, Kletke C, Singh JK, Kimura R, Tsao EI, Folena-Wasserman G. 1999. Comparability testing of a humanized monoclonal antibody (Synagis$^{(R)}$) to support cell line stability, process validation, and scale-up for manufacturing. Biologicals 27:203-215.

Schmelzer AE, Miller WM. 2002. Hyperosmotic stress and elevated pCO2 alter monoclonal antibody charge distribution and monosaccharide content. Biotechnol Prog. 18:346-353.

Shalliker RA, Broyles BS, Guiochon G. 2003. Axial and radial diffusion coefficients in a liquid chromatography column and bed heterogeneity. J Chrom A. 994: 1-12.

Shields RL, Lai J, Keck R, O'Connell LY, Hong K, Meng YG, Weikert SH, Presta LG. 2002. Lack of fucose on human IgG1 N-linked oligosaccharide improves binding to human Fc-γ RIII and antibody-dependant cellular toxicity. J Biol Chem. 277:26733-26740.

Singh V. 1999. Disposable bioreactor for cell culture using wave-induced agitation. Cytotechnology. 30:149-158.

Slamon DJ, Leyland-Jones B, Shak S, Fuchs H, Paton V, Bajamonde A, Fleming T, Eiermann W, Wolter J, Pegram MD, Baselga J, Norton L. 2001. Use of chemotherapy plus a monoclonal antibody against HER2 for metastatic breast cancer that overexpresses HER2. N Eng J Med. 344:783-792.

Sofer GK, Nystrom L-E. 1989. Process chromatography: a practical guide. 56. Academic Press Inc. San Diego.

Sommerfeld S, Strube J. 2005. Challenges in biotechnology production – generic processes and process optimization for monoclonal antibodies. Chem Eng Process 44: 1123-1137.

Soriano GA., Titchener-Hooker NJ. & Shamlou PA. 1997. The effects of processing scale on the pressure drop of compressible gel supports in liquid chromatographic columns. Bioprocess Engineering 17:115-119.

Sotiriadis A, Keshavarz T, Keshavarz-Moore E. 2001. Factors affecting the production of a single-chain antibody fragment by *Aspergillus awamori* in a stirred tank reactor. Biotechnol Prog. 17:618-623.

Stickel JJ, Fotopoulos A. 2001 Pressure-Flow Relationships for Packed Beds of Compressible Chromatography Media at Laboratory and Production Scale. Biotechnol. Prog. 17:744-751.

Stowers AW, Chen Lh LH, Zhang Y, Kennedy MC, Zou L, Lambert L, Rice TJ, Kaslow DC, Saul A, Long CA, Meade H, Miller LH. 2002. A recombinant vaccine expressed in the milk of transgenic mice protects Aotus monkeys from a lethal challenge with *Plasmodium flaciparum*. Proc Natl Acad Sci USA. 99: 339-344.

Stryer L. 1995. Antibodies and T-Cell receptors. In Biochemistry 4th Ed 361-391. WH Freeman and Company. New York.

Thiel KA. 2004. Biomanufacturing, from bust to boom...to bubble? Nature Biotech 22:1365-1372.

Titchener-Hooker NJ, Zhou Y, Hoare M, Dunnill P. 2001. Biopharmaceuticals process development: Part II, Methods of reducing development time. BioPharm Europe. September: 68-74.

Tong JM, Kettel M, Perry M, Pain DJ, Valentine DM, Westlake AJ, Wrankmore M, Brown M. 2004. A case study on the application of disposable technologies in cGMP manufacturing processes for a therapeutic antibody. ACS 227th National Meeting.Anaheim, CA. March 28th -April 1st.

Tsuchiya N, Endo T, Matsuta K, Yoshinoya S, Aikawa T, Kosusge E, Takeuchi F, Miyamoto T, Kobata A. 1989. Effects of galactose depletion from oligosaccharide chains on immunological activities of human IgG. J Rheumatol. 16:285-290.

Tylka S, 2003. Microwell centrifugation. MSc research project.

van der Pol L, Tramper J. 1998. Shear sensitivity of animal cells from a culture-medium perspective. Trends Biotechnol. 16:323-328.

van Reis R, Goodrich EM, Yson CL, Frautschy LN, Dzengeleski S, Lutz H. 1997. Linear scale ultrafiltration. Biotech Bioeng. 55:737-746.

van Reis R, Leonard LC, Hsu CC, Builder SE.1991. Industrial scale harvest of proteins from mammalian cell culture by tangential flow filtration. Biotech Bioeng. 38:413-422.

van Reis R. Zydney A. 2001. Membrane separations in biotechnology. Curr Opin Biotech. 2001. 12:208-211.

Willoughby N, Martin P, Titchener-Hooker NJ. 2004. Extreme scale-down of expanded bed adsorption: Purification of an antibody fragment directly from recombinant E. coli culture. Biotech Bioeng. 87:641-7.

Winter G, Griffiths A D, Hawkins R E & Hoogenboom H R. 1994. Making antibodies by phage display technology. Annu Rev Immunol. 12:433-55.

Winter G, Milstein C. 1991 Man-made antibodies. Nature. 349:293 – 299.

Wurm FM, Gwinn KA, Kingston RE. 1986. Inducible overexpression of the mouse c-myc protein in mammalian cells. Proc Natl Acad Sci USA 83:5414-5418.

Wurm FM. 2004. Production of recombinant protein therapeutics in cultivated mammalian cells. Nature biotech. 22:1393-1398.

Yang J-D, Angelillo Y, Chaudhry M, Goldenberg C, Goldenberg DM. 2000. Achievement of high cell density and high antibody productivity by a controlled-fed perfusion bioreactor process. Biotech Bioeng. 69:74-82.

Zettlmeissl G, Wirth M, Hauser HJ, Kupper HA. 1988. Isolation of overproducing recombinant mammalian cells by a fast and simple selection procedure. Gene 73:419-426.

Zoon KC. 1997. Points to consider in the manufacture and testing of monoclonal antibody products for human use. CBER. FDA.

Publications List

Hutchinson N, Bingham N, Murrell N, Farid S, Hoare M. 2006. Shear stress analysis of mammalian cell suspensions for prediction of industrial centrifugation and its verification. Biotech Bioeng. 95. 483-491.

Hutchinson N, Hoare M. 2003. Shear stress analysis for the prediction of industrial centrifugal clarification. *Recovery of Biological Products XI*, 14-19th September, Banff, Canada.

Hutchinson N, Hoare M. 2005. Shear stress analysis of mammalian cell suspensions for prediction of industrial centrifugation performance. *ESACT-UK*, 6-7th January, Leicester, UK

Willoughby, N., Salte, H., Tustian, A., Hutchinson, N., Hoare, M. (2005) Ultra-scale-down of centrifugation – applications in recovery from high cell density systems, *CAP 05,* Phoenix, Arizona, USA, May.

Willoughby, N., Salte, H., Tustian, A., Hutchinson, N., Hoare, M. (2005) Ultra-scale-down of centrifugation – applications in recovery from high cell density systems, *WCCE 7,* Glasgow, UK, July.

Green K, Kauten J, Blanchard D, Kenny A, Willoughby N, Hutchinson N. 2005 Design, scale-up, characterization and validation of a 20,000L primary recovery

process for mammalian cell culture. Accepted for *Biochemical Engineering XIV,* 10-14th July 2005, Harrison Hot Springs, Canada.